DYNAMIC ANALYSIS AND SEISMIC RETROFIT OF THE POINT SUR LIGHTHOUSE

A Thesis

presented to

Faculty of California Polytechnic State University,

San Luis Obispo

In Partial Fulfillment

of the Requirements for the Degree

Master of Science in Architectural Engineering

by

Nicholas Dekker

June 2020

COMMITTEE MEMBERSHIP

TITLE:	Dynamic Analysis and Seismic Retrofit of the Point Sur Lighthouse
AUTHOR:	Nicholas Dekker, EIT
DATE SUBMITTED:	June 2020

COMMITTEE CHAIR:	Cole McDaniel, PhD, PE Professor of Architectural Engineering
COMMITTEE MEMBER:	Graham Archer, PhD Professor of Architectural Engineering
COMMITTEE MEMBER:	Peter Laursen, PhD, PE Professor of Architectural Engineering

ABSTRACT

Dynamic Analysis and Seismic Retrofit of the Point Sur Lighthouse

Nicholas Dekker

The Point Sur Lighthouse is an unreinforced stone masonry building completed in 1889 on the central coast of California. The lighthouse is listed on the National Register of Historic Places and is still an active aid to navigation. The original first-order Fresnel lens was removed from the lantern room and placed in safekeeping due to its high risk of damage in the event of a strong earthquake. The lens has been approved to return to its original setting but the seismic performance of the building must first be assessed in order to ensure the safety of the lens and lighthouse, specifically the out-of-plane behavior of the unreinforced masonry walls, the implementation of possible seismic retrofit schemes, and the effects of the lens's added weight.

This research focuses on the dynamic behavior of the lighthouse in its current state and the changes in the dynamic behavior each of the proposed seismic retrofit schemes might cause. For the purposes of this research, dynamic behavior is considered as natural frequencies, mode shapes, and related structural properties. The dynamic behavior of the lighthouse was assessed using two main methods: forced vibration testing and finite element computer modeling. Forced vibration testing is a nondestructive testing method that can be used to directly characterize dynamic behavior of a structure, and finite element computer modeling is useful for the design and simulation of dynamic behavior of both new and existing structures. The combination of these two methods on the Point Sur Lighthouse will work to develop and prove state-of-the-art seismic retrofitting techniques.

Keywords: Unreinforced Masonry, Seismic Retrofit, Forced Vibration Testing, Finite Element

ACKNOWLEDGMENTS

I would like to thank my family and friends for supporting me through the completion of this project and encouraging me to pursue a subject I am passionate about. A big thank you to my advisor Cole McDaniel for all the careful guidance, as well as Peter Laursen and Graham Archer. Thank you to the faculty and staff of the Architectural Engineering Department for the time and energy they invested in me throughout my time as an undergraduate and graduate student and for making the ARCE program so rad. Thank you also to RISA Tech, Inc., the Central Coast Lighthouse Keepers, California State Parks, and the Cal Poly Office of Graduate Education.

TABLE OF CONTENTS

LIST OF TABLES

LIST OF FIGURES

1.0 INTRODUCTION

1.1 Overview

The Point Sur Lighthouse is a historic unreinforced masonry structure that is susceptible to damage in an earthquake due to a number of factors, mainly its inadequate lateral load resistance capacity coupled with the high seismicity of its location. The tall unreinforced masonry walls and weak roof diaphragms have a particularly high risk of damage. Though the original first-order Fresnel lens is not currently in the lighthouse, its repatriation has been approved by the U.S. Coast Guard and it will also have a high risk of damage when it returns. The goal of this thesis was to determine the most effective seismic retrofit schemes for the lighthouse using a combination of ultra-low forced vibration testing [1,2] and finite element computer modeling. This combination is unusual in seismic retrofitting because it is time and labor intensive, but it was justified in this case because of the extreme care that needs to be taken to preserve the historic structure. The lighthouse is shown in Figure 1.1-1.

Figure 1.1-1: Point Sur Lighthouse

1.2 Purpose of Research

The purpose of this research was to develop and prove state-of-the-art seismic retrofitting procedures by implementing a combination of analysis methods on the historic Point Sur Lighthouse. One relatively uncommon seismic analysis method is ultra-low forced vibration testing, which is nondestructive, simple to conduct, and has a wide range of applications including structural damage detection [4] and system behavior identification [5]. Finite element computer modeling is an analysis method commonly used in the design of new construction. Finite element programs allow a structure to be modeled according to the architect's and engineer's specifications to meet structural loading criteria. However, finite element modeling is just as useful in studying existing structures. These methods are considered state-of-the-art because they have only recently been made possible by advances in technology including sensors, computers, and programming, but are not yet commonly used in the majority of structural engineering practices.

The combination of these two techniques on a single retrofit project is unusual because neither technique follows prescriptive procedures like the ones found in building codes, instead they rely on engineering judgement and experience in structural design. These techniques are also time and labor intensive. Ultra-low forced vibration testing requires an extensive amount of field work and subsequent data analysis, while finely tuned finite element computer modeling requires a high attention to detail and informed user input between solution operations. With an increasing need for careful seismic retrofitting of historic structures, the combination of these techniques may one day be a viable option for historic structures or even commonplace buildings, and this research is an important step in its widespread use.

1.3 Scope and Topics

Before this research began, the lighthouse was evaluated according to tiered screening procedures found in the American Society of Civil Engineers ASCE 41-17: Seismic Evaluation and Retrofit of Existing Buildings [6] and basic retrofit components were designed to satisfy the structural deficiencies that were discovered. The ASCE 41-17 retrofit designs and other designs developed during this research made up the collection of designs that were evaluated. The lighthouse was also subjected to ultra-low forced vibration testing and data was collected that gave insight into the dynamic behavior of the lighthouse as it currently stands. This data was essential in the confirmation of the finite element model created in RISA-3D as it validated the results that were found under various loading scenarios and guided decisions that were made in the modeling process.

The majority of this research focused on the analysis of the lighthouse and potential seismic retrofit schemes that may be implemented in the lighthouse. At the start of this research, a finite element model was created of the as-built lighthouse to serve as a base model and was then modified to include each of the retrofit designs. In each of the models, a modal analysis was conducted in order to obtain natural periods and frequencies, mass participation, and mode shapes. These results provided only a start of the comparison between retrofit schemes, and a comparison of mode shapes proved especially difficult because of their unitless nature. Next, a linear static design level seismic load was applied to each of the models in order to achieve a more qualitative assessment based on the comparison of the deflections of components. Similar analyses were conducted again with the addition of the Fresnel lens, which was modeled as a point mass in its original location in the lantern room. Finally, a modal response spectrum

analysis was conducted in each both plan directions to compare the retrofit schemes. The final analysis was effective at highlighting the differences in the retrofit schemes that the other analyses could not. These analyses were used to evaluate the effectiveness of various retrofit schemes on improving the dynamic behavior of the lighthouse as a whole and of its major components individually. Only estimated member sizes and configurations for each of the retrofit schemes were proposed in this research and their complete design was left to a design professional at a later stage in the retrofit process.

1.4 Literature Review

The Piedras Blancas Lighthouse is a historic lighthouse located roughly 65 miles south of the Point Sur Lighthouse on California State Route 1. The two lighthouses began operation in the late 1800s and share a similar elevated historical status. Like Point Sur, the Piedras Blancas Lighthouse is also unreinforced brick masonry construction and was evaluated according to a similar combination of forced vibration testing and finite element computer modeling in order to determine the best course of action for retrofitting the structure. The forced vibration testing was used to confirm the accuracy of the dynamic behavior simulated in the finite element model. The finite element model was also used to inform the possible retrofit options [7]. The work done on the Piedras Blancas Lighthouse has a similar scope and timeline as the work started on the Point Sur Lighthouse with this research and will continue with future research. The retrofit decisions made for one lighthouse will help inform the decisions for the other lighthouse, as the lighthouses have a similar course of action: analyze the lighthouse with forced vibration testing and finite element modeling, design and implement a seismic retrofit scheme, and evaluate the accuracy of the original analysis using the same analysis methods. The structural systems that

will be used to retrofit each of the lighthouses may be different since the Point Sur Lighthouse is a tower with adjoining rooms while the Piedras Blancas Lighthouse is only a freestanding tower, but the methodology is the same.

Sourer et al. [8] tabulated the results of tests performed on full-scale stone masonry walls of a similar construction and material to the ones found in the Point Sur Lighthouse. The purpose of the research was to determine material properties of typical sandstone masonry buildings of a particular era. The walls were tested past their peak axial capacities both in-plane and out-of-plane. Tests by others on smaller material samples were also included in the results to compare material properties such as Young's modulus and shear modulus. Even though the walls of the Point Sur Lighthouse are not expected to reach, let alone exceed, their peak axial capacities in any foreseeable loading scenario, some amount of strength degradation may be assumed to be present due to the age of the construction and proximity to the ocean. The data from Sourer et al. was useful in determining proper material properties to use in the finite element model of the lighthouse.

Furtmüller and Adam [9] gave recommendations on material properties of historical brick and mortar to be used in numerical models based on sample testing. Brick and mortar samples were extracted from buildings constructed in Vienna, Austria within a certain range of years that include the year the Point Sur Lighthouse was constructed. A mean and standard deviation were provided for the tested properties due to the large number of tests that were conducted. The test samples' material properties were matched with numerical models. The purpose of the research was to determine material properties of brick masonry for more accurate and efficient numerical modeling on a number of different modeling scales. The data from Furtmüller and Adam was

useful for accurate material property inputs in the finite element model since a portion of the lighthouse's tower is constructed with brick masonry.

Vaculik [10] developed both force and displacement-based seismic design methodologies for unreinforced masonry walls out-of-plane. The focus of the research was displacement-based methodologies for two-way spanning unreinforced masonry walls, which is one of the primary areas of study needed at the Point Sur Lighthouse. Even though the main unreinforced masonry typology studied by Vaculik is not the same as that found in the lighthouse, Vaculik generalized the final recommendations of the research so that they may have a wide range of applications. Two-way walls were found to have a much larger strength and displacement capacity than vertically spanning walls and parameters were identified for two-way walls that are beneficial to the wall's out-of-plane resistance capabilities. Advantages of two-way spanning walls over vertically spanning walls were found to diminish with the failure of connections to adjacent walls acting as supports.

1.5 Future Research

This research may continue with more advanced finite element modelling of the lighthouse and its potential retrofit schemes. The finite element program used in this research was RISA-3D because of its user-friendly interface and the ease with which a user can model and manipulate 8-node solid elements, though other programs may be used to supplement the analyses conducted. There are many model input parameters that may be fine-tuned to better reflect the dynamic behavior of the lighthouse. A number of other types of loading scenarios may be run in RISA-3D that were not already run for this research, and they could be used to further compare the proposed retrofit solutions.

This research may also continue with additional ultra-low forced vibration testing on the lighthouse as it stands and if/when a retrofit scheme is eventually installed. If one of the retrofit schemes that has been recommended in this research is installed, the finite element model for that retrofit scheme can be compared directly to the additional ultra-low force vibration testing results. If a new retrofit scheme is installed, that scheme can easily be modeled in the as-built lighthouse finite element model and compared to the corresponding forced vibration testing results.

2.0 CURRENT LIGHTHOUSE

2.1 Overview

The Point Sur light was first activated in 1889 along the Big Sur coast of Central California and is still an active aid to navigation. The lighthouse (and other buildings used to support the lighthouse) was constructed of unreinforced sandstone masonry hewn from the hills nearby. Though the sandstone walls are approximately 20″ thick and portions of the lighthouse's tower are even thicker, there are still significant structural deficiencies present that must be addressed in order to preserve the lighthouse and protect the valuable first-order Fresnel lens once it returns to its original setting in the lighthouse's lantern room. The most glaring deficiencies in the lighthouse are the tall gabled walls, which are expected to have poor dynamic behavior out-of-plane should a strong earthquake occur, the roof lateral force resisting system deficient in both strength and stiffness, and uncertainties in the foundation capacity [11].

2.2 History

The Point Sur Lighthouse is located approximately halfway between San Francisco and San Luis Obispo on California State Route 1 at the northern end of the Big Sur coast, shown in Figure 2.2-1. The Big Sur coast became known for its heavy fog and high winds by Spanish explorers and later tallow and hide traders. The beginning of the California gold rush in 1849 quickly increased coastal shipping through the area and it became clear that a light was needed at Point Sur to fill the gap between the Piedras Blancas light approximately 55 miles to the south by sea and the Pigeon Point light approximately 65 miles to the north by sea. President Andrew Johnson signed an Executive Order in 1866 that reserved the site for a lighthouse [12]. The wreck of the steamer *Ventura* in 1875 motivated petitions to the U.S. Lighthouse Service Board

(a) (b)

Figure 2.2-1: a) Central Coast Lighthouses [13], b) Point Sur Lighthouse Location [14]

for funds to build a light at Point Sur, but the first funds were not allocated until 1886. Congress allocated $50,000 for construction of the lighthouse in 1886, another $50,000 in 1887 to continue the construction that had stopped [15], and a final $69,100.69 in 1887-1888 to fund the project to completion [16] for a total of $169,100.69, or about $4,600,000 in 2020 dollars.

The lighthouse was equipped with a first-order Fresnel lens, the largest class of Fresnel lenses, which is a compact type of lens adapted for use in lighthouses by Augustin-Jean Fresnel. The entire lens assembly stands 18′ tall and weighs almost 10,000 lbs. The lens alone stands 8′ tall by 6′ in diameter and weighs 4,330 lbs. The lens consists of panels of concentric rings of glass prisms that focus light rays from the inner light source into a single large beam. An example of a first-order lens is shown in Figure 2.2-2. Each lighthouse along the coast broadcasted light with a unique pattern and color combination so that ships could determine their

location by triangulation; the Point Sur light alternated red and white flashes spaced 15 seconds apart. The light from the Point Sur Lighthouse was first activated on August 1, 1889 and could be seen for 23 nautical miles.

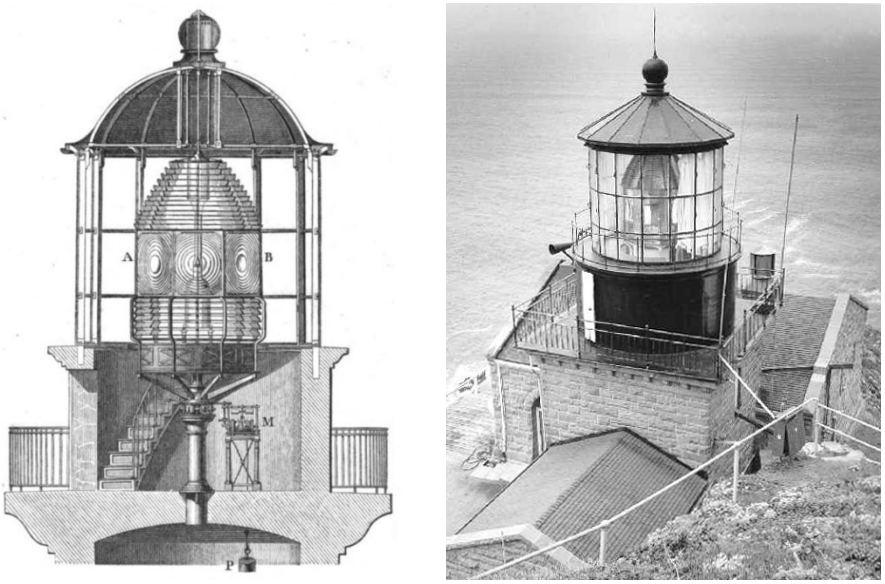

(a) (b)

Figure 2.2-2: a) Example of First-Order Fresnel Lens in Section
b) First-Order Fresnel Lens at Point Sur [17]

A lighthouse keeper and a number of keeper's assistants lived on the rock with their families in order to maintain the lighthouse and fog signal 24 hours a day. Though the lighthouse improved navigations along the Big Sur coast, there were still shipwrecks that occurred nearby. The most famous wreck off Point Sur was the USS *Macon* airship which fell into the ocean in 1935 and whose wreckage was not located until 1991. The U.S. Coast Guard assumed responsibility for all aids-to-navigation in 1939 and automated the Point Sur Lighthouse in 1974; the lighthouse is an active aid to navigation to this day. The Point Sur Light Station was placed on the National Register of Historic Places in 1980 and along with the area nearby, makes up the Point Sur State Historic Park, shown in Figure 2.2-3.

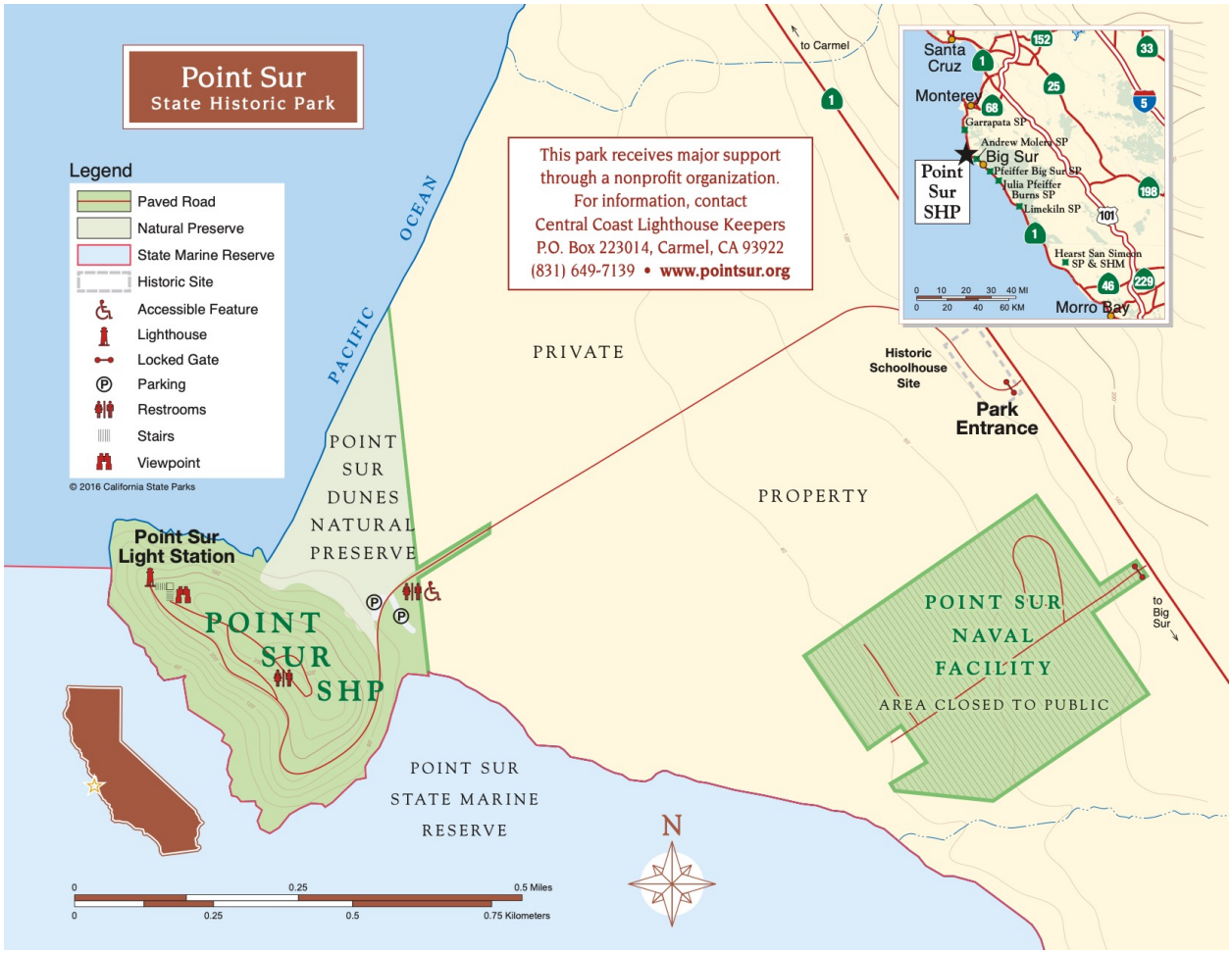

Figure 2.2-3: Point Sur State Historic Park [18]

2.3 Building Description

2.3.1 Lighthouse

The lighthouse consists of three main sections that form a T-shape in plan: the fog room, the tower, and the radio room, shown in Figure 2.3-1. The fog room is the section located furthest to the west and is 33′4″ by 40′0″ in plan. The walls are constructed of unreinforced sandstone masonry roughly 20″ thick and range in height from 13′10″ at the rectangular walls on the east and west sides to 22′6″ at the peak of the gabled walls on the north and south sides. The roof is supported by trusses that span in the east-west direction and are constructed of 4x wooden

members of various depths and 1″ steel rods. Atop the wooden trusses are purlins, subpurlins, 1″ straight sheathing, and roofing material.

The radio room is the section located furthest to the east and is 17′8″ by 16′0″ in plan. The walls are also constructed of unreinforced sandstone masonry roughly 20″ thick and range in height from 12′9″ at the rectangular walls on the north and south sides to 18′8″ at the peak of the gabled wall on the east side. The roof is supported by trusses that span the 16′ direction and are constructed of 2x and 1x members of various depths. Atop the trusses is straight sheathing and roofing material, though this is not directly visible like it is in the fog room because the ceiling and walls are plastered over.

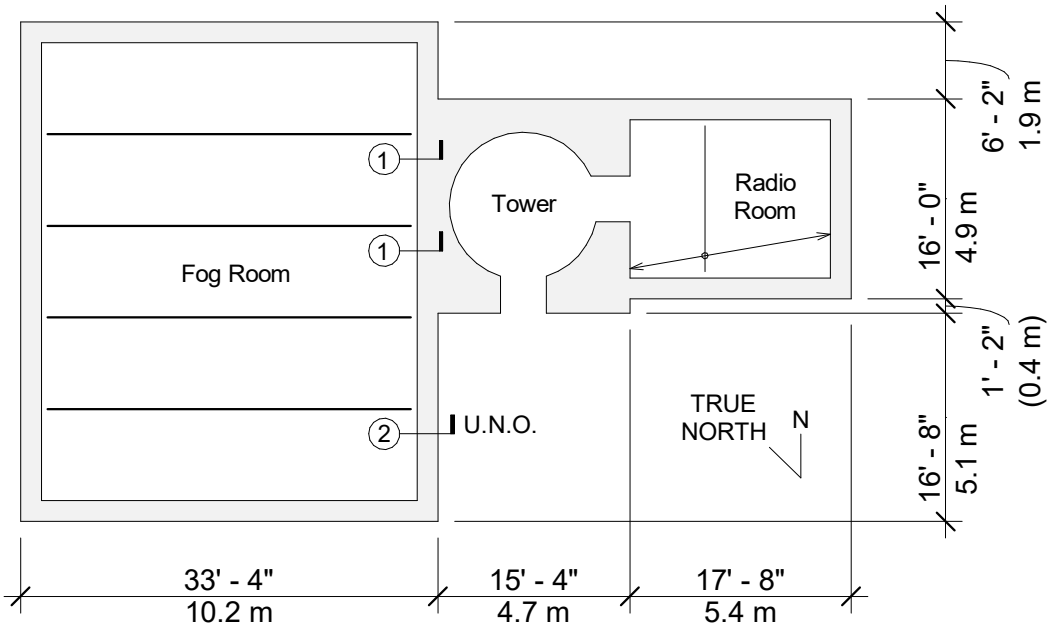

Figure 2.3-1: Point Sur Lighthouse Plan

The tower is located between the fog room and the radio room in plan, forming the west wall of the radio room and coinciding with a portion of the east wall of the fog room. The outer surface of the tower's section is rectangular in plan and was constructed with unreinforced

sandstone masonry, measuring 17′0″ by 17′2″. The inner surface of the tower's section is circular in plan with a diameter of 12′0″ and was constructed with roughly 12″ of unreinforced brick masonry. The spiral staircase that runs the height of the tower is broken up by an intermediate landing 13′4″ from the ground level and reaches the watch room level 24′8″ from the ground level. The tower's section changes at the watch room level from a square to a circle, with an inside diameter of 12′0″ and an outside diameter of 15′4″, constructed solely with unreinforced sandstone masonry. Both the inside and outside of the watch room level is clad in steel plate. The south elevation of the lighthouse is shown in Figure 2.3-2.

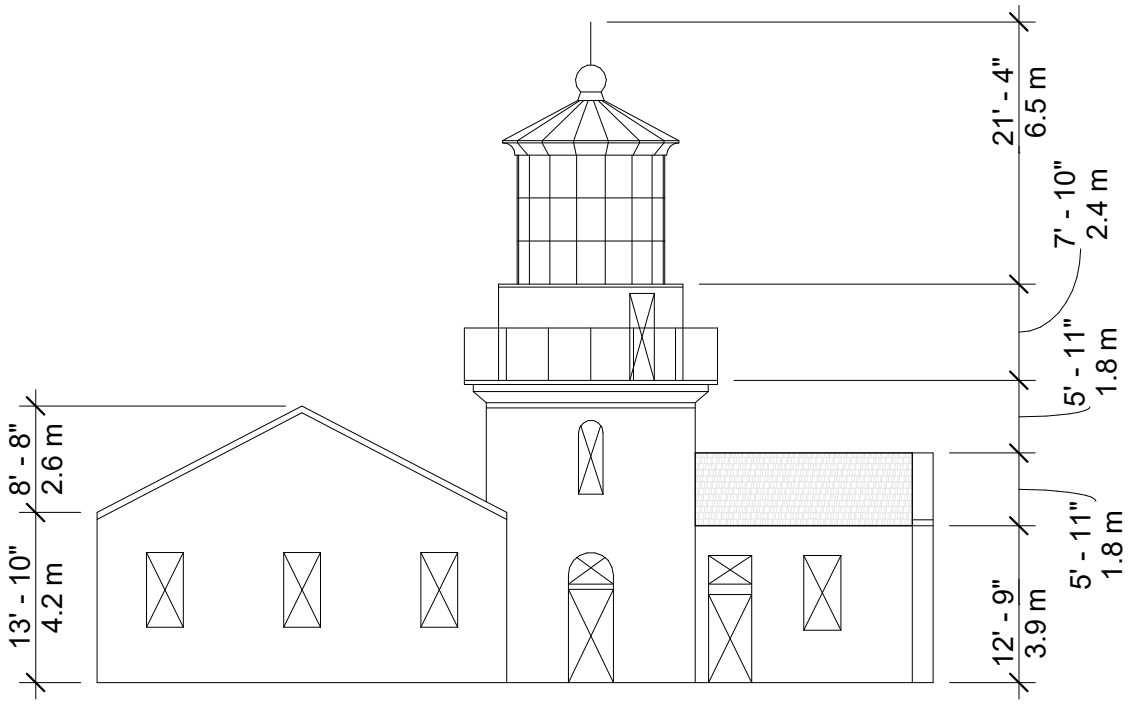

Figure 2.3-2: Point Sur Lighthouse South Elevation

The watch room extends 7′3″ up to an elevation of 31′11″ and is where the Fresnel lens stand was originally mounted. The lamp inside the lens was rotated by a mechanism powered by descending weights. The shaft that housed those weights extends from the ground level up to the

watch room floor level. The lantern room is directly above the watch room and extends another 9′6″ up to an elevation of 41′5″. The lens filled the lantern room and was accessible from the inside by a small staircase and from the outside by a narrow catwalk. The roof above the lantern room was constructed with cast iron fixtures and copper plate. The height of the tower to the top of the ventilator ball, not including the lightning rod, is 49′6″.

2.3.2 Lens Removal and Repatriation

The lighthouse's lens was manufactured in 1887 by a firm in Paris and its light was produced first by a kerosene lamp and later by an incandescent lightbulb. The United States Coast Guard automated the lighthouse's operations in 1974, shifting the function of producing light from the Fresnel lens to a modern aero beacon mounted outside the lantern room nearby. The Coast Guard removed the Fresnel lens from the lantern room in 1978 for safekeeping and moved the aero beacon into the lantern room. The lens was taken from storage and loaned to a maritime museum in Monterey from 1992 to 2017. The lens is currently back in storage but has been approved to return to the lighthouse following a request to the United States Coast Guard by the Central Coast Lighthouse Keepers. Point Sur's lens may be repatriated on the condition that a seismic evaluation and retrofit be performed on the lighthouse, making it the only first-order Fresnel lens that has been approved to return to its original setting in the country. This research aimed to contribute to the seismic evaluation of the lighthouse as it currently stands, but also to analyze the lighthouse with the added weight of the lens before the lens returns. Any retrofit scheme that was studied must take into account the added weight of the lens including the effects on the dynamic behavior of the lighthouse.

2.3.3 Other Light Station Buildings

Other buildings were built on Point Sur at the same time as the lighthouse to support the people and operations necessary to maintain the lighthouse's light and later its fog signal. Many of those buildings are still standing and available for tour along with the lighthouse, making the Point Sur Light Station the only complete turn of the century light station open to the public in California [19]. The light station is shown on its perch on Point Sur rock in Figure 2.3-3.

Figure 2.3-3: Point Sur Light Station [3]

The head keeper's quarters are one story constructed in unreinforced sandstone masonry with a second story of light wood framing added later. The assistant keeper's quarters is three stories and also built in unreinforced sandstone masonry. Restoration projects were undertaken for both of those buildings that included refurbishing the interior and exterior and strengthening the structure. These buildings have many of the same deficiencies as the lighthouse, for example weak walls out-of-plane and weak lateral force resisting system components. Unlike the lighthouse, the seismic strengthening components that were added in the living quarters will be

hidden with plaster once the restoration projects are complete. The strengthening components and techniques used in the living quarters will be used as examples when designing the retrofit components for the lighthouse.

The main difficulty in adding components to the lighthouse is their intrusion on the original architectural features, since any modern additions to the building must maintain the building's historic character. Figure 2.3-4 shows a new lateral force resisting connection installed in the assistant keeper's quarters. In the lighthouse, sufficient anchorage into the unreinforced masonry like the anchorage shown will be necessary no matter what retrofit scheme is selected because all schemes require improved load transfer between the heavy masonry walls and the light roof diaphragm. New members in the lighthouse will most likely be stainless steel rather than wood so they can be smaller and corrosion resistant, also like the ones shown in the figure.

Figure 2.3-4: Example of Anchorage into Unreinforced Masonry

2.4 Lighthouse Structural Deficiencies

Before the original lens may be repatriated to the lighthouse, a seismic evaluation of the lighthouse must be completed to ensure the valuable lens will be safe in the event of strong

ground motions. Even though the lens would be entirely supported by the lighthouse's tower, the entire lighthouse will be considered in the evaluation. The unreinforced masonry construction and deficient lateral force resisting system components raise some of the most obvious concerns but a more in-depth survey of the building shows there are a number of other vulnerabilities that will need to be addressed. The unreinforced masonry in the building is expected to have very low strength and URM is known to suffer from catastrophic failure in large seismic events. In the case of the lighthouse, there are very few locations where such a failure might occur, but a failure could still cause irreparable damage due to the fact that the building is small and has a simple floorplan; any one failure could result in a large portion of the building being damaged. A catastrophic failure could also occur within components of the lateral force resisting system.

2.4.1 Unreinforced Masonry

The majority of the lighthouse is constructed of unreinforced sandstone masonry cut from the surrounding hills while the interior surface of the lighthouse's tower is constructed from unreinforced brick masonry. The in-plane shear strength properties of unreinforced masonry walls have been studied in depth for better understanding of similar lateral force resisting systems in URM buildings, since in-plane shear failures make up a large portion of all URM failures in large seismic events. Out-of-plane failures of walls are known to be a deficiency of URM construction and make up another large portion of URM wall failures in large seismic events. Despite the similar hazards of in-plane and out-of-plane URM failure modes, there is still a significant disparity between the research, assessment, and design techniques of the two main types of failures [10]. One aspect of out-of-plane unreinforced masonry failure modes that has received disproportionately little research is the behavior of two-way spanning walls because

research has mainly focused on one-way spanning walls. This disparity in out-of-plane research is unfortunate because two-way spanning wall failures are much more common in practice. Figure 2.4-1 shows common crack patterns in one- and two-way spanning walls, where one-way spanning walls usually exhibit cracking in only one direction while the crack patterns of two-way walls are generally more complex and segmented with cracks that run in a combination of horizontal, vertical, and diagonal directions.

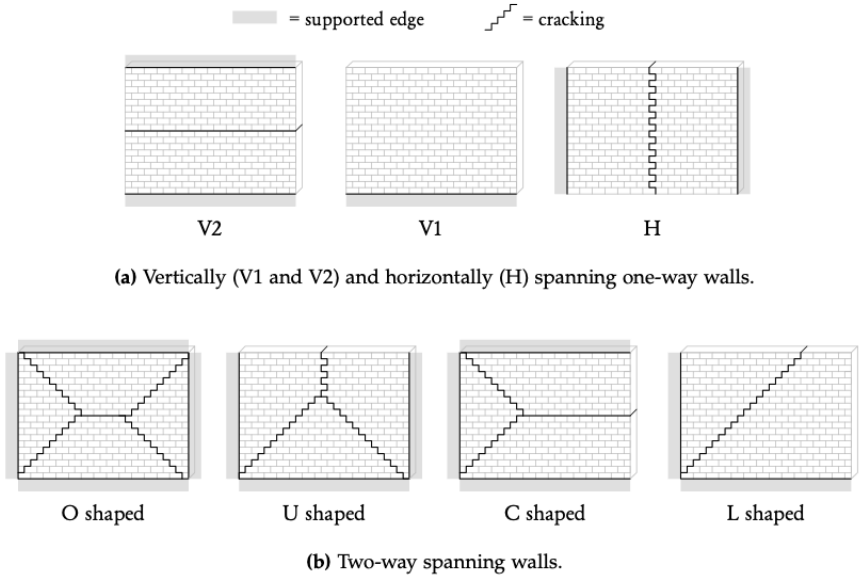

Figure 2.4-1: Expected URM Crack Patterns Based on Wall Span Direction [10]

In the case of the lighthouse, the expected mode of failure in the unreinforced masonry is out-of-plane failure in two-way spanning walls, specifically at the north, south, and west walls of the fog room. Even though the large thickness of the walls offsets the low strength of the masonry and mortar system, the large height of the walls coupled with the large thickness and inadequate restraint at the top edges of the walls still poses a risk of poor out-of-plane dynamic behavior. The trends found in the crack patterns shown in Figure 2.4-1 were applied to some of the walls of interest in the lighthouse, and the expected crack patterns of the walls are shown in

Figure 2.4-2 as dashed lines. These crack patterns are based on the crack patterns of brick masonry and may vary greatly due to the random ashlar bond pattern and varying dimensions of the stones, shown in Figure 2.4-3.

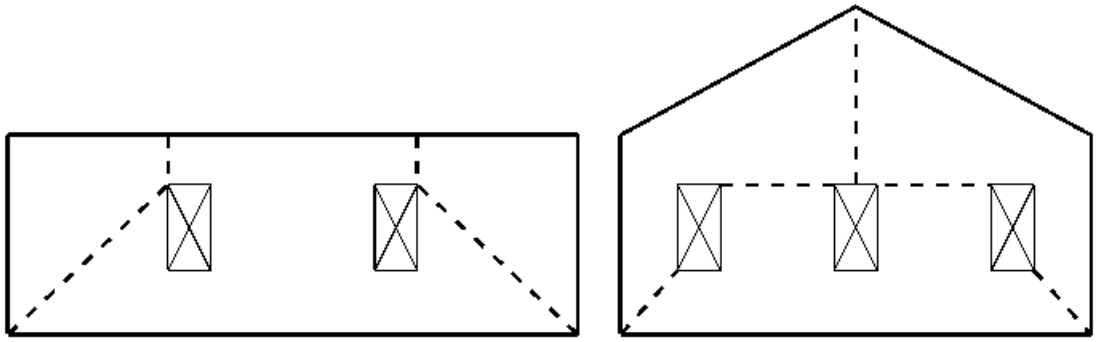

Figure 2.4-2: Expected URM Crack Patterns in the Lighthouse

Figure 2.4-3: Random Ashlar Sandstone Masonry Bond Pattern

The expected mode of failure in the URM walls is out-of-plane due to their large height and lack of restraint at the roof. The lighthouse is only one story and the roof assembly is extremely light, therefore the vast majority of the in-plane loads that the walls might experience in a seismic event are inertial loads due to the walls' own self weight. The portions of the walls

that act as spandrels over doorways or piers between windows are the most vulnerable to in-plane loading since they have a vastly reduced section compared to the portions of the walls without openings. In general, the walls are expected to sufficiently resist in-plane loads because the strength capacity of the walls in-plane is directly proportional to the thickness of the walls. The expectation is the same in the tower because all areas of the cross section are as thick or thicker than the walls.

Another complication that arises from the unreinforced masonry in the lighthouse is the formation of proper connections between the masonry and new and/or existing components of various materials. An example of sufficient anchorage into the masonry is shown in Section 2.3.3, though the instance described has the advantage of being concealed inside a wall cavity. It will be important to balance the strength of the anchorage with the intrusion of the connection on the historical character of the building. It also appears that the walls are constructed of more than one vertical layer of stone masonry, further complicating any future anchorage design. Fortunately, there are a number of different methods to properly anchor into the unreinforced masonry that are minimally intrusive. These include drilling through the wall to attach a small backing plate or coring down the center of the wall, inserting a bolt or rod, and filling the rest of the cavity with grout.

2.4.2 Strength and Stiffness

Two of the most important considerations in basic elastic structural engineering are strength and stiffness. Strength involves a structure's ability to adequately resist applied forces while maintaining stability, and stiffness involves a structure's ability to adequately resist applied forces without excessive deflection or vibration. The strength and stiffness properties of

a member or system of members are related but are not directly proportional, and a good example of this relationship is found in the lighthouse.

The gabled walls in the fog room are expected to have adequate strength in-plane, and possibly out-of-plane, but low stiffness out-of-plane is the expected failure mode. The gabled walls' inadequate connection to the roof diaphragm suggests that the walls will behave more like a cantilever than a simply supported beam and the geometry of a cantilever leads to a much lower overall stiffness. Similarly, the rectangular wall in the fog room has adequate strength to resist in-plane and possibly out-of-plane loading, but its long, inadequately unsupported top edge could lead to excessive out-of-plane deflections as the controlling failure mode. A proper connection to the roof diaphragm would greatly increase the overall stiffness out-of-plane for the western rectangular wall as well, and the rectangular wall already benefits greatly from its connection to the stiff tower through the fog room trusses. The tower is expected to perform well in terms of both strength and stiffness because of the immense thickness of its cross section. The stiffness of the tower is so great that reinstalling the lens in the tower is expected to have a very small effect on the tower's dynamic behavior.

The roof diaphragms in the fog and gable rooms are expected to be extremely deficient in both strength and stiffness based on the assumed properties of their construction. In modern construction, roof diaphragms are integral to the overall strength and stiffness of a building because they are used to transfer lateral forces and unify lateral force resisting elements. In the lighthouse, the diaphragms' straight sheathing construction and inadequate connection between walls and diaphragm means that the diaphragms will be incapable of properly transferring even small lateral loads, let alone design level seismic loads.

2.4.3 Lateral Force Resisting System

The lateral force resisting system (LFRS) as a whole is considered deficient because of its undefined and discontinuous load path. To begin, the roof diaphragm itself is considered deficient and is not expected to adequately resist the inertial loads placed on it by the heavy sandstone walls in a major seismic event. The roof diaphragm also provides inadequate restraint to the walls out-of-plane. One advantage that the roof diaphragm has is the very small inertial loading due to its own self-weight. The simple floorplan is also an advantage because the four walls of the fog and radio rooms can all act as LFRS elements between the roof levels and the foundation. The simple floorplan also means that collectors are not directly necessary because the sandstone walls that carry the lateral load to the foundation are practically continuous along each wall line. However, chords are necessary for proper load resistance and there are no continuous chords along any of the walls in the fog or radio rooms. The direct connection between the roof diaphragm and the gabled walls of the fog room is either hidden or nonexistent and the connection between the roof diaphragm and the rectangular walls of the fog room is uncertain. Any information about the connections to the roof diaphragm must be obtained from visual inspection. Figure 2.4-4 highlights the interface between the walls and roof diaphragm and Figures 2.4-5 and 2.4-6 show the connections between the roof diaphragm and fog room rectangular walls in detail. The detail numbers correspond to the detail callouts in Figure 2.3-1.

Figure 2.4-4: Roof Diaphragm and Wall Interface

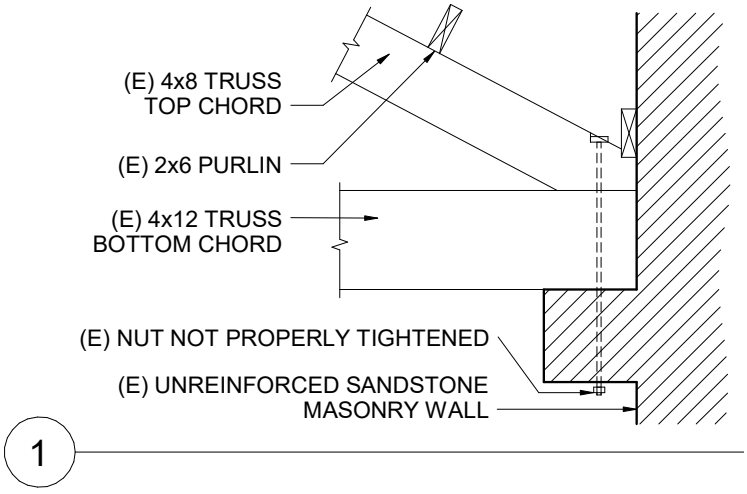

Figure 2.4-5: Truss to URM Wall Detail #1

The LFRSs in the fog and radio rooms are incapable of working as a cohesive system due to the lack of proper connectivity between elements. The unreinforced sandstone masonry walls are expected to have sufficient strength in-plane, but significant damage may occur in a seismic event due to the lack of restraint at the roof out-of-plane. The tower benefits from a simpler construction layout than the adjacent rooms and is expected to have sufficient lateral strength due to its thick and sturdy section.

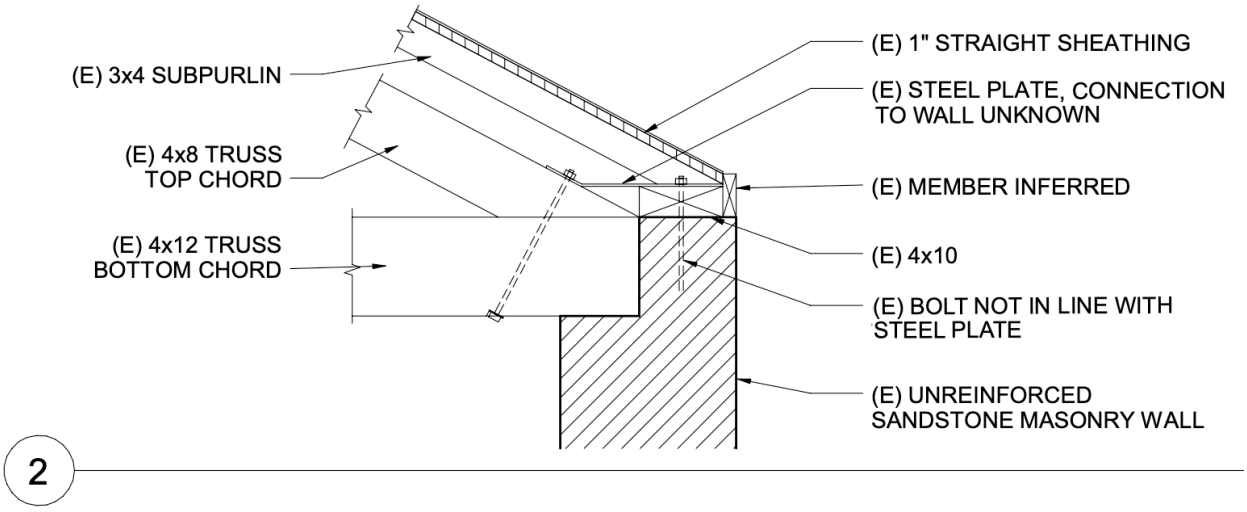

Figure 2.4-6: Truss to URM Wall Detail 2

2.4.4 Gravity Force Resisting System

The main gravity force resisting components are wooden trusses in the fog and radio rooms. The trusses in the fog room have top chords of 4x8 wood members, bottom chords of 4x12 wood members, and a web of 4x6 wooden members and 1″ steel rods. The fog room trusses support 2x6 purlins, 3x4 subpurlins, 1″ straight sheathing, and roofing. The trusses in the radio room have a much smaller span than the trusses in the fog room and have top chords of 2x6 wood members and web members of 1x6 and 2x6 wood members. The radio room's trusses support only 1″ straight sheathing and roofing. The trusses in the fog room bear directly on the sandstone masonry walls in a small groove cut into the wall where the tower and fog room walls do not coincide, or on a small projection extending into the fog room where the tower and fog room walls do coincide. The bearing area on the masonry walls is sufficient for the members and gravity loading conditions but the connections may still be deficient for lateral loading.

The main gravity force resisting components in the tower are steel beams, used only to support the stairs and landings at this time since the lens is not currently in the lantern room. The

beams bear directly into the brick masonry of the inner section of the tower, though there may be a more developed connection inside the walls. The beams are expected to have adequate strength to support the lens once it returns to the lighthouse. The landings are ribbed steel plate and bear into the brick masonry in a fashion similar to the beams. All gravity framing has been deemed sufficient by inspection since member sizes are large and gravity loads are generally low. Even though the added weight of the repatriated lens in the lantern room should not damage the existing framing, the existing gravity connections may need to be strengthened to more safely transfer higher inertial loads in the event of an earthquake.

2.4.5 Foundation

The condition and full extent of the lighthouse's foundation is uncertain. At the time of construction of the lighthouse, reinforced concrete technology was still relatively new and the need for deformed rebar to improve the concrete's tensile capacity was not yet fully understood. Deformed rebar is known today to be an essential component of standard concrete construction. A lack of deformed rebar, the building's age, and possible degradation due to the proximity to the ocean and 130-year lifespan of lighthouse could result in a foundation state of only limited strength. Figure 2.4-7 shows portions of the lighthouse's foundation that are exposed and whose strength may be deteriorated, located near the southwest corner of the lighthouse. A number of retrofit schemes proposed later in this research are centered around strengthening techniques that would require contact with the foundation. When evaluating retrofit schemes, careful consideration of any additional loads placed on the foundation were made, and final retrofit recommendations were conservative due to the unknown strength of the foundation.

Figure 2.4-7: Exposed Portions of Lighthouse Foundation, Southwest Corner

Even though some edges of the foundation sit near steep drop-offs and eroding soil, the foundation as a whole is expected to allow the lighthouse to remain stable in the event of a strong seismic event. This confidence is based on the fact that the foundation was constructed very near, if not directly on, bedrock and changes in slope stability have historically been minimal. The site of the lighthouse and the roads leading to it were cut directly from bedrock and it can be assumed that the concrete foundation extends sufficiently close to bedrock to avoid overturning, sliding, liquefaction, or any other foundation failure, similar to other locations on the point [20].

2.5 Retrofit Timeline

The timeline for retrofitting the Point Sur Lighthouse is currently unknown. Much of the retrofitting process depends on available funds raised by the Central Coast Lighthouse Keepers, who are the main supporters of all the light station's restoration projects. The full design of any proposed retrofit scheme is outside the scoop of this research and would therefore need to be completed by an engineering professional.

3.0 PAST EVALUATIONS

3.1 Overview

The Point Sur Lighthouse was subjected to ultra-low forced vibration testing before this research began. The ultra-low forced vibration testing used a linear mass shaker to induce a small sinusoidal load at a point on a structure and the resulting accelerations were measured around the building using piezoelectric accelerometers. Data was collected that gives insight into the dynamic behavior of the lighthouse as it currently stands, including mode shapes and load path deficiencies. The data was also essential in the confirmation of the finite element model created in RISA-3D, as it validated the results that were found under various loading scenarios and guided modeling decisions. The lighthouse was also evaluated before this research began according to the tiered screening procedures found in the American Society of Civil Engineers ASCE 41-17: Seismic Evaluation and Retrofit of Existing Buildings [6], an accepted standard for seismic retrofit procedures. Each of the three tiers of procedures increase in complexity and inspection from the next, where the first tier includes only a preliminary review of construction drawings or the structure itself and the third tier involves designing solutions. A basic retrofit scheme was developed in order to resolve the structural deficiencies identified in the screenings. The retrofit scheme served as a starting point for the design of other schemes and a baseline when studying the dynamic behavior of the building before and after modification.

3.2 Ultra-Low Forced Vibration Testing

3.2.1 Description

Forced vibration testing (FVT) is a method of studying the dynamic properties of an existing building using a mass shaker to induce a load and accelerometers to measure the

building's response. Large scale FVT typically involves an eccentric mass shaker anchored to the building that induces a load using a series of weights eccentrically attached to a rotating shaft. This method of testing is difficult because the mass shaker is often very large and heavy, making it challenging to transport and install. The anchorage of the device to the building requires additional equipment and may damage architectural finishes. Ultra-Low Forced Vibration Testing (UL-FVT) is a relatively new concept in forced vibration testing that uses portable equipment and a small linear mass shaker to induce a test load at ultra-low amplitudes with resulting accelerations that are imperceptible to occupants. The UL-FVT test of a building can be conducted by a single engineer using equipment with a total cost of less than $15,000 and compact enough to be transported on a handcart [1]. For these reasons, it is the ideal method of structural testing for the remote Point Sur Lighthouse.

The equipment necessary for a UL-FVT test is limited to a signal generator, amplifier, and linear mass shaker for the loading and accelerometer(s), data acquisition device, and laptop computer for the response recording, all shown in Figure 3.2-1. The linear mass shaker and eccentric mass shaker produce load in a similar way but the linear mass shaker exerts its load on the structure through friction at its base instead of mechanical anchorage. The shaker is not limited to only sinusoidal load patterns but is capable of receiving and replicating seismic ground motion signals from the signal generator. The maximum load amplitude that the shaker used in this research can consistently produce is roughly 30 lbs. between the frequencies of 2-20 Hz. The accelerometers used for the tests in this research can measure the response of the building down to a resolution of 1-3 μg, or $1x10^{-6}$ times the acceleration due to gravity.

Figure 3.2-1: UL-FVT Equipment [21]

The UL-FVT method is characterized by four different activities: an initial broad-range ambient vibration test (AVT) used to find likely natural frequencies, a forced vibration test that sweeps through smaller ranges of frequencies to pinpoint the exact natural frequencies identified in the AVT, another forced vibration test that sweeps through smaller ranges of frequencies centered around a natural frequency to determine the frequency's damping ratio, and finally an extended forced vibration test at a particular natural frequency to record the mode shape at steady state vibration. The position of the shaker and accelerometers can have a large effect on the clarity of the results so great care must be taken during both testing and data processing. The shaker should be positioned to maximize the response of the mode of interest but minimize the response of other modes.

The accelerations recorded during the AVT are generated by occupants or equipment in the building and are generally in the range of 5-10 μg. Large HVAC units may generate ambient vibrations of up to 100 μg. The first forced vibration test sweeps through the range of

frequencies centered on the expected natural frequency continuously. In the second forced vibration test, frequencies of interest are determined manually. Frequencies of interest can be identified by their peak accelerations recorded in forced vibration tests, which in large buildings typically range from 20-40 μg when the shaker's excitation frequency is not at the natural frequency but can reach 1000 μg when the shaker's frequency is at the natural frequency.

3.2.2 Theory and Methodology

The basis for any ambient or forced vibration testing method is dynamic amplification, which relates the deformations of a structure due to a statically applied load to the deformations of a structure due to a harmonically applied load of the same amplitude. The amount of dynamic amplification depends on the ratio of the structure's natural frequency to the loading frequency and the damping of the structure. The closer the natural and loading frequencies, the larger the dynamic amplification, but when the loading frequency is significantly larger than the natural frequency, dynamic deformations will be smaller than their corresponding static deformations. Dynamic amplification is useful in an ambient or forced vibration test because it allows for clear identification of natural frequencies and mode shapes of large structures even though the harmonic load amplitude is significantly smaller than the design loads of the building.

The derivation of the dynamic amplification factor begins with the basic equation of motion for a damped structure subjected to a harmonic load and may be adapted for a structure with a single degree of freedom or multiple degrees of freedom. A more complete derivation may be found in Chopra [22] or Ramos [5]. The variables in Equation 3.2-1 represent the following values: m, c, and k are the mass, damping, and stiffness of the structure, respectively,

$\ddot{u}$, $\dot{u}$, and u, are the acceleration, velocity, and displacement functions of the structure, respectively, and p_o is the amplitude of the harmonic load at circular frequency ω.

$$m\ddot{u} + c\dot{u} + ku = p_o \sin(\omega t) \qquad \text{(Equation 3.2-1)}$$

Initial conditions used to solve the differential equation are shown in Equation 3.2-2.

$$u = u(0) \quad \text{and} \quad \dot{u} = \dot{u}(0) \qquad \text{(Equation 3.2-2)}$$

The solution to the differential equation is shown in Equation 3.2-3 and only includes the particular solution since the complementary (transient) solution will gradually decrease to zero.

$$u(t) = C \sin(\omega t) + D \cos(\omega t) \qquad \text{(Equation 3.2-3)}$$

Variables C and D are defined in Equations 3.2-4 and 3.2-5, respectively, where ζ is the damping ratio and ω_n is the natural circular frequency of the structure.

$$C = \frac{p_o}{k} \frac{1 - (\omega/\omega_n)^2}{[1 - (\omega/\omega_n)^2]^2 + [2\zeta(\omega/\omega_n)]^2} \qquad \text{(Equation 3.2-4)}$$

$$D = \frac{p_o}{k} \frac{-2\zeta(\omega/\omega_n)}{[1 - (\omega/\omega_n)^2]^2 + [2\zeta(\omega/\omega_n)]^2} \qquad \text{(Equation 3.2-5)}$$

Rewriting Equation 3.2-3 and substituting in C and D gives Equations 3.2-6, displacement as function of time. Double differentiation of Equation 3.2-6 yields Equation 3.2-7, acceleration as a function of time.

$$u(t) = \frac{p_o}{k} R_d \sin(\omega t - \phi) \qquad \text{(Equation 3.2-6)}$$

$$\ddot{u}(t) = -\frac{p_o}{m} R_a \sin(\omega t - \phi) \qquad \text{(Equation 3.2-7)}$$

The deformation response factor R_d , defined in Equation 3.2-8, relates the maximum static deformation to the maximum dynamic deformation, while the acceleration response factor R_a ,

defined in Equation 3.2-9, is the acceleration equivalent to R_d. Plots of the deformation and acceleration response factors versus frequency ratio ω/ω_n are shown in Figure 3.2-2.

$$R_d = \frac{1}{\sqrt{[1-(\omega/\omega_n)^2]^2 + [2\zeta(\omega/\omega_n)]^2}} \qquad \text{(Equation 3.2-8)}$$

$$R_a = (\omega/\omega_n)^2 R_d \qquad \text{(Equation 3.2-9)}$$

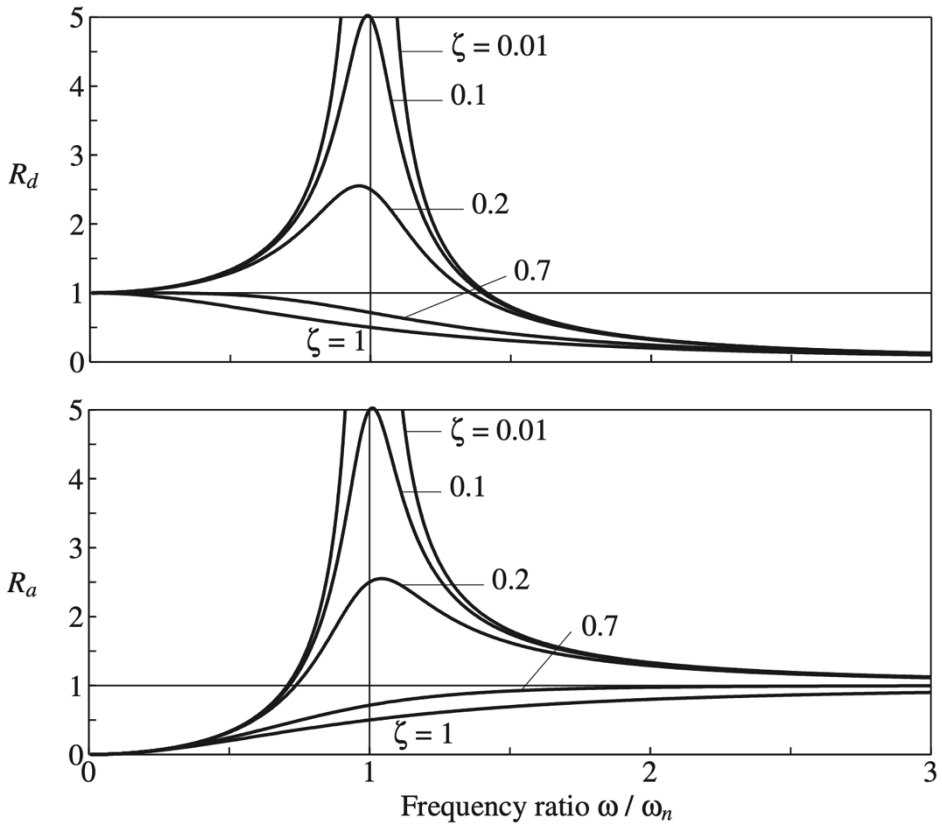

Figure 3.2-2: Response Factors R_d and R_a vs. Frequency Ratio ω/ω_n [22]

The response of a structure with low damping increases dramatically when excited close to the structure's natural frequency. The expected acceleration response factor for the Point Sur Lighthouse is roughly 16 because of its low average damping of 3.13%. The sharp increase in response due to dynamic amplification allows for clear identification of a resonant frequency on

a plot of acceleration amplitude versus excitation frequency. This frequency-response curve is a useful format for data recording in forced vibration testing. A resonant frequency on a frequency-response curve is effectively equal to the natural frequency for small damping ratios. Before the acceleration response data from UL-FVT may be plotted against excitation frequency, it must be converted from the time domain to the frequency domain. This conversion is done continuously and in real time during testing by the laptop's software using a fast Fourier transform (FFT). A graphical representation of the FFT process is shown in Figure 3.2-3.

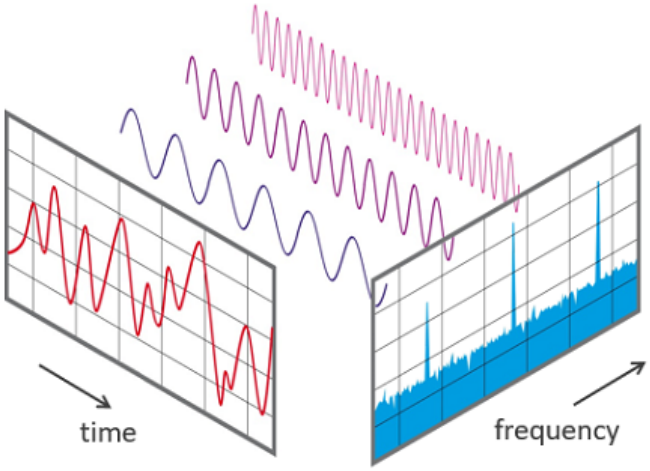

Figure 3.2-3: Graphical Representation of a Fast Fourier Transform [23]

The damping for the structure at a certain natural frequency can be found using the frequency-response curve and half-power bandwidth method. The half-power bandwidth method is useful in a forced vibration testing because the value of the applied force is not required in the calculation. The damping ratio ζ as a percent of the critical damping can be calculated using Equation 3.2-10, where f_n is the natural frequency and f_a and f_b are the frequencies with a

response amplitude of $1/\sqrt{2}$ of the natural frequency's response amplitude. A graphical representation of this calculation is shown in Figure 3.2-4.

$$\zeta = \frac{f_a - f_b}{2f_n} \times 100 \qquad \text{(Equation 3.2-10)}$$

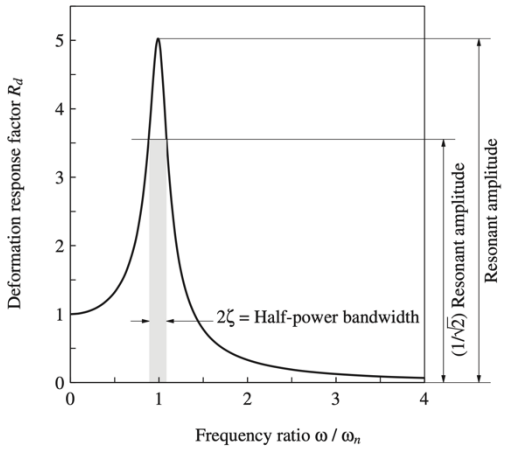

Figure 3.2-4: Half-Power Bandwidth on Frequency-Response Curve [22]

The variable ϕ in Equations 3.2-6 and 3.2-7 represents the phase angle or phase lag of the response with respect to the loading, and it is calculated using Equation 3.2-11. The phase angle of a mode defines how long the maximum response lags behind the maximum force amplitude, and it may not be ignored in forced vibration testing when modes have closely spaced frequencies such as in the Point Sur Lighthouse. Exciting a structure at one of its natural frequencies when its other natural frequencies have a similar value (especially when they are below the frequency of interest), could lead to an "impure" mode shape that is made up of not only the mode shape of the natural frequency of interest but also the mode shapes of lower natural frequencies. A low enough damping ratio would theoretically minimize the interference of the phase angle, but sufficient experience with forced vibration testing in the real world shows

that this is not always the case. A plot of phase angle versus frequency ratio ω/ω_n is shown in Figure 3.2-5.

$$\phi = tan^{-1}\left(\frac{2\zeta(\omega/\omega_n)}{1-(\omega/\omega_n)^2}\right) \qquad \text{(Equation 3.2-11)}$$

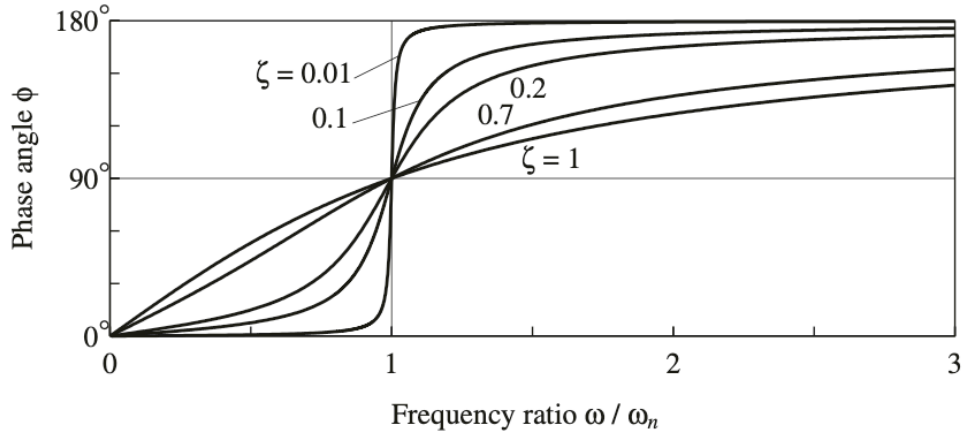

Figure 3.2-5: Phase Angle ϕ vs. Frequency Ratio ω/ω_n [22]

One practical method of reducing the phase angle and interference from other mode shapes on the mode shape of interest is by fine-tuning the placement of the shaker within the building. The best shaker position for a natural frequency is one that mimics the mode shape of that natural frequency. Shaker placement is known to alter results considerably and proves difficult in buildings with irregular floorplans or lateral system configurations [21]. The available areas for shaker placement in the Point Sur Lighthouse are limited to inside the tower, making it difficult to single out the mode shape and natural frequency of only one of the modes whose main response occurs in the tower.

The response of a structure at a certain natural frequency may be maximized by mimicking the mode shape of that natural frequency because the response of a structure in real

space is proportional to the response of the structure in modal space. Equations 3.2-12 and 3.2-13 are the modal equivalents of Equations 3.2-6 and 3.2-7, modal displacement and acceleration of mode *n* due to a harmonic load as functions of time.

$$q_n(t) = \frac{P_n}{K_n} R_d \, sin(\omega t - \phi_n) \qquad \text{(Equation 3.2-12)}$$

$$\ddot{q}_n(t) = -\frac{P_n}{M_n} R_a \, sin(\omega t - \phi_n) \qquad \text{(Equation 3.2-13)}$$

The mass *m*, stiffness *k*, and harmonic load $p(t)$ in real space may be related to equivalent terms in modal space M_n , K_n , and $P_n(t)$ through Φ_n and Φ_n^T, the mode shape vector of mode *n*. These relationships are shown in Equation 3.2-14, 3.2-15, and 3.2-16. It should be noted that ϕ_n represents the phase angle of mode *n* while Φ_n represents the mode shape vector of mode *n*.

$$M_n = \Phi_n^T \, m \, \Phi_n \qquad \text{(Equation 3.2-14)}$$

$$K_n = \Phi_n^T \, k \, \Phi_n \qquad \text{(Equation 3.2-15)}$$

$$P_n(t) = \Phi_n^T \, p(t) \qquad \text{(Equation 3.2-16)}$$

Equations 3.2-17 and 3.2-18 are the final expressions relating real and modal displacements and accelerations $q(t)$ and $\ddot{q}(t)$, where Φ is the mode shape matrix of the system.

$$u(t) = \Phi q(t) \qquad \text{(Equation 3.2-17)}$$

$$\ddot{u}(t) = \Phi \ddot{q}(t) \qquad \text{(Equation 3.2-18)}$$

Further applications of these relationships are discussed in Section 7.3.4 and may be explored in future research.

3.2.3 Example Research – Piedras Blancas

The Piedras Blancas Lighthouse is another historic lighthouse located approximately 65 miles south of the Point Sur Lighthouse on California State Route 1. It began operation in 1875

and is also listed on the National Register of Historic Places. Like Point Sur, this lighthouse is unreinforced brick masonry and was evaluated according to a similar combination of forced vibration testing and finite element computer modeling in order to determine the best course of action for retrofitting the structure. This research used a similar procedure to evaluate the Point Sur Lighthouse.

The UL-FVT test setup for the Piedras Blancas Lighthouse included a number of accelerometers along the lighthouse's 70′ height and a linear mass shaker placed on the concrete slab that caps the tower. The same UL-FVT method described in Section 3.2.1 was used to test the lighthouse, starting with an ambient vibration test that yielded accelerations in the range of 20-30 μg and then a forced vibration test that yielded resonant accelerations in the range of 3000 μg. The large increase in response at resonance can be attributed to very low damping. The fundamental period (frequency) of the structure was found to be roughly 0.20 seconds (5 Hz).

The data collected during UL-FVT was used to validate the results of a finite element computational model created to explore possible retrofit options. The model's fundamental period was approximately 0.15 seconds and normalized mode shapes corresponded closely to the mode shapes found experimentally. The accuracy of the dynamic behavior simulated in the finite element model will give confidence to the future retrofit designers that any retrofit design can be realistically modeled before it is installed. Adding possible retrofit components to the finite element model of the lighthouse will allow designers to check the strength capacity of the component against seismic loading demands and also determine its effects on the dynamic behavior of the building, which is much more difficult to do using building code procedures [7].

3.2.4 Test Setup

The UL-FVT test on the Point Sur Lighthouse was conducted in August 2018 and data was recorded at six locations of interest around the building. Each location of interest was equipped with two accelerometers oriented in orthogonal directions and aligned in the local north-south and east-west directions, parallel and perpendicular to the walls of the lighthouse. The lighthouse is oriented so that true "global" north is roughly 45° west of what will be called "local" north and specified directions will be based on local north for clarity. The approximate locations of the accelerometers are shown in plan, south elevation, and isometric view in Figure 3.2-5. The approximate accelerometer locations given are within a margin of accuracy that will not significantly affect the quality of the data. Accelerometer A was placed on the floor of the watch room, accelerometers B, C, and D were placed at the top of the walls oriented in the north-south direction on the interior of the building, accelerometer E was placed on top of the wall oriented in the north-south direction on the exterior of the building, and accelerometer F was placed in the north window sill of the intermediate landing in the tower. The shaker was placed in the watch room at the same location as accelerometer A and oriented in the local north-south or east-west direction as well. The available areas for shaker placement in the Point Sur Lighthouse were limited to the intermediate landing in the tower, watch room floor, and lantern room catwalk. The intermediate landing in the tower was not used because the connections to the surrounding masonry would not effectively transfer the shaker's load and the lantern room catwalk was not used because the shaker could not be placed at the center of the tower's section. The best location for the shaker was therefore the watch room floor.

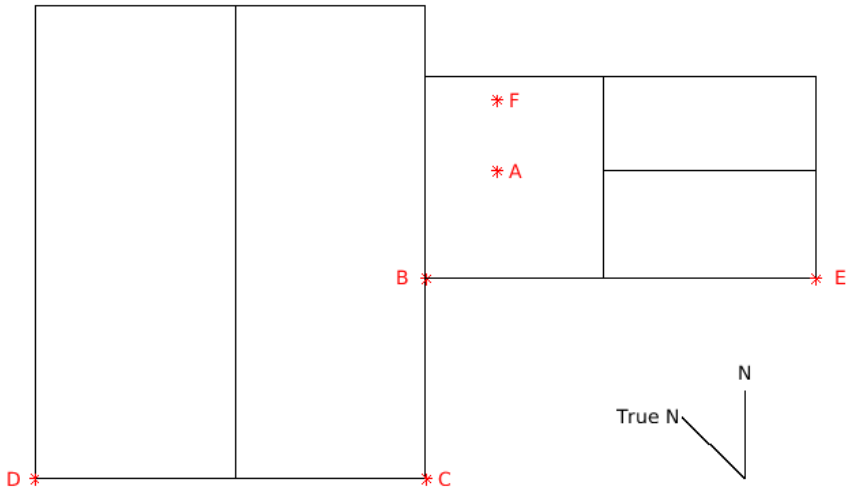

(a)

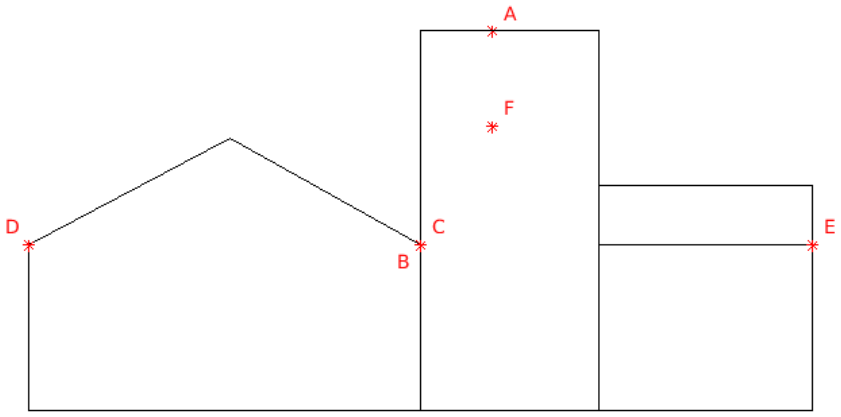

(b)

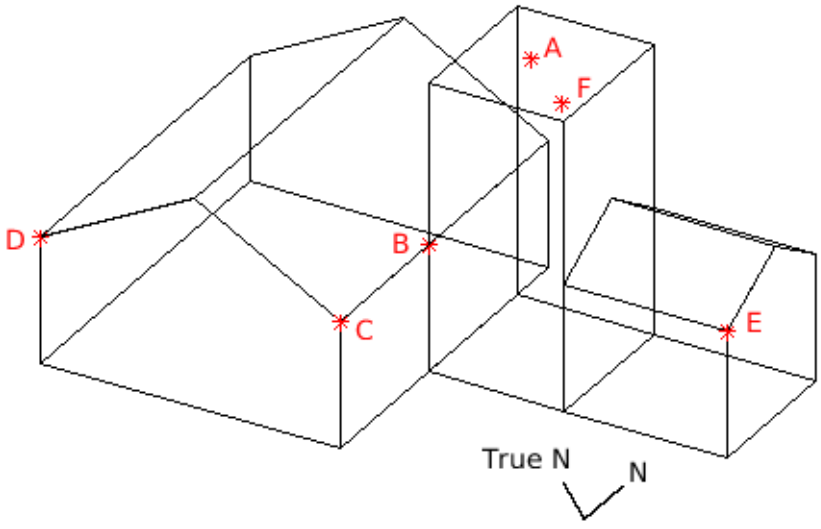

(c)

Figure 3.2-6: Accelerometer Locations in (a) Plan, (b) South Elevation, and (c) Isometric View

3.3 Ultra-Low Forced Vibration Testing Results

Even though the ultra-low forced vibration data was limited, it was still used to draw a variety of conclusions about the lighthouse's stiffness and strength. The frequency sweep data was used to determine natural frequencies and damping characteristics, which are related to the stiffness of the lighthouse. The relative accelerations recorded at each location were used to compare the stiffnesses of the walls both in-plane and out-of-plane, as well as characterize the connections between key system components.

3.3.1 Natural Frequencies

A preliminary sweep was performed to determine estimates for the natural frequencies in the north-south and east-west directions. Next, a more precise frequency sweep was performed at 0.10 Hz increments centered around the estimated natural frequency from the preliminary sweep that moved slowly outward until sufficient data was recorded to determine the damping of the system. The sweep data for the east-west and north-south directions is shown as a frequency-response curve in Figures 3.3-1 and 3.3-2, respectively. The natural frequency in the east-west direction was found to be 9.7 Hz and the natural frequency in the north-south direction was found to be 9.6 Hz, identified from the peaks of their respective frequency-response curves. The natural frequency and period data for each direction is summarized below in Table 3.3-1.

Table 3.3-1: UL-FVT Natural Frequencies and Periods

Direction	Freq. (Hz)	Period (s)
E/W	9.70	0.103
N/S	9.60	0.104

The proximity of the natural frequencies can potentially produce a number of errors when trying to understand the true dynamic behavior of the lighthouse. Using the mass shaker to induce a load at either one of the natural frequencies in either of the orthogonal directions would excite both modes to a similar extent, leading to "impure" mode shapes for both natural frequencies. Adjusting the position of the shaker to maximize the response of the mode of interest and minimize the response of other modes is often possible in typical buildings but is exceptionally difficult in buildings such as the Point Sur Lighthouse where there are limited options for the placement of the shaker. The frequency-response curve for the east-west direction is fairly smooth and has a much clearer peak than the curve for the north-south direction. The irregularities in the north-south frequency-response curve could be contributions from other modes with frequencies around 9.40 Hz and 9.90 Hz.

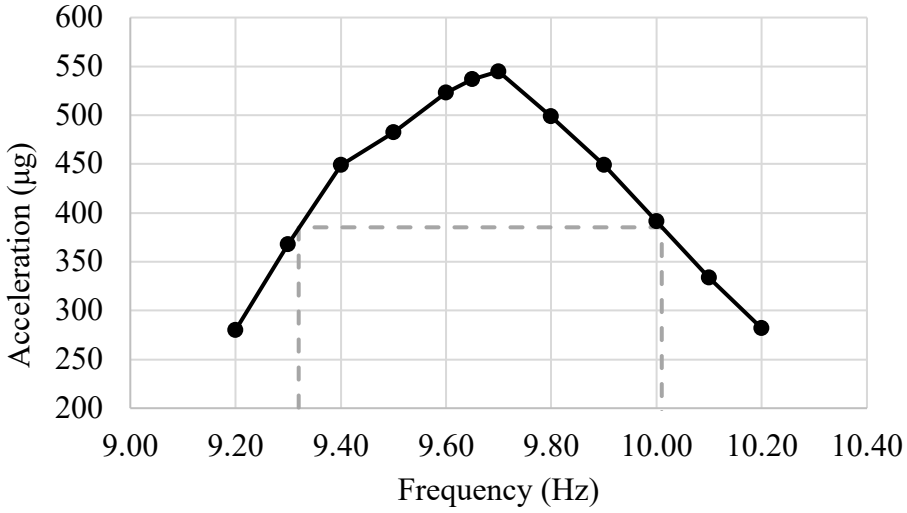

Figure 3.3-1: UL-FVT Frequency Sweep E/W

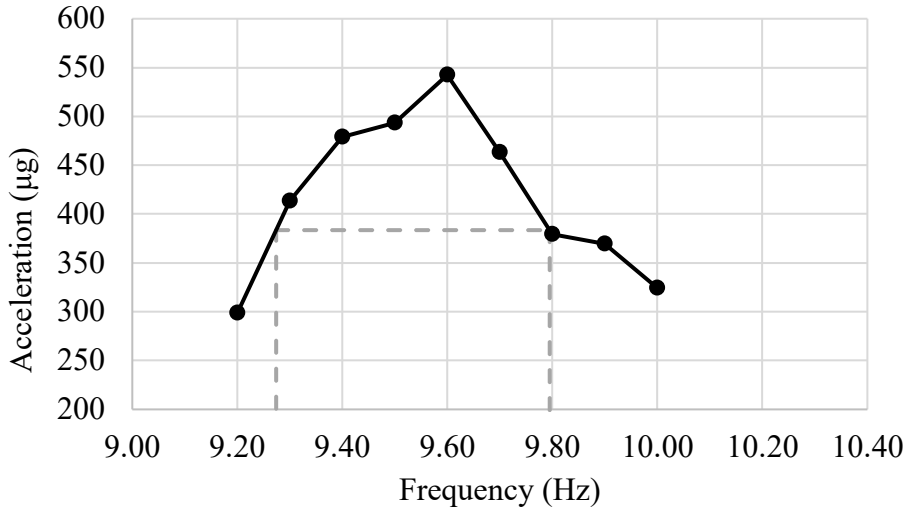

Figure 3.3-2: UL-FVT Frequency Sweep N/S

3.3.2 Damping

The damping for the natural frequencies in each direction was calculated using the data from the frequency-response curve and the half-power bandwidth method. The frequencies used to calculate the damping are represented by the dashed lines in Figures 3.3-1 and 3.3-2 and the results for each natural frequency as a percentage of critical damping are given in Table 3.3-1. An average damping value of 3.13% was used for all structural analyses in the finite element model for simplicity and limitations in the program. The effects of the small simple floorplan of the lighthouse and heavy masonry construction balance to a damping ratio of about what was expected. The difference in damping ratios between the two natural frequencies could be the result of differences in stiffness of the tower and masonry walls in-plane and out-of-plane, especially where the tower section adjoins the east wall of the fog room.

Table 3.3-2: UL-FVT Damping

Direction	Freq. (Hz)	Period (s)	Damping (%)
E/W	9.70	0.103	3.55
N/S	9.60	0.104	2.71

3.3.3 Mode Shapes

The acceleration data from the six accelerometer locations obtained from the UL-FVT test gave a good description of the dynamic response of the lighthouse as a whole but it was difficult to tell if the total response consisted of the response of the mode of interest only or if there were contributions from other modes as well. Either way, the displacement, velocity, and acceleration responses at any one location are all proportional and related by the natural circular frequency. This proportional relationship allowed the acceleration data recorded in the test to be plotted directly as displacement data for easy visualization. The accelerations recorded at locations B, C, D, and E are plotted as points, each displaced by their own north-south and east-west components and connected with straight lines. The accelerations recorded at locations A and F are plotted as the entire circle of the inner surface of the tower section displaced by their own north-south and east-west components. When shaking the lighthouse in either the east-west direction or north-south direction, the largest response occurred at location A, the location of the shaker, and the smallest response occurred at location D. Even though the placement of the shaker should minimize the response at location A perpendicular to the direction of shaking, there was still a small response in the perpendicular direction, perhaps due the mode shape itself or the irregular T-shape of the lighthouse in plan.

When shaking the lighthouse in the east-west direction, locations A and F at different heights in the tower had similar proportions of north-south and east-west response, indicating that there was only a small amount of twist or bend in the tower. The twist in the tower may be because of eccentric stiffness in the tower, but more likely it was because the modal axis and the shaker's axis were not aligned. The east-west response was much larger than the north-south response at locations A and F. Location B had the next largest response after locations A and F, and its response consisted of roughly equal east-west and north-south components. The response at location C also had roughly equal east-west and north-south components, though the response was smaller than the response at location B. Locations D and E had the smallest response and a majority of their response was in the north-south direction despite the shaking in the east-west direction. The relative responses in the east-west and north-south directions due to shaking in the east-west direction are given in Table 3.3-2, where all the response components were normalized by the largest response component. The mode shape is shown graphically in Figure 3.3-3.

Table 3.3-3: UL-FVT Mode Shape E/W

Accel. Location	E/W	N/S
A	1.00	0.32
B	0.22	0.25
C	0.18	0.13
D	0.04	0.14
E	0.06	0.18
F	0.59	0.21

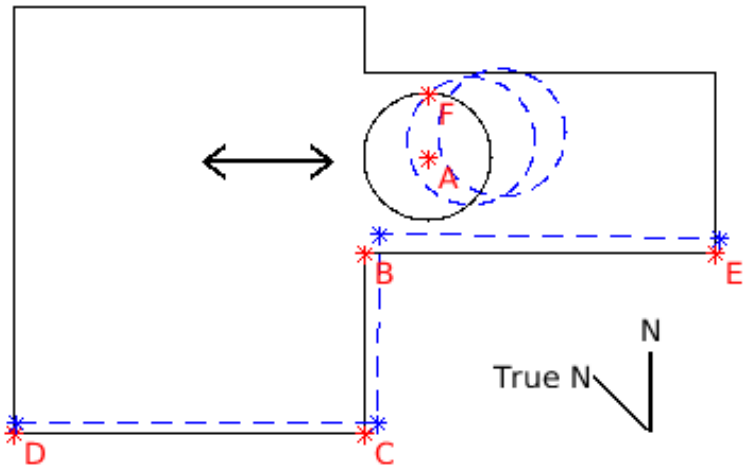

Figure 3.3-3: UL-FVT Mode Shape E/W

The small response at locations D, and E was evidence of a weak and discontinuous diaphragm. The shaker excited the tower into the fog room, bent the adjoining wall, and produced a similar response at B and C. A stiffer diaphragm in the fog room would likely produce a response at location D that is closer to the response at locations B and C because the diaphragm would be able to transfer the load of the intruding tower to the opposite side of the fog room. The discontinuity of the load path across the fog room from the tower to location D in terms of both strength and stiffness was believed to be the largest factor in the small response at location D. Although the trusses span east-west, they were ineffective in transferring tensile east-west loads between the walls of the fog room because of the inadequate lateral strength of their connections. An increase in the strength and stiffness of the roof diaphragm would also aid in transferring full inertial loads of the connected elements in the event of strong ground motions.

When shaking the lighthouse in the north-south direction, locations A and F at different heights in the tower again had similar but not equal proportions of north-south and east-west response, also indicating that there is a small amount of twist or bend in the tower, attributed to

the misalignment of the modal axis and shaker axis. The north-south response was much larger than the east-west response at locations A and F as well. Locations B and E had the next largest response after locations A and F, and their response consisted of roughly equal proportions of east-west and north-south components, the north-south being the larger of the two. The response at location C was similarly proportioned to the responses at locations B and E, though the north-south response was slightly less. Location D had the smallest response of all the locations and a majority of its response was again in the north-south direction. The relative responses in the east-west and north-south directions from shaking in the east-west direction are given in Table 3.3-3, where all the response components were normalized by the largest response component. A graphical representation of the mode shape is shown in Figure 3.3-4.

Table 3.3-4: UL-FVT Mode Shape N/S

Accel. Location	E/W	N/S
A	0.25	1.00
B	0.11	0.56
C	0.09	0.26
D	0.02	0.24
E	0.07	0.53
F	0.16	0.56

In general, shaking in the north-south direction produced a much larger response at locations outside of the tower than shaking in the east-west direction. The response of the lighthouse as a whole was also much more cohesive, since the response at each location is predominantly in the north-south direction. Locations C and D responded in a similar way as did locations B and E. One of the main reasons for this behavior is the difference in the in-plane and

out-of-plane stiffnesses for the walls of the lighthouse. A weak and discontinuous diaphragm may also be a reason. The response at location B was more closely related to the response at location C due to the higher in-plane stiffness of the wall shared between the two locations. The response at location D was more closely related to the response at location C because the out-of-plane behavior of the wall shared between the two locations is more effective than the diaphragm at transferring loads.

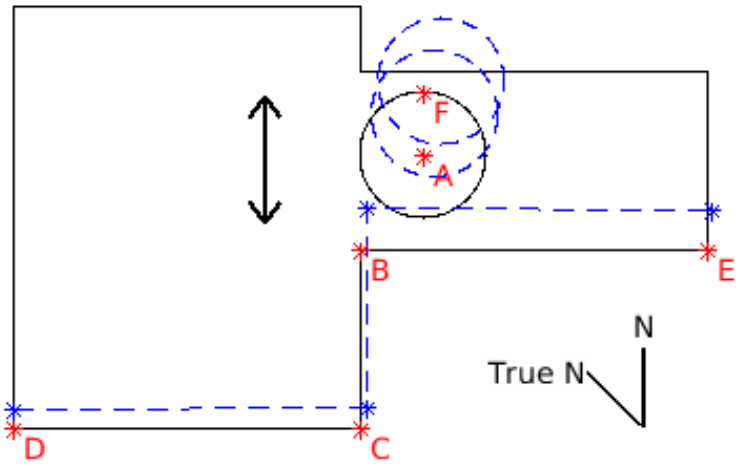

Figure 3.3-4: UL-FVT Mode Shape N/S

3.4 ASCE 41-17 Evaluations

The tiered screening procedures found in ASCE 41-17 are a systematic way of identifying potential structural deficiencies in a building and developing retrofit measures in order to bring the building into compliance with a selected performance objective. The scope of a Tier 1 screening only includes identification of potential deficiencies for a basic building of any type as well as deficiencies specific to the building type, for example URM. A Tier 2 evaluation takes the potential deficiencies identified in the Tier 1 screening and develops retrofit components or systems that will bring the deficient areas of the building within the acceptable

limits set by the selected performance objective. A Tier 3 evaluation must be performed when a Tier 2 evaluation is not permitted based on performance objective requirements or building characteristics, and it includes a more thorough analysis of the building as a whole with new retrofit measures as well as construction documents that describe in detail the proposed retrofit measures.

The tiered screening procedures were used to evaluate the lighthouse according to the Basic Performance Objective for Existing Buildings defined in ASCE 41-17 Chapter 2. This objective defines the level of performance that the structure must meet for each of the seismic events considered, the two Basic Safety Earthquakes. Basic Safety Earthquake-1 (Existing) has a probability of exceedance of 20% in 50 years and a 225-year return period and the Basic Safety Earthquake-2 (Existing) has a probability of exceedance of 5% in 50 years and a 975-year return period. The structural performance level that the lighthouse must meet after the Basic Safety Earthquake-1 (Existing) is life safety, defined as a "damage state in which a structure has damaged components but still retains a margin of safety against the onset of partial or total collapse." The structural performance level that the lighthouse must meet after the Basic Safety Earthquake-2 (Existing) is collapse prevention, defined as a "damage state in which a structure has damaged components and continues to support gravity loads but retains no margin against collapse" [6].

The Tier 1 screening identified the following potential deficiencies in the lighthouse: The lighthouse does not contain a complete and well-defined load path that would serve to transfer inertial forces to the foundation. A torsional irregularity may be present because the estimated distance between the center of mass and the center of rigidity is more than 20% of the lighthouse

width in either of the plan dimensions. The lighthouse may be subject to overturning since the base/height ratio exceeds the allowable limit defined by the seismicity of its location. In addition, there are no ties from the walls into the foundation that might be used to resist seismic forces. The shear stress in the unreinforced masonry shear walls may exceed the allowable limit defined by quick check procedures. Exterior unreinforced masonry walls are dependent on the roof diaphragm for lateral support but are not anchored out-of-plane at the roof level. A number of structural concerns were identified upon investigation of the roof diaphragms, including improper connectivity to the masonry walls, an absence of continuous cross ties, and straight-sheathed diaphragms with large spans and aspect ratios.

The first stage of retrofit recommendations was centered around strengthening the roof diaphragms and their connections to the walls. The walls in the fog room, and to a lesser extent, the walls in the radio room, require additional restraint out-of-plane along their top edges. One of the most straightforward methods of providing out-of-plane restraint is by anchoring them to the roof diaphragm using structural holdowns like the ones shown in Figure 3.4-1. Improvements to the connections between the roof trusses and the masonry walls will also provide significant out-of-plane restraint. Structural holdowns are designed to provide a strong connection between wood members and concrete or masonry using large anchor bolts. However, providing a better connection between the walls and roof will increase the inertial loads that are directed to the roof diaphragm, so the roof diaphragm itself must also be strengthened. One way to increase the strength of the roof diaphragm is by adding blocking at regular intervals and straps between larger members. Straps are designed to transfer tension loads across discontinuities in a tension load path, for example between larger framing members in the lighthouse where the nature of the

connection between members and the outer walls are unknown. A common type of strap is shown in Figure 3.4-1. The roofing in the lighthouse may need to be removed to install the straps, in which case structural panels could also be installed to supplement the straight sheathing already present in the roof diaphragm.

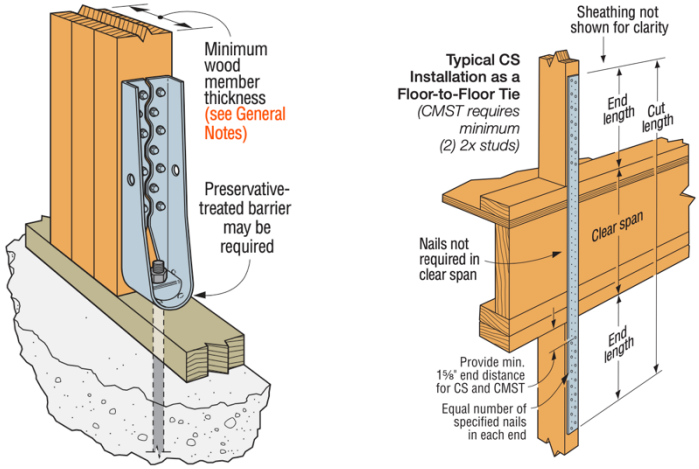

(a) (b)

Figure 3.4-1: Example a) Holdown and b) Strap for Connection Strengthening [24]

Other locations in the lighthouse that would benefit from strengthened connections are the lantern room and interior of the tower. Neither the type nor strength of the connection between the lantern and watch rooms is known and regularly spaced anchorage may be added as a precaution. Historic sections of the lighthouse tower show a small gap between the outer sandstone masonry and inner brick masonry, most likely for ventilation. Regularly spaced anchorage in both directions may also be installed to bridge the gap between masonry types.

The next stage of retrofit recommendations included the addition of structural members in order to resolve the deficiencies identified in the tiered screenings. The first option for an additional member was a strong-back, which is usually a steel member anchored directly to an

unreinforced masonry wall and spans either vertically or horizontally. If the strong-back spans vertically, it is anchored into the foundation at the base of the wall and tied into the roof diaphragm at the top of the wall. If the strong-back spans horizontally, it may span between vertical strong-backs or adjacent walls. Strong-backs are a common retrofit solution for increasing the out-of-plane strength and stiffness of deficient URM walls and strong-backs are simple to install.

Another alternative for the next retrofit stage was a bundle of rebar or post-tensioning cables in cored shafts inside the walls. The bundles may span vertically or horizontally, and bundles of post-tensioned cables have been shown to be successful at mitigating URM deficiencies during large seismic events when spanning in either direction [25]. However, the option of adding rebar or post-tensioned cables was not considered a feasible solution because the required coring into the walls is labor intensive and expensive, and extreme caution must be taken when considering any disturbances to the foundation. The following section describes the retrofit schemes that were considered.

3.5 Retrofit Schemes

The following retrofit schemes were developed to mitigate some of the deficiencies present in the lighthouse while also providing various options for secondary considerations including the costs of hardware and labor, architectural intrusion, and the need for further engineering design. There was no one retrofit scheme developed that will resolve all individual deficiencies because the retrofit schemes are focused on improving the dynamic behavior of the fog room and lighthouse overall.

3.5.1 Connections Scheme

The first and most basic retrofit scheme developed for this research, designated the "Connections" scheme for reference, involved strengthening the connections between existing components in the lighthouse, namely the connections between the roof diaphragm and the masonry walls. Proper anchorage of the roof trusses was also addressed. While this retrofit scheme did not address all of the deficiencies identified in the ASCE 41-17 screenings, it did include all of the first stage of recommendations and provided significant structural improvements to the lighthouse with minimal expenses for hardware and labor. The Connections scheme also provided minimal intrusion on the architectural character of the lighthouse's interior, which is an important consideration for a historic building. The connection hardware was discreet and the most noticeable change to the lighthouse was the addition of small anchor plates on the exterior of the lighthouse to aid in connection anchorage through the walls.

3.5.2 Strong-Backs Scheme

The next retrofit scheme developed for this research, designated the "Strong-Backs" scheme for reference, included all of the improvements made in the Connections scheme as well as the installation of two large steel strong-backs at each of the gabled walls in the fog room. Though this scheme did not address all of the individual deficiencies identified in the lighthouse, it did begin to include the next stage of recommendations that the Connections scheme did not address. The strong-backs were specifically designed to improve both the strength and stiffness of the masonry walls in order to meet ASCE 41-17 requirements. An initial strong-back design assumed the walls were sufficiently restrained at their top edges, but further investigation revealed that this is not the case and the strong-back design was improved. The Strong-Backs

scheme is shown in plan and elevation in Figure 3.5-1 and intruded on the architectural features more than the Connections scheme due to the presence of full members. The Strong-Backs scheme was more expensive and labor intensive than the Connections scheme, but strong-backs are a common retrofit solution and their installation is simple.

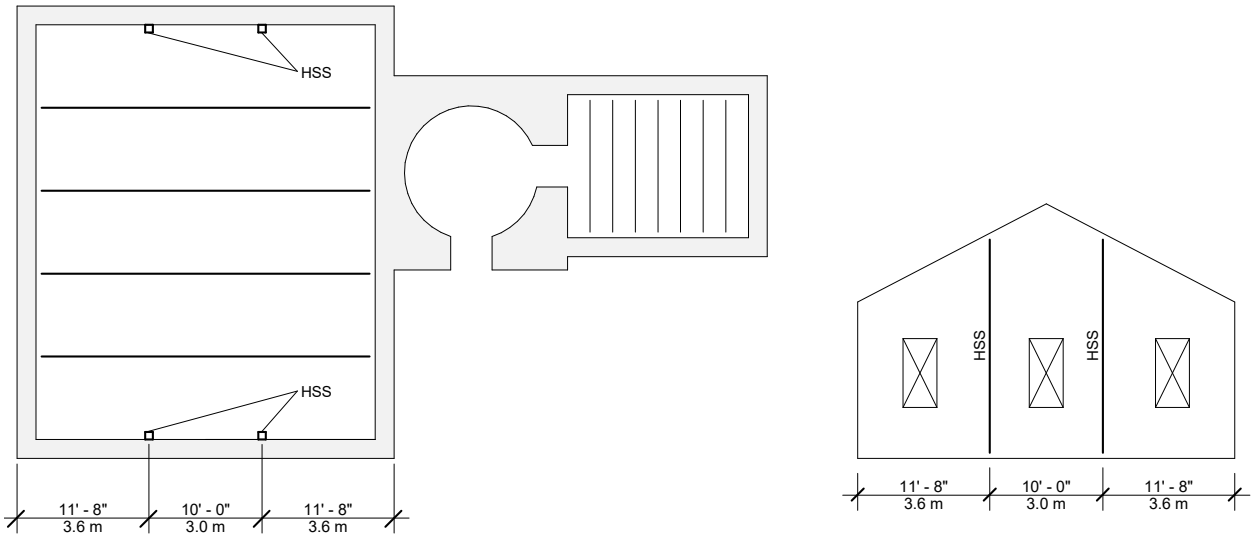

Figure 3.5-1: Strong-Backs Retrofit Scheme Plan and Elevation

3.5.3 Diamond Braces Scheme

Another retrofit scheme developed for this research, called the "Diamond Braces" scheme for reference, included all of the improvements made in the Connections scheme and used steel braces in the planes of the gabled roof to address the deficiencies in the masonry walls. Similar to the Strong-Backs scheme, the Diamond Braces scheme did not address all of the deficiencies in the lighthouse but was expected to significantly improve the deficiencies in the masonry walls in the fog room. The main goal of the diamond braces was to restrain the top edges of the gabled walls in the fog room by connecting them directly to the tower and the perpendicular rectangular walls. The brace size was selected based on the available space above

the roof trusses, shown in Figure 2.4-5, and had sufficient strength for inertial loads from the masonry walls. The main challenge with the Diamond Braces scheme was the anchorage of the braces to the rectangular walls and tower, but this was left to a design professional. The Diamond Braces scheme was much less architecturally intrusive than the Strong-Backs scheme, and it is shown in plan and elevation in Figure 3.5-2. The horizontal member in the elevation view was included to aid in restraining the wall and the anchorage of the braces to the wall.

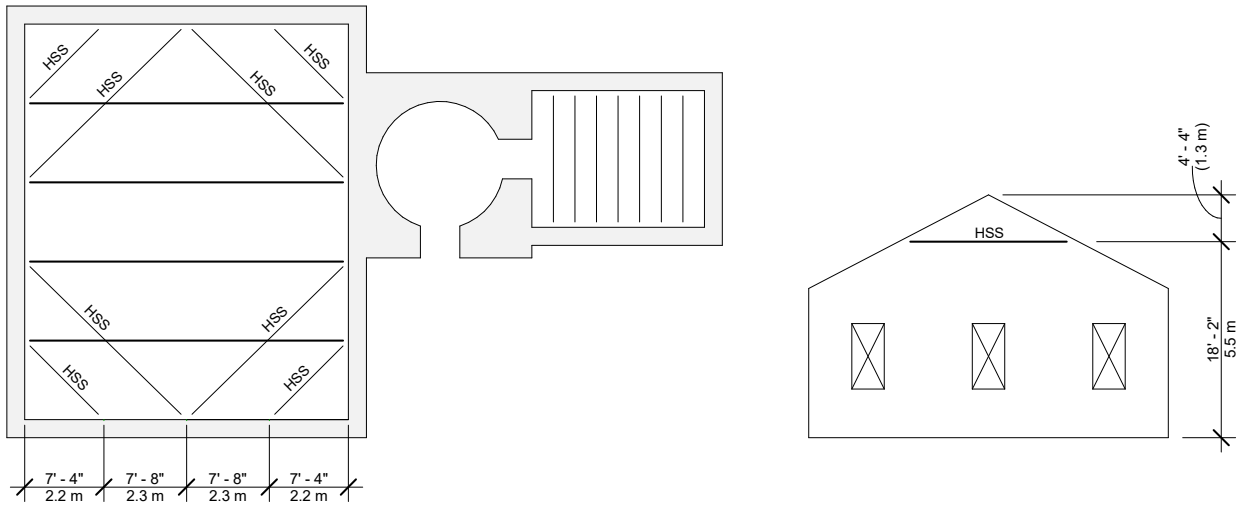

Figure 3.5-2: Diamond Braces Retrofit Scheme Plan and Elevation

3.5.4 Horizontal Strong-Backs Scheme

The next retrofit scheme developed for this research, called the "Horizontal Strong-Backs" scheme for reference and the "HSB" scheme for short, was simply a modified version of the Strong-Backs scheme in that the strong-backs span horizontally instead of vertically. The horizontal strong-backs were designed to meet the same code criteria for the wall deflection as the vertical strong-backs using a single member spanning the entire length of the gabled wall, resulting in a much larger section size. An elevation of the HSB scheme would look similar to

the elevation of the Diamond Brace scheme shown in Figure 3.5-2 except the horizontal member would be located between the top of the windows and the start of the gable's incline. Even though the HSB scheme included only one member per gabled wall, it was arguably more architecturally intrusive due to the much larger member size.

3.5.5 Diamond Braces and Horizontal Strong-Backs Scheme

The final retrofit scheme developed for this research, designated the "Diamond Braces and Horizontal Strong-Backs" scheme for reference and DB+HSB scheme for short, was a combination of the Diamond Braces and Horizontal Strong-Backs schemes. Preliminary studies showed that the benefits of each of the schemes complemented each other well as did the configurations of their members. Early versions of the Diamond Braces scheme were effective at restraining the top edges of the walls while early versions of the Horizontal Strong-Backs scheme were effective at reducing deflection near the mid-height of the wall. The diamond braces were in the planes of the gabled roof and the horizontal member connecting them leaves plenty of space for a horizontal strong-back below it. The DB+HSB scheme was by far the most intrusive on the undecorated interior of the lighthouse but was the superior scheme based on its structural benefits to the lighthouse.

4.0 FINITE ELEMENT MODELING

4.1 Overview

The finite element modeling program used in this research was RISA-3D, a fairly common program in structural engineering offices. One of the main reasons RISA-3D was chosen was due to its easy-to-use interface and because its modeling tools lent themselves better to modeling the irregular tower section and walls than the tools of other common finite element programs. The presentation of the solution results is also compatible with the other computer programs used in this research. However, any finite element program is not without its own set of limitations and some assumptions were made in order to translate the real structure into an acceptable finite element model. Once the basic structure of the lighthouse was modeled, fine-tuning the element mesh and material properties was necessary to make the model a more accurate representation of the real lighthouse. The most important adjustments to the mesh and material properties were made to the sandstone masonry elements since those elements made up the majority of the lighthouse's structure and had the largest effect on the dynamic behavior of the building as a whole. Once a base model of the lighthouse was completed, the retrofit schemes determined earlier were implemented into the model in order to simulate their effects on the dynamic behavior of the lighthouse should they be implemented in real life.

4.2 Purpose

The purpose of creating a finite element model of the Point Sur Lighthouse was to virtually study the dynamic behavior of the lighthouse as it stands and the effects of retrofit components on the lighthouse as if they were implemented. The ultra-low forced vibration testing of the building provided a basis for determining whether or not the results from the

analyses of the finite element base model were valid or whether more work had to be done to better capture the characteristics of the lighthouse. Once the base model was deemed acceptable and its dynamic behavior was within a reasonable margin of the dynamic behavior measured in the real lighthouse, various retrofit solutions were added to the model and their effects studied as well. Closely matching the real lighthouse's characteristics in the finite element model gave reasonable assurance that the retrofit solutions added to the finite element model will have the same effects on the real lighthouse.

4.3 Modeling Process

The modeling process began by placing eight-node "solid" elements in the general layout of the lighthouse using the dimensions shown in Figures 2.3-1 and 2.3-2. Once a basic framework of unreinforced masonry was in place, the solid elements were meshed for proper connectivity. Proper connectivity of elements means elements are joined at their nodes only and no element nodes meet adjacent elements anywhere between nodes. This step is essential in all finite element modeling so that groups of elements behave as they are meant to and the analyses can run properly. Next, the solid elements were meshed to a smaller size by subdividing existing elements in all three directions, X, Y, and Z. This level of meshing was necessary to accurately model the stiffness of the components of the lighthouse, mainly the walls in the fog and radio rooms, but also the tower. Numerical finite element formulations are known for overestimating the stiffnesses of their analytical counterparts, but this can be compensated for by using multiple finite elements to model a single component, known as meshing. Finally, other minor components were added to the model such as trusses in the fog and radio rooms, the lantern room mullions, glass, roof, and roof diaphragms in the fog and radio rooms.

4.3.1 Modeling Limitations

There were modeling limitations due to the fact that some characteristics of the lighthouse are simply unknown, impossible to determine exactly, and some characteristics that are known could not be modeled accurately. Because the condition and exact configuration of the foundation is unknown, modeling the lighthouse began at the ground level. Information about the foundation is impossible to obtain without excavating. The true boundary conditions of the masonry elements at the ground level are most likely somewhere in between pinned and fixed, but solid elements in RISA-3D do not support boundary conditions other than pinned. The strength and ductility of connections between many components is unknown. The exact modulus of elasticity and density of the sandstone and brick masonry is unknown so values were estimated and bounded from outside sources [8,9]. The sandstone masonry in the lighthouse was laid in a random ashlar bond, shown in Figure 2.4-3, but this is impossible to model exactly in RISA-3D due to its complexity and because solid elements would not reach proper connectivity in that pattern. The amount and extent of brick masonry within the sandstone masonry tower is unknown so estimates were made from historic images and plans. These limitations will keep the finite element model from perfectly representing the lighthouse in a number of ways, but the goal of the finite element model is not to create an identical virtual lighthouse. The goal of the finite element model is to accurately reproduce the strength and stiffness characteristics of the lighthouse, and this is still possible despite the limitations of the program.

4.3.2 Modeling Assumptions

A variety of assumptions must be made when creating a model in a finite element program in order to simplify the model and make up for the limitations in information and

modeling capabilities. The connections between members were modeled as pinned or as moment connections. Also, nonlinear material and connection properties are not supported in RISA-3D. Beam elements are typically modeled along their centerlines, which poses a problem at some major element intersections. Short link members were used to connect members whose intersection did not occur at a single point which is not expected to significantly influence the results. In order to achieve proper connectivity of elements around opening in the walls for windows and doors and allow for more efficient modeling, some dimensions of the wall openings were rounded off to align with the wall openings around the lighthouse. The rounded top door into the fog room was also modeled as rectangular. The main benefit of rounding off dimensions was that each of the mesh layers parallel to the ground could be a uniform thickness and at a constant elevation. These assumptions were necessary and useful in finite element modeling because they allow a user to accurately capture the essential characteristics of a structure without a complete knowledge of the structure's construction.

4.4 Model Meshing

4.4.1 Meshing for Connectivity

Proper connectivity between elements is important in finite element modeling because element boundary conditions are an essential part of element formulations. For this reason, model results will be invalid and misleading if elements are not properly joined at their nodes. A finite element can only respond to an action, for example a force, moment, or displacement, if the action is applied at a node. An action that is applied to an element between nodes must be converted to equivalent actions at the nodes. Proper connectivity of elements means elements are joined at their nodes only and no element nodes meet adjacent elements anywhere between

nodes. Meshing elements in the finite element modeling process is also important so that analyses can run quickly and smoothly without errors.

The process of meshing elements to achieve proper connectivity in the lighthouse finite element model was most applicable to the solid elements that make up the walls and tower section. The gabled walls, intersections of walls, and openings for doors and windows required careful attention to make sure that elements were properly connected while also retaining an accurate representation of the lighthouse. A preliminary mesh of a gabled test wall that contains the minimum number of elements to capture the openings and gabled shape is shown in Figure 4.4-1. Solid elements are marked with a "+" and one of the many improper intersections between elements is bolded in red. The trapezoidal element above the intersection and the rectangular element below are not properly joined because the rectangular element's upper left node meets the trapezoidal element between its bottom two nodes.

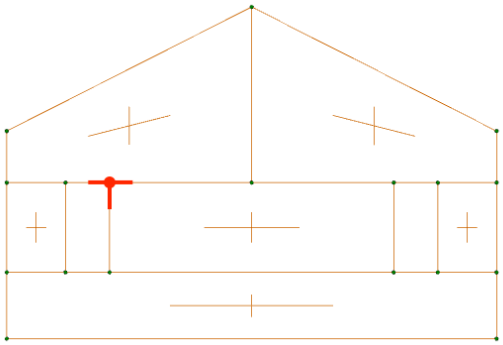

Figure 4.4-1: Improper Connection of Solid Elements

The same wall is shown in Figure 4.4-2 with a proper mesh for connectivity for all special features of the wall, namely the windows and gabled shape. The wall has the minimum number of solid elements needed to model the special features and achieve proper connectivity, corresponding to the maximum mesh size for flexibility.

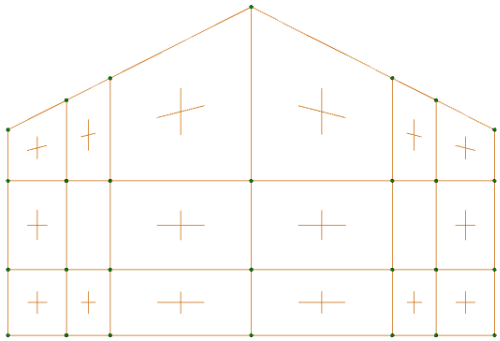

Figure 4.4-2: Proper Connection of Solid Elements

4.4.2 Meshing for Flexibility

Accurate modeling of a component or structure's stiffness in a finite element program is important because deflections and modal properties are largely based on stiffness and are used heavily in design. It is common for numerical finite element formulations to result in overestimating the stiffnesses of their analytical counterparts which can lead to lower deflections and higher natural frequencies. When comparing deflections in a structure to code-allowed limits, a higher stiffness can incorrectly show that the structure is acceptable. The two best ways to decrease the stiffness of a finite element are by changing the element's formulation or by subdividing the element into multiple smaller elements. Changing an element's formulation is usually impossible in finite element programs so the only practical way to decrease stiffness is to increase the number of elements used to model a building component.

Once again, the process of meshing elements to achieve reasonable flexibility in the lighthouse finite element model was most applicable to the solid elements that make up the walls and tower. Even though a smaller element size, referred to as "mesh size", is generally more accurate to the real component or structure, a balance between accuracy and usability was considered when subdividing the solid elements in the lighthouse. Smaller elements represented

the true stiffness of the lighthouse better, but more elements slowed the computer's graphics and computational abilities. The mesh size of the test wall modeled in the previous section represents the maximum mesh size that captures proper meshing for connectivity. Figure 4.4-3 shows the same test wall with four other levels of mesh size, each labeled with the average dimension of the solid elements that make up the wall.

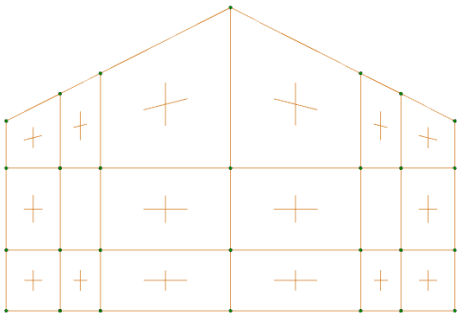

Maximum Mesh Size

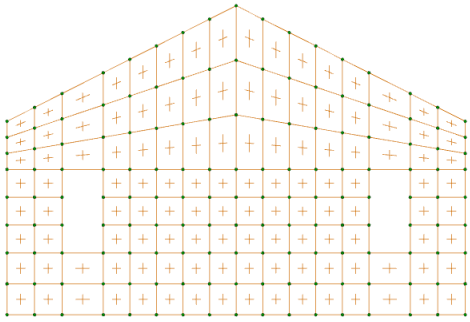

2′ Mesh Size

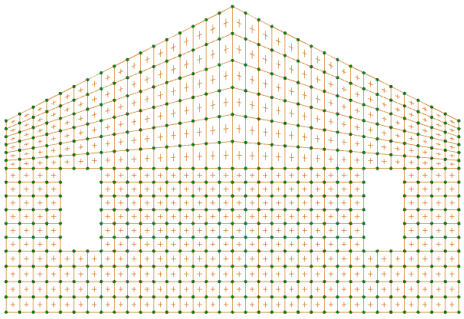

1′ Mesh Size

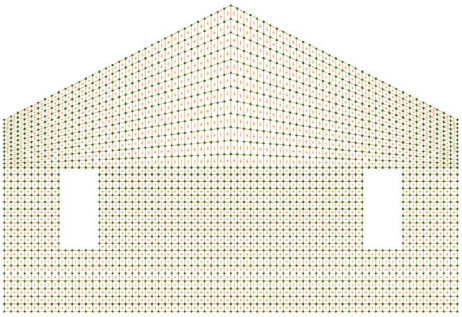

6″ Mesh Size

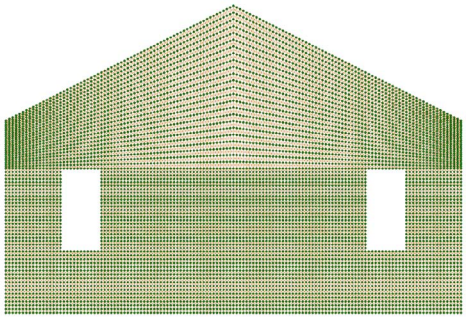

3″ Mesh Size

Figure 4.4-3: Mesh Sizes for a Test Wall

An analysis of the test wall with each of the mesh sizes was run and the results are summarized in Table 4.4-1. Decreasing the mesh size of the wall just one level represented a 36% drop in natural frequency and a 3.5% increase in mass participation. The natural frequency is an indicator of the wall's stiffness and the mass participation is an indicator of a mode's contribution to the dynamic response. Further decreases in mesh size allowed the modal properties to converge on a value at the expense of adding a very large number of elements to the model. The mesh size with the best combination of accuracy and usability and the one used in the lighthouse model was 1' because its natural frequency and mass participation values were close to those of the 3" mesh size but with a fraction of the elements.

Table 4.4-1: Effects of Mesh Density on Natural Frequencies of a Test Wall

Mesh Size	# of Solids	Freq. (Hz)	Period (s)	MP (%)
Max	32	20.6	0.049	44.4
2'	244	13.2	0.076	47.9
1'	1016	11.6	0.086	48.9
6"	4064	11.1	0.090	49.1
3"	32512	11.0	0.091	49.2

4.4.3 Final Mesh

The final mesh configuration for the entire lighthouse with the meshing for both connectivity and flexibility is shown in plan in Figure 4.4-4. The best aspect ratio for a solid element's length, width, and height is 1:1:1, and most solid elements in the model were rectangular in plan except for those in the tower. The elements in the tower were not rectangular in order to integrate the circular inner section of the tower with the rectangular outer section, but they were modeled to be as rectangular as possible. Another constraint placed on the modeling of the elements in the tower was the inclusion of the brick masonry. A roughly 12″ thick layer of

unreinforced brick masonry lines the circular inner section of the tower and was modeled in the lighthouse as accurately as possible.

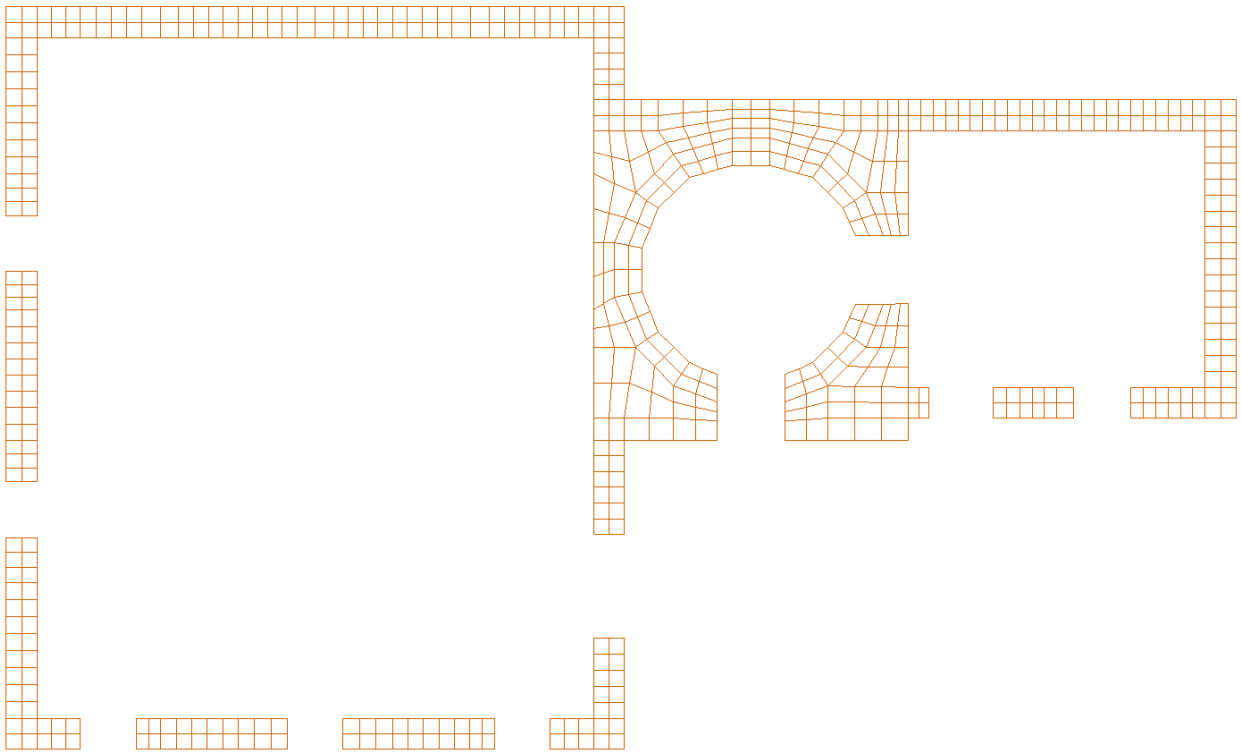

Figure 4.4-4: Final Finite Element Model Mesh

4.5 Element Properties

4.5.1 Sandstone Masonry

Unreinforced sandstone masonry makes up the majority of the Point Sur Lighthouse's mass, so it was crucial to model its material properties accurately. The unreinforced nature of the sandstone masonry construction also accounts for a large portion of the structural deficiencies present in the lighthouse. The most important material property of the sandstone masonry in the finite element model was its modulus of elasticity, which is the measure of a material's ability to

deform when subjected to outside opposing forces. The modulus of elasticity is computed as the ratio of stress to strain and it is expressed in units of stress.

Sourer et al. [8] tested full-scale unreinforced sandstone masonry walls loaded axially and laterally both in-plane and out-of-plane in order to investigate the material properties of typical sandstone masonry construction from a particular era. The results were compared to compression tests by others conducted on sandstone masonry sample types such as in situ or small standalone sandstone samples. Data was continuously gathered throughout the wall tests as the axial load was increased up to and past the walls' peak axial capacities. Even though the walls of the lighthouse are not expected to reach, let alone exceed, their peak axial capacities in any foreseeable loading scenario, some amount of strength degradation may reasonably be assumed in the walls due to their 130-year age and proximity to the ocean. The data of interest from Sourer et al. is summarized in Table 4.5-1. IP denotes in-plane, OOP denotes out-of-plane.

Table 4.5-1: Sandstone Elastic Modulus, Sourer et al. [8]

Test Results	Min (ksi)	Max (ksi)	Avg (ksi)
Before damage	236	328	286
After damage, IP	107	340	246
After damage, OOP	-	-	239

After the full lighthouse was modeled and the meshing of elements was complete, the factor that had the largest effect on the modal properties of the lighthouse was the modulus of elasticity of the sandstone masonry. In order to determine which value for the sandstone's modulus of elasticity was most appropriate out of the data in Table 4.5-1, an analysis of the model was run with each of the values in the "After damage, IP" row of the table and the lighthouse model's natural frequency was compared to the natural frequency of the real

lighthouse found by UL-FVT. The results are shown in Figure 4.5-1, where Tower Mode 2 is the fundamental tower mode in the east-west direction, Tower Mode 1 is the fundamental tower mode in the north-south direction, Wall Mode is the fundamental wall mode out-of-plane, and UL-FVT 1 & 2 are the natural frequencies found of the real lighthouse.

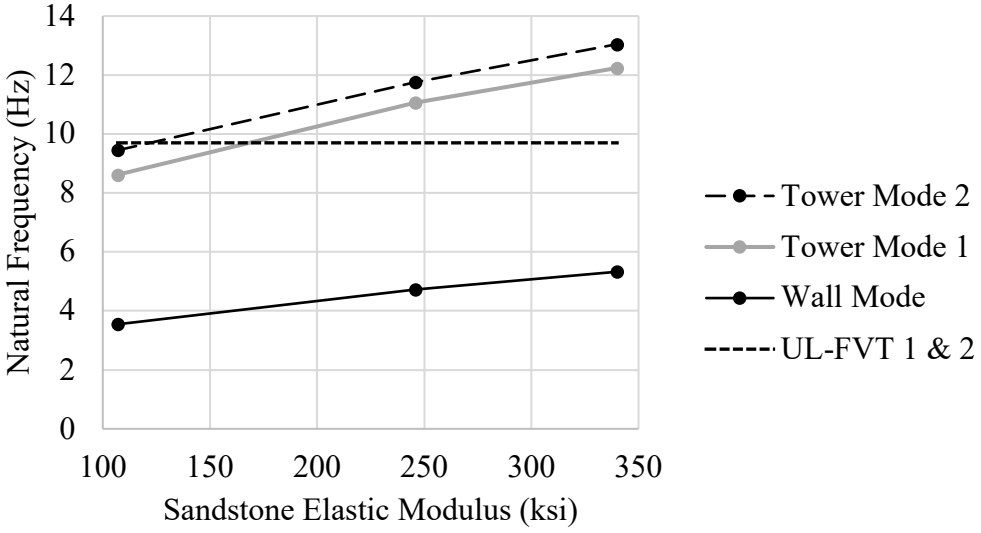

Figure 4.5-1: Model Natural Frequencies vs. Sandstone Elastic Modulus

The natural frequency of the model increased with an increase in modulus of elasticity as expected, and the fundamental tower modes began at a natural frequency close to that of the real lighthouse and quickly became too high. The lowest value in the table, 107 ksi, was deemed acceptable for use as the sandstone's modulus of elasticity.

4.5.2 Brick Masonry

The next most common material by mass in the lighthouse is unreinforced brick masonry and it was important to model the material properties accurately because a significant portion of the tower's section at its base is brick masonry. Fürtmuller and Adam [9] used the results of

historic brick material tests in their numerical modelling to achieve more accurate models at multiple modelling scales. The brick samples were extracted from buildings constructed in Vienna, Austria over a range of years that included 1889, the year the Point Sur Lighthouse was constructed. Statistical data of the material properties from the experimental test results was given and then the tests were simulated numerically. The same brick masonry properties were then backed out of the numerical models and compared to the experimental results. The numerical values were the ones used in this research and are summarized in Section 4.5.4.

4.5.3 Flexible Diaphragm

One of the limitations of many finite element programs, including RISA-3D, is their inability to accurately model flexible diaphragms. Fortunately, it is possible to "trick" a program into modeling a flexible diaphragm using a variety of different methods. The method used in this research made use of plate elements and material properties to model the in-plane stiffness of the lighthouse roof diaphragm.

The deformations in a flexible diaphragm are theoretically made up of both shear and bending components but in practice may be idealized to only consider the shear component. Equation 4.5-1 describes the deformation at the tip of a point-loaded cantilever, in this case a thin cantilever modeled using plate elements in RISA-3D, where the first term represents the deformation due to bending and the second term to shear. *P* represents the point load applied to the end of the cantilever, *L* the length, *E* the modulus of elasticity, *I* the moment of inertia, *A* the cross-sectional area, and *G* the shear modulus.

$$\Delta = \frac{PL^3}{3EI} + \frac{1.2PL}{AG} \qquad \text{(Equation 4.5-1)}$$

In a finite element program like RISA-3D, setting the modulus of elasticity *E* of a material to an extremely large number effectively reduces the deformation due to bending to zero, leaving only shear deformation. The bending term in Equation 4.5-1 may be dropped, and rearranging the remaining variables yields Equation 4.5-2. A graphical representation is shown in Figure 4.5-X.

$$\frac{AG}{1.2L} = \frac{P}{\Delta} \qquad \text{(Equation 4.5-2)}$$

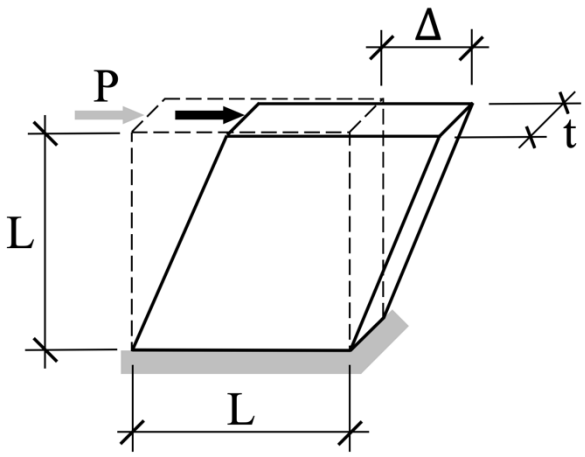

Figure 4.5-2: Thin Cantilevered Plate Deflecting in Shear

Both sides of Equation 4.5-2 are in the form of a stiffness, force per distance. Setting the plate length and height equal allows the stiffness of the plate element to be independent of the size of the plate element and makes the elements easier to model in RISA-3D. With an equal plate length and height, the cross-sectional area of the cantilevered plate is now described by Equation 4.5-3 where *L* represents the side length of the plate and *t* represents the thickness.

$$A = L \times t \qquad \text{(Equation 4.5-3)}$$

Equation 4.5-4 defines a new variable for shear stiffness k_V, force *P* divided by displacement Δ.

$$k_V = P/\Delta \qquad \text{(Equation 4.5-4)}$$

Substituting Equations 4.5-3 and 4.5-4 into Equation 4.5-2 and setting the thickness *t* equal to 1" yields Equation 4.5-5, a proportional relationship between shear modulus and shear stiffness.

$$G = 1.2k_V \qquad \text{(Equation 4.5-5)}$$

This final relationship between shear modulus *G* and shear stiffness k_V for a square plate element of 1" thickness was the key to modeling the roof diaphragm in the lighthouse. The shear modulus of the diaphragm's assigned material is only a function of shear stiffness and default expected values of shear stiffness may be drawn from ASCE 41 based on the diaphragm construction and material. The default recommended shear stiffness for the diaphragm type found in the lighthouse, 1" straight sheathed, is 2.0 k/in. which yielded a shear modulus of 2.4 ksi. The properties for the diaphragm material used in the lighthouse model are summarized in the following section.

4.5.4 Other Members

There are few components in the lighthouse besides the sandstone masonry, brick masonry, and roof diaphragms. The remaining elements are the roof trusses in the fog and radio rooms, the glass, mullions, and roof of the lantern room, and the steel plates cladding the inside and outside of the watch room level. The only elements that were added to the model lighthouse that are not in the real lighthouse are wood members used to brace the bottom chords of the roof trusses. These wood members had no effect on the dynamic behavior of the gabled walls to which they connect but had a large effect on the dynamic behavior of the trusses themselves. Without the bracing on the bottom chords of the trusses, the program calculated a number of minor modes that were irrelevant to this research. Complete lists of members, plates, solids, and materials used to model the lighthouse are summarized in Tables 4.5-2 and 4.5-3.

Table 4.5-2: Finite Element Model Members, Plates, and Solids

Element	Section	Material
Members		
1 in. Rod	1" Diameter	A36 Gr. 36
1x1	1" x 1"	Douglas Fir General
1x6	1" x 6"	Douglas Fir General
2x6	1.5" x 5.5"	Douglas Fir
2x8	1.5" x 7.5"	Douglas Fir
4x10	3.5" x 9.25"	Douglas Fir
4x12	3.5" x 11.25"	Douglas Fir
4x6	3.5" x 5.5"	Douglas Fir
4x8	3.5" x 7.5"	Douglas Fir
Diamond Brace	HSS5½x5½x1/2	A500 Gr. B Rect.
Gable Brace	HSS12x6x1/4	A500 Gr. B Rect.
Horiz. Strong-Back	HSS20x12x1/2	A500 Gr. B Rect.
Rigid	-	Rigid
Strong-Back 1	HSS8x8x3/8	A500 Gr. B Rect.
Strong-Back 2	HSS14x14x7/8	A500 Gr. B Rect.
Tower Cap Bar	0.5" x 2"	A36 Gr. 36
Tower Mullion Horiz.	0.5" x 2"	General Steel
Tower Mullion Vert.	1.2" x 4"	A36 Gr. 36
Plates		
Roof Diaphragm	1" Thick	Diaphragm
Lantern Glass	3/16" Thick	Glass
Steel Plate	1/4"-5/8" Thick	Steel - General
Solids		
Brick Masonry	Varies	Sandstone
Sandstone Masonry	Varies	Brick

The values represented by asterisks in Table 4.5-3 are calculated by RISA-3D based on the member section, and the values represented by dashes do not apply to the material.

Table 4.5-3: Finite Element Model Materials

Material	E (ksi)	G (ksi)	ν	F_y (ksi)	ρ (k/ft^3)
Brick	1088	508	0.07	-	0.094
Diaphragm	1.0E+06	2.4	0	-	0.035
Douglas Fir	*	*	*	-	0.035
Douglas Fir - General	1600	800	0	-	0.035
Glass	10150	4160	0.22	-	0.158
Rigid	1.0E+06	-	0	-	0
Sandstone	107	40	0.35	-	0.150
Steel - A36 Gr. 36	29000	11154	0.3	36	0.490
Steel - A500 Gr. B Rect.	29000	11154	0.3	46	0.527
Steel - General	29000	11154	0.3	-	0.490

The final lighthouse base model is shown in Figure 4.5-3, with solid elements shown in brown, roof diaphragm plate elements in red, steel plate elements in blue, and glass plate elements in green. Next, the simplified lens model and retrofit schemes were added.

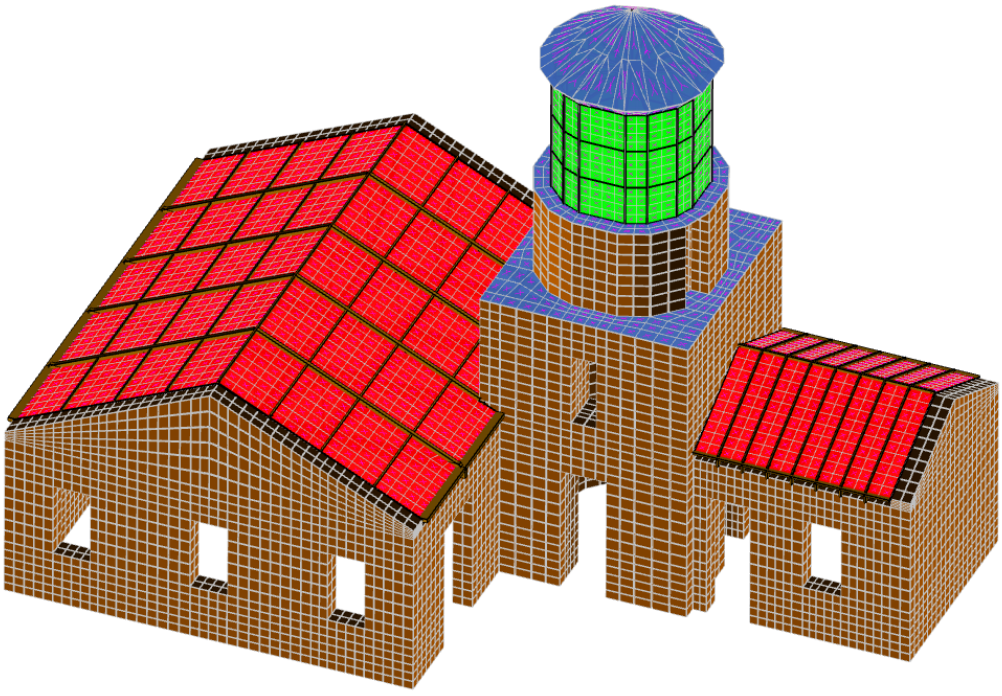

Figure 4.5-3: Final Finite Element Model

4.5.5 Addition of Lens

The first-order Fresnel lens was modeled in the base lighthouse model using rigid elements in a double pyramid configuration with peaks at the approximate locations of the lens and stand centers of mass. Rigid elements were used because the new connections between the repatriated lens and the real lighthouse will be designed to remain elastic in a design level seismic event. The lens itself was modeled as rigid because its construction is unknown but assumed to be sufficient to withstand its own inertial loads. The rigid elements are shown in Figure 4.5-4 between the rectangular solid elements and are bolded in yellow where they overlap the image of the lens. The weights of the lens and stand were applied to the pyramid peaks as point loads and their total is compared to the weights of other lighthouse components in Table 4.5-4. Even though the lens and stand assembly weighs almost 10,000 lbs., it still represents less than 1% of the total lighthouse weight.

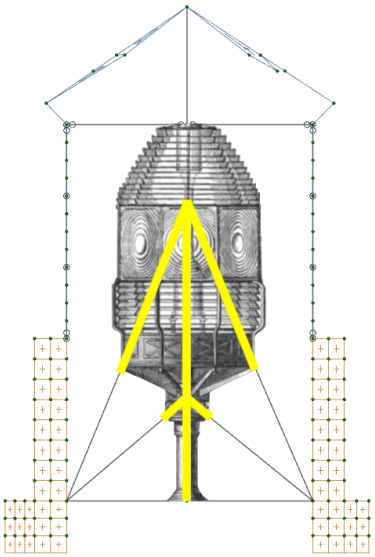

Figure 4.5-4: Rigid Member Lumped Mass Fresnel Lens Model

Table 4.5-4: LH Component Weights

Room	Weight (k)	% of Total
Fog	464	35.3
Tower	682	51.9
Radio	168	12.8
TOTAL	1314	100
Lens	*9.57*	*0.73*

4.6 Retrofit Schemes

4.6.1 Connections Scheme

There were no elements added to the base lighthouse finite element model in order to model the Connections retrofit scheme. It is not possible to model the deficiencies of any of the connections in the lighthouse due to the limitations of RISA-3D, so the connections between elements in the base model were already modeled as sufficient by default. An isometric view of the fog room's gabled wall is shown in Figure 4.6-1 for comparison in later sections.

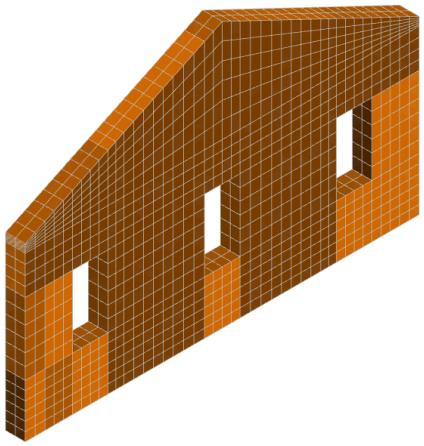

Figure 4.6-1: Isometric View of Fog Room Gabled Wall, Connections Scheme

4.6.2 Strong-Backs Scheme

The only elements that were added to the base lighthouse finite element model in order to model the Strong-Backs retrofit scheme were the strong-backs themselves. Each strong-back shared a node with two adjacent solids at the ground and the boundary condition were modeled as fixed. Though solid elements in RISA-3D do not support fixed boundary conditions, the fixed condition could be applied to the strong-back's beam element. An isometric view of the fog room's gabled wall with the supporting strong-backs is shown in Figure 4.6-2.

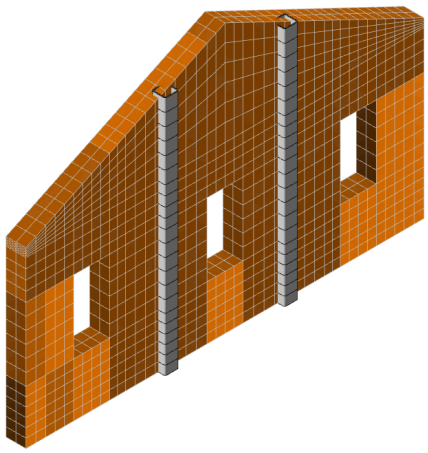

Figure 4.6-2: Isometric View of Fog Room Gabled Wall, Strong-Backs Scheme

4.6.3 Diamond Braces Scheme

The elements that were added to the base lighthouse finite element model in order to model the Diamond Braces retrofit scheme were the braces themselves in the plane of the roof, the horizontal brace at the top of the wall, and minor elements for proper connectivity to solid elements. A number of minor elements were needed to connect the braces to the fog room walls and tower but they had small sections and did not affect the analysis results. An isometric view of the fog room's gabled wall with the supporting braces is shown in Figure 4.6-3.

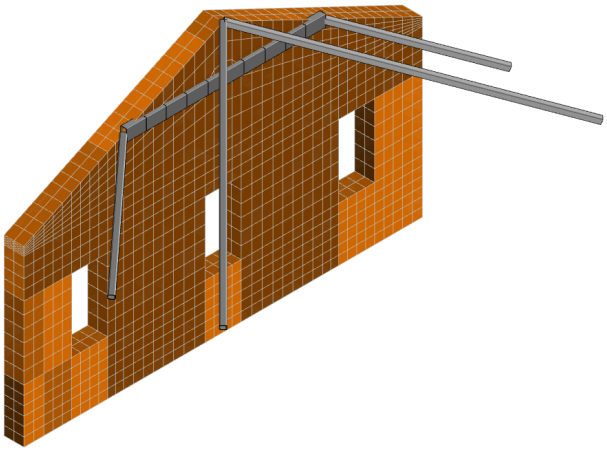

Figure 4.6-3: Isometric View of Fog Room Gabled Wall, Diamond Braces Scheme

4.6.4 Horizontal Strong-Backs Scheme

The elements that were added to the base lighthouse finite element model in order to model the HSB retrofit scheme were the strong-backs themselves and minor elements to allow for proper connectivity to solid elements. Again, the minor elements were needed to connect the braces to the fog room walls but they had small sections and did not affect the analysis results. An isometric view of the fog room's gabled wall with the supporting strong-backs is shown in Figure 4.6-4.

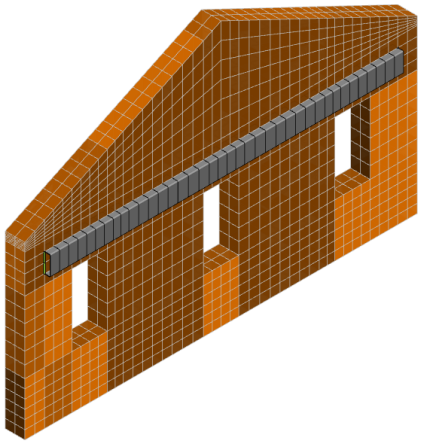

Figure 4.6-4: Isometric View of Fog Room Gabled Wall, HSB Scheme

4.6.5 Diamond Braces and Horizontal Strong-Backs Scheme

The elements that were added to the base lighthouse finite element model in order to model the DB+HSB retrofit scheme were the same elements that were added to model the Diamond Braces and HSB retrofit scheme. One advantage of combining the Diamond Braces and HSB retrofit schemes is that the member configuration of one scheme does not need to be altered to accommodate the member configuration of the other. An isometric view of the fog room's gabled wall with the supporting braces and strong-backs is shown in Figure 4.6-5.

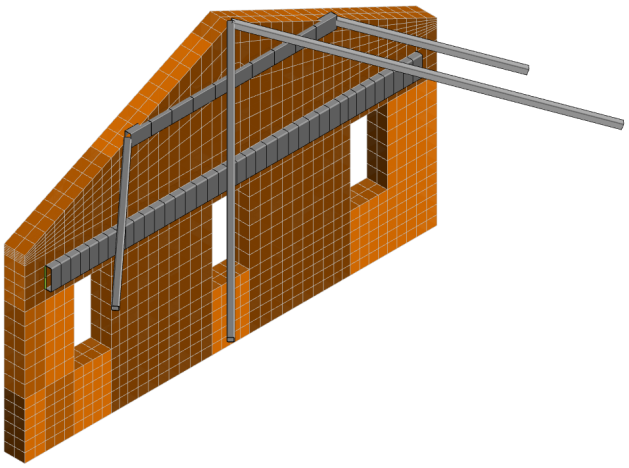

Figure 4.6-5: Isometric View of Fog Room Gabled Wall, DB+HSB Scheme

4.7 Finite Element Model Analyses

4.7.1 Modal Analysis

The first analysis that was conducted on the finite element models was a modal analysis and included studies into the natural frequencies and periods, translational mass participation, and mode shapes of the lighthouse. While an investigation into many lighthouse modes might be valuable, limiting the analysis scope to the fog room gabled wall's fundamental mode out-of-plane and a fundamental mode for the tower in each direction was sufficient for this research.

The natural frequencies and periods of a fundamental mode are a function of the stiffness of the lighthouse's components, which can be altered by the addition of various retrofit schemes. The mass participation of a mode is an indicator of the mode's contribution to the overall response of the building. A high mass participation for a single mode indicates that many different components of the lighthouse are contributing to the response, which is a good measure of how closely a building is vibrating like a single degree of freedom system. The consideration of enough modes to achieve a sum of 90% mass participation is required by ASCE 41-17 to accurately capture the dynamic behavior of the finite element model.

The mode shape at a natural frequency gives a picture of the relative stiffness of each of the sections in a building as well as the uniformity of the structure's response. A mode shape represents a set of relative response values, whether they are displacements, velocities, or accelerations, and this is advantageous in UL-FVT and in the comparison of retrofit schemes. Comparing the differences in mode shapes due to the addition of retrofit schemes is one way to compare the effects of retrofit schemes on isolated sections of the lighthouse or even the lighthouse as a whole.

4.7.2 Equivalent Lateral Force Procedure

The next analysis conducted on the finite element model follows the Equivalent Lateral Force Procedure (ELFP). The basic outline of the ELFP conducted on the Point Sur Lighthouse finite element model was as follows: the site-specific seismic parameters were determined and used to construct a design acceleration response spectrum, shown in Figure 4.7-1. The fundamental frequencies of the lighthouse were used to determine a spectral acceleration from the response spectrum. The spectral acceleration was applied to the lighthouse laterally and the

resulting deflections of the members of the lighthouse were recorded. The response spectrum represents the maximum acceleration a structure would undergo at a specific site based on its natural period. The equation used to determine the pseudo seismic force based on the spectral acceleration was ASCE 41-17 Equation 4-1, shown here as Equation 4.7-1, where *V* represents the total pseudo seismic force, *C* is a factor based on building construction, S_a is the spectral acceleration, and *W* is the total weight of the building.

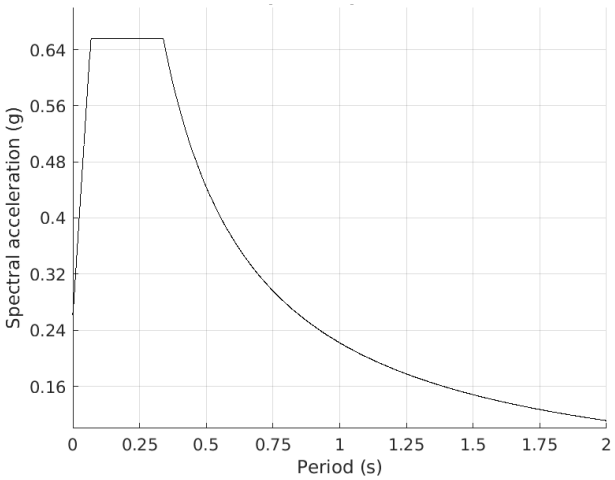

Figure 4.7-1: Point Sur Design Acceleration Response Spectrum

$$V = CS_aW \qquad \text{(Equation 4.7-1)}$$

Using a value of $C = 1$ for unreinforced masonry and dropping the weight variable *W* turns the pseudo seismic force into a pseudo seismic acceleration, which was simple to apply to all elements in the lighthouse simultaneously in RISA-3D. The main objective of using the ELFP as another analysis tool was to compare the differences in deflections of the lighthouse with different retrofit schemes. The deflection in each of the sections of the lighthouse will provide a concrete basis for comparing each of the schemes. However, the equivalent lateral force

procedure is not technically allowed by code for the full design of a retrofit scheme because of the lighthouse's structural irregularities, so additional analysis procedures were required.

4.7.3 Modal Response Spectrum Analysis

The final analysis conducted on the finite element model was a modal response spectrum analysis (MRSA). The MRSA procedure is similar to the ELFP procedure in that it depends heavily on the site-specific response spectrum, but the MRSA also uses the modal properties of the structure to produce a more comprehensive investigation than the ELFP. Another reason why a MRSA analysis of a structure gives a more comprehensive investigation than an ELFP analysis is because the MRSA analysis results are the combination of a series of smaller analyses, one analysis for each mode of the structure. A MRSA analysis combines the results of any number of dynamic analyses and is more effective in identifying important design subtleties than a single analysis for this reason. The required number of modes and analyses for an ASCE 41-17 approved MRSA analysis is the number of modes that corresponds to 90% mass participation.

The basic outline of the MRSA analysis conducted on the Point Sur Lighthouse finite element model was as follows: for each mode under consideration, the natural frequency, mode shape, and estimated damping ratio were determined. The natural period and damping were used to determine the maximum deformation from the design displacement response spectrum, shown in Figure 4.7-2 for the Point Sur Lighthouse. The final maximum displacements were determined using the modal participation factors, mode shapes, and maximum deformations. The final displacements of all the modes considered were then combined using the CQC method, which is a method of combining the modal responses with closely spaced natural frequencies. The MRSA analyses were performed completely by RISA-3D.

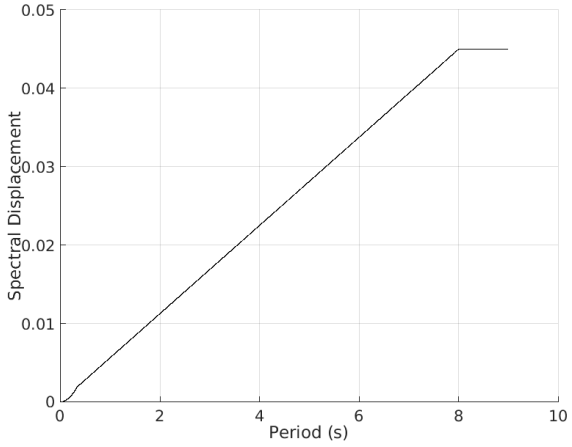

Figure 4.7-2: Point Sur Design Displacement Response Spectrum

While the modal and ELFP analyses were of some benefit when comparing the retrofit schemes, the MRSA analysis was expected to provide the best comparison of the schemes because it provided the most comprehensive analysis of the lighthouse and the effects of the retrofit schemes. The results of the MRSA analysis were used to compare retrofit schemes but can also be used to design the retrofit schemes themselves since they represent real demands on the lighthouse members, though a full design of a retrofit scheme was left to a professional.

5.0 FINITE ELEMENT MODEL ANALYSIS RESULTS

5.1 Overview

The results of the modal analysis provided a good starting point for the comparison of the proposed retrofit schemes, but they were not the only criteria by which the retrofit schemes should be evaluated. The natural frequencies and periods of the fundamental wall mode changed drastically due to the various amounts of additional stiffness the retrofit schemes contributed, while the natural frequencies of the tower modes changed relatively little. What did change in the fundamental tower modes between retrofit schemes was the amount of mass participation, which was a good indicator of the engagement of the gabled walls and the tower. The mode shapes of the lighthouse with each of the retrofit schemes also changed drastically though it was difficult to compare mode shapes directly because of their unitless nature.

The results of the equivalent lateral force analysis provided a better point of comparison than the modal properties, but they did not provide an all-around indicator of a retrofit scheme's effectiveness either. Applying an equivalent lateral force in each orthogonal direction only showed how effective a retrofit scheme was for a particular section of the lighthouse, for example, the fog room's gabled walls. The best retrofit scheme for each section of the lighthouse individually was then clear because the retrofit schemes may be ranked by the amount of deflection that occurred due to the applied load. Even so, a better analysis method would provide a clear picture of the best retrofit scheme for the lighthouse as a whole.

The results of the modal response spectrum analysis provided the best measure of a retrofit scheme's potential because they represented the most comprehensive analysis of the retrofit scheme's effects on the lighthouse. The MRSA analysis results for each scheme were a

combination of the results from the number of modes required to reach approximately 90% mass participation. The displaced shapes of the lighthouse with each of the retrofits due to the MRSA analysis were similar, but not identical to, the displaced shapes from the ELFP analysis. The MRSA analysis was the best tool for comparing retrofit schemes of the three considered because it gave the clearest picture of how a retrofit scheme changed the dynamic behavior of the whole lighthouse.

In general, the effects of adding the first-order Fresnel lens back into the lighthouse model were negligible because the lens represented such a small percentage of the building's weight and the stiffness of the tower is so great. The lens represented a small percentage of just the tower's weight as well. The modal properties and ELFP results only changed by small percentages and the MRSA results changed more than the other results did, but all the changes were still within a small enough margin that it was clear that any retrofit scheme had a much larger effect on the dynamic behavior of the lighthouse than the repatriation of the lens.

5.2 Natural Frequencies, Periods, and Mass Participation

5.2.1 FE Model vs. UL-FVT

The results of the modal analysis of the base finite element model were in very close agreement with the UL-FVT natural frequencies; the natural frequency of the fundamental tower mode in the north-south direction was 0.04 Hz away from the corresponding UL-FVT natural frequency and the natural frequency for the tower mode in the east-west direction was within one Hertz for its corresponding UL-FVT natural frequency. The finite element model and UL-FVT natural frequencies are shown in Tables 5.2-1 and 5.2-2.

Table 5.2-1: E/W Mode Comparison

Mode	Freq. (Hz)	Period (s)
UL-FVT	9.70	0.103
FEM	8.74	0.114

Table 5.2-2: N/S Mode Comparison

Mode	Freq. (Hz)	Period (s)
UL-FVT	9.60	0.104
FEM	9.56	0.105

One of the main reasons for the difference in natural frequencies of the fundamental tower modes in the finite element model is the difference in direction and stiffness of the walls adjoining the tower section. Even though the northern radio room wall is relatively stiff and the adjoining walls running in the north-south direction are relatively flexible because they are short or contain a door opening, the walls running north-south also benefit from the intersection with the gabled walls. The reason the UL-FVT natural frequencies were so close is because the interaction between the walls in the finite element model is dependent on idealized connections between elements, but the true interaction between walls in the lighthouse is reduced by weaker connections and is more dependent on the stiffness of the tower itself.

5.2.2 Connections Scheme

The Connections retrofit scheme had relatively low mass participation (MP) for its fundamental wall and tower modes compared to participation of finite element models of typical buildings. The number of modes required to meet or exceed 90% mass participation for the Connections scheme (and all other schemes) was 210 since a large majority of the lighthouse's modes had less than 1% mass participation. The modal property data for the 210 modes of the

Connections scheme model is shown in the Appendix in Table A.2-1. The natural frequencies of the fundamental tower modes were fine-tuned to closely match the frequencies of the real lighthouse found by UL-FVT and the natural frequency of the wall mode is reasonable based on the relative stiffnesses of the gabled walls out-of-plane and the stiff tower section. The modal properties for the Connections scheme are summarized in Table 5.2-3.

Table 5.2-3: Modal Properties for Connections Scheme

Mode	Freq. (Hz)	Period (s)	MP E/W (%)	MP N/S (%)
1	3.64	0.275	-	11.4
3	8.74	0.114	24.0	4.32
6	9.56	0.105	0.07	20.0

The three modes considered in Sections 5.2.2 through 5.2.7 are the fundamental mode of the fog room gabled walls out-of-plane (called the fundamental wall mode for reference), the fundamental mode of the tower in the east-west direction, and the fundamental mode of the tower in the north-south direction (called the fundamental tower modes for reference). A response in the gabled walls out-of-plane is in the north-south direction and a response in-plane is in the east-west direction. The fundamental modes for each section of the lighthouse were the modes with the first instance of significant mass participation at the lowest natural frequency. The fundamental wall mode was always the first mode of the lighthouse as a whole, but the order of appearance of the fundamental tower modes changed based on the change in stiffness of the fog room gabled walls that each of the retrofit schemes provided. Modes between the fundamental wall mode and each of the fundamental tower modes for the retrofit schemes were modes with a majority of their response in the fog room gabled walls only and usually had very little mass participation.

5.2.3 Strong-Backs Scheme

The Strong-Backs retrofit scheme provided enough stiffness to the fog room gabled walls to increase the natural frequency of the fundamental wall mode by almost one full Hertz from the Connections scheme, yet the natural frequencies of the fundamental tower modes changed very little. The mass participation (MP) increased significantly for the fundamental tower mode in the east-west direction, possibly due to the increased stiffness of the gabled walls. The order of the fundamental modes also changed dramatically from the Connections scheme. The modal properties for the Strong-Backs scheme are summarized in Table 5.2-4.

Table 5.2-4: Modal Properties for Strong-Backs Scheme

Mode	Freq. (Hz)	Period (s)	MP E/W (%)	MP N/S (%)
1	4.63	0.216	-	11.6
2	8.88	0.113	38.4	3.15
3	9.53	0.105	4.33	20.4

5.2.4 Diamond Braces Scheme

The Diamond Braces scheme significantly increased the stiffness of the fog room's gabled walls over the Connections scheme, as both the fundamental wall mode's natural frequency and mass participation nearly doubled. The increase in mass participation for the wall mode was due to the increased stiffness as well as the direct connection to the stiff tower. The natural frequencies and mass participation of the fundamental tower modes also increased from the Connections model, the mass participation for the east-west tower mode increasing significantly. The increase in mass participation of the fundamental tower mode in the north-south direction was due to the engagement of the fog room gabled wall out-of-plane by its

connection to the tower and the fog room rectangular walls. The modal properties for the Diamond Braces scheme are summarized in Table 5.2-5.

Table 5.2-5: Modal Properties for Diamond Braces Scheme

Mode	Freq. (Hz)	Period (s)	MP E/W (%)	MP N/S (%)
1	6.75	0.148	0.01	19.6
3	9.22	0.108	41.3	6.88
4	9.82	0.102	8.69	27.6

5.2.5 Horizontal Strong-Backs Scheme

The Horizontal Strong-Backs scheme did not have a large effect on the natural frequencies over the Connections scheme, though it did have a large effect on the mass participation of the fundamental tower modes. One reason the natural frequencies were unvarying was because the horizontal strong-backs did not provide the gabled walls with any additional stiffness when bending about their base out-of-plane, nor did they engage the tower directly. The mass participation may have increased because the horizontal strong-backs provided additional stiffness to the gabled walls in-plane, but more likely because they aided in a more unified response of the lighthouse as a whole. The modal properties for the HSB scheme are summarized in Table 5.2-6.

Table 5.2-6: Modal Properties for HSB Scheme

Mode	Freq. (Hz)	Period (s)	MP E/W (%)	MP N/S (%)
1	4.11	0.244	-	11.8
3	8.96	0.112	40.2	2.45
4	9.61	0.104	0.51	31.2

5.2.6 Diamond Braces and Horizontal Strong-Backs Scheme

The DB+HSB scheme had the largest overall effect on the natural frequencies and mass participation of the lighthouse. The additional members contributed enough additional stiffness to the fog room's gabled walls that the natural frequency of the fundamental wall mode almost doubled from the wall mode frequency of the Connections model. The changes in modal properties of the lighthouse model due to the DB+HSB scheme were almost the direct sum of the changes due to the individual retrofit schemes, though it was interesting to note that the mass participation of the fundamental tower mode in the north-south direction was less than that of the Diamond Braces and HSB schemes individually. The modal properties for the DB+HSB scheme are summarized in Table 5.2-7.

Table 5.2-7: Modal Properties for DB+HSB Scheme

Mode	Freq. (Hz)	Period (s)	MP E/W (%)	MP N/S (%)
1	7.20	0.139	0.03	22.6
3	9.28	0.108	41.5	7.88
4	9.86	0.101	10.6	24.4

5.2.7 Summary

In general, the retrofit schemes that provided the largest increase in out-of-plane stiffness and increased the natural frequency of the fundamental wall mode the most also provided the largest increase in mass participation to all three of the fundamental modes considered. The modal results presented in Tables 5.2-3 through 5.2-7 are summarized to include natural frequency and mass participation in the major direction for each of the fundamental modes and are shown in Tables 5.2-8 through 5.2-10. The retrofit schemes that only provided the gabled walls with additional stiffness and did not increase the wall mode's mass participation did not

provide a direct connection from the gabled walls to the tower, for example the Strong-Backs scheme. The retrofit schemes that provided a large increase in mass participation for the fundamental tower modes were also the ones that provided a direct connection between the gabled walls and tower.

The HSB and Strong-Back schemes provided an unexpectedly large increase in mass participation for the fundamental tower mode in the east-west direction based on the change in mass participation that they provided to the fundamental wall mode in the north-south direction. The horizontal strong-backs and strong-backs clearly provided a much larger benefit to the gabled walls in-plane (east-west) than out-of-plane (north-south). The HSB scheme also provided a significant increase in mass participation for the second fundamental tower mode, so much so that it surpassed the schemes that use diamond braces to directly engage the tower.

Table 5.2-8: Modal Prop. Summary for Fund. Wall Mode OOP

Retrofit Model	Freq. (Hz)	Period (s)	MP N/S (%)
DB+HSB	7.20	0.139	22.6
Diamond Braces	6.75	0.148	19.6
Strong-Backs	4.63	0.216	11.6
HSB	4.11	0.244	11.8
Connections	3.64	0.275	11.4

Table 5.2-9: Modal Prop. Summary for Fund. Tower Mode E/W

Retrofit Model	Freq. (Hz)	Period (s)	MP E/W (%)
DB+HSB	9.28	0.108	41.5
Diamond Braces	9.22	0.108	41.3
HSB	8.96	0.112	40.2
Strong-Backs	8.88	0.113	38.4
Connections	8.74	0.114	24.0

Table 5.2-10: Modal Prop. Summary for Fund. Tower Mode N/S

Retrofit Model	Freq. (Hz)	Period (s)	MP N/S (%)
HSB	9.61	0.104	31.2
Diamond Braces	9.82	0.102	27.6
DB+HSB	9.86	0.101	24.4
Strong-Backs	9.53	0.105	20.4
Connections	9.56	0.073	20.0

With all the changes in natural frequencies of the fundamental modes due to the various retrofit schemes, the frequencies still did not change enough to decrease the spectral acceleration based on the response spectrum constructed for the site of the lighthouse. The design acceleration response spectrum is shown in Figure 5.2-1, and the periods that give a spectral acceleration on the "plateau" of the response spectrum are between 0.068 and 0.338 seconds. The smallest natural period for any of the fundamental modes with any retrofit scheme was 0.101 seconds and the largest was 0.275 seconds; the spectral acceleration remained on the "plateau" and yielded a value of $S_a = S_{DS} = 0.656\ g$ [26].

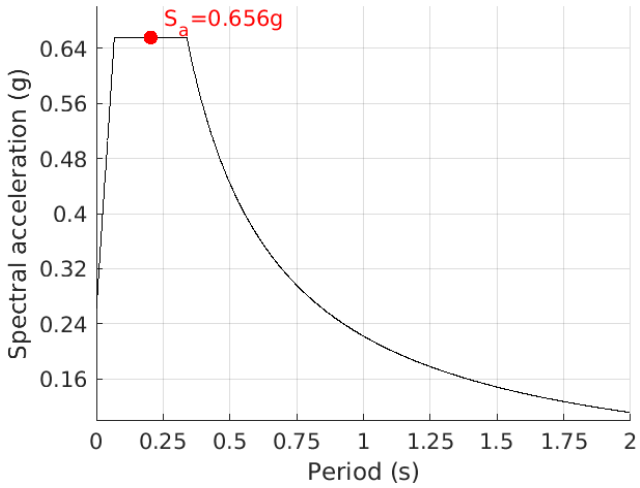

Figure 5.2-1: Point Sur Design Acceleration Response Spectrum with S_a

Even though the mass participation changed drastically between the least effective and most effective retrofit schemes for the three fundamental modes under consideration, a modal analysis for all of the retrofit schemes needed to consider more than 200 modes to achieve 90% mass participation. The modal property data for the 210 modes needed to exceed 90% mass participation for the Connections scheme is shown in the Appendix Table A.2-1. The main reason for the large number of modes was because the lighthouse was modeled with its mass assigned directly to its elements instead of lumped at its floor levels like in simple finite element models. In the case of the lighthouse, a large majority of the 210 modes considered had less than 1% mass participation.

The most effective retrofit schemes overall when only considering natural frequencies and mass participation were the schemes that engaged the tower and perpendicular walls to support the fog room gabled walls out-of-plane. A direct connection between the fog room gabled walls, fog room rectangular walls, and the tower was beneficial to the out-of-plane stiffness of the gabled walls, yet it had comparatively little effect on the tower itself.

5.3 Mode Shapes

5.3.1 FE Model vs. UL-FVT

The mode shapes of the finite element model were plotted as a series of points in the same way the UL-FVT mode shapes were plotted in Section 3.3.3, using only the modal displacements of nodes in the finite element model that corresponded to the approximate accelerometer locations from the UL-FVT test. The mode shapes of the finite element model of the lighthouse showed a resemblance to the mode shapes of the real lighthouse found by UL-FVT but they failed to capture a number of important characteristics.

The finite element model's mode shape that corresponded to UL-FVT shaking in the east-west direction showed similar displacement patterns but the proportions of the displacement components in each direction were clearly different. A comparison of the mode shapes is shown in Figure 5.3-1, where the UL-FVT mode shape is represented by a blue dashed line and the finite element model mode shape is represented by a magenta dotted line. Both mode shapes were normalized to their largest displacement components then scaled up the same amount for visualization. The finite element model's displacements at accelerometer locations A and F in the tower were much smaller than the UL-FVT displacements and suggest that the tower moved in the northeast-southwest direction rather than the nearly east-west direction of the UL-FVT mode shape. The model's displacements at locations B, C, D, and E all overestimated the east-west response of the UL-FVT mode shape but accurately estimated small north-south responses. One reason that the finite element's mode shape was so different from the UL-FVT mode shape was because the model overestimated the stiffness of the element connections and the UL-FVT mode shape may consist of more than the fundamental mode shape in the east-west direction.

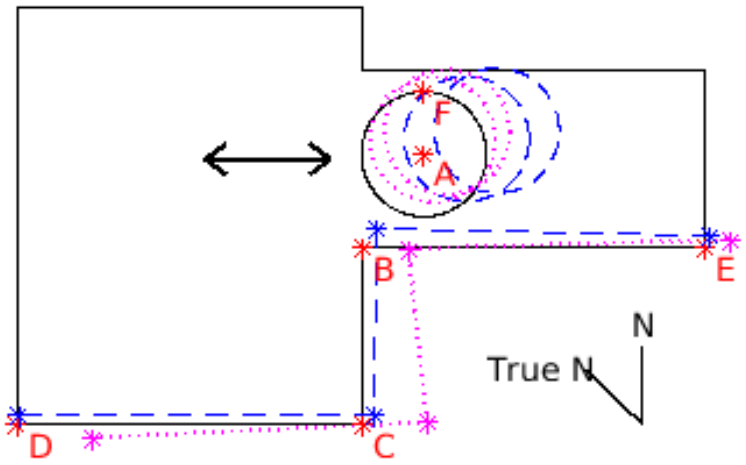

Figure 5.3-1: FEM and UL-FVT Mode Shape E/W
(··· FEM - - - UL-FVT)

The finite element model's mode shape that corresponded to UL-FVT shaking in the north-south direction also showed similar displacement patterns but the proportions of the displacements in each direction were still clearly different. A comparison of the mode shapes is shown in Figure 5.3-2, with the UL-FVT mode shape represented as a blue dashed line and the finite element model mode shape represented as a magenta dotted line. Both mode shapes were normalized to their largest displacement components then scaled up the same amount for visualization. The displacements at accelerometer locations A and F of the finite element model were proportioned correctly to accurately simulate the mode shape found during UL-FVT testing, but they greatly underestimated the magnitude of the UL-FVT displacements. The displacements at locations B and E were similar in magnitude and direction between the finite element model and UL-FVT but the displacements at locations C and D were not. The displacements at locations C and D from the finite element model mode shape greatly overestimated the magnitude of the response of the UL-FVT mode shape and the direction of the displacement was completely inaccurate. The modal displacements at locations A, B, E, and F were very similar between the model and the real lighthouse but a number of factors could have contributed to the inaccuracies at locations C and D.

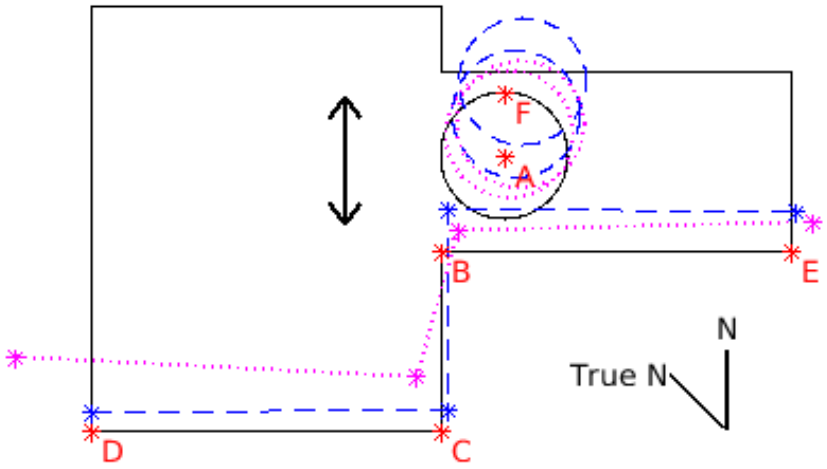

Figure 5.3-2: FEM and UL-FVT Mode Shape N/S
(··· FEM - - - UL-FVT)

5.3.2 Full Lighthouse

The mode shapes for the fog room's gabled wall fundamental mode out-of-plane (called the fundamental wall mode for reference) and fundamental tower mode in the east-west direction (called the fundamental tower mode for reference) of the lighthouse model with each of the retrofit schemes are shown in isometric view in Figure 5.3-3 and in plan in Figure 5.3-4. The wall mode's modal displacements of the gabled walls were the largest at the top edge without diamond braces providing restraint, and when diamond braces were included, the largest modal displacements occurred near the mid-height of the wall. It was difficult to compare the magnitude of the gabled wall modal displacements because the displacements are unitless, but it was clear that the retrofit schemes aided in reducing the modal displacements of the gabled walls in the fundamental tower mode. The large stiffness of the tower kept its modal displacements relatively constant between retrofit schemes.

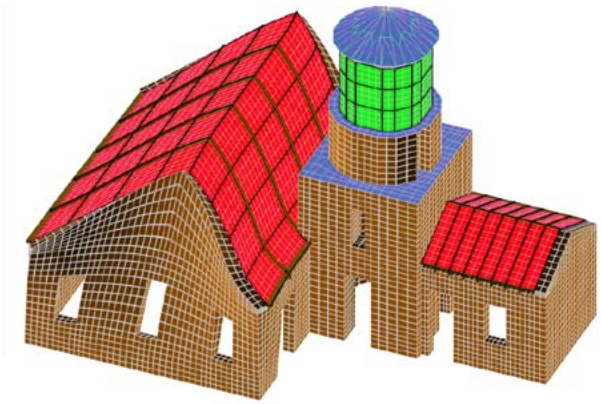

Connections Fund. Wall Mode

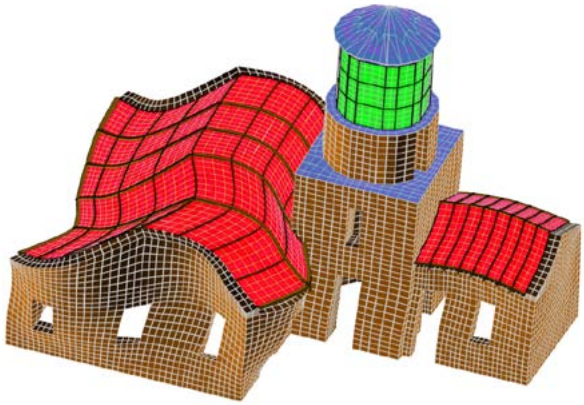

Connections Fund. Tower Mode

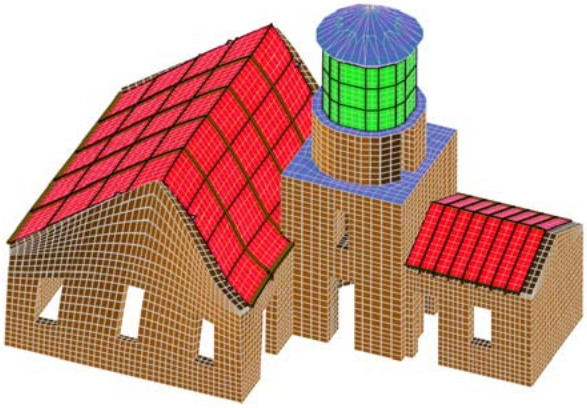

Strong-Backs Fund. Wall Mode

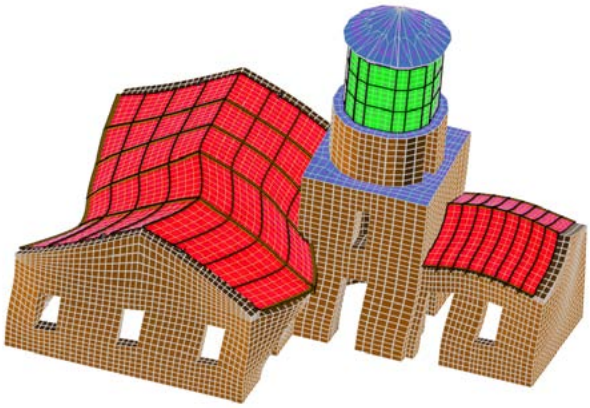

Strong-Backs Fund. Tower Mode

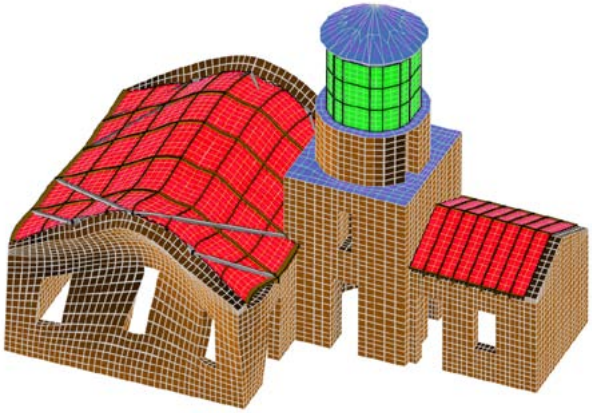

Diamond Braces Fund. Wall Mode

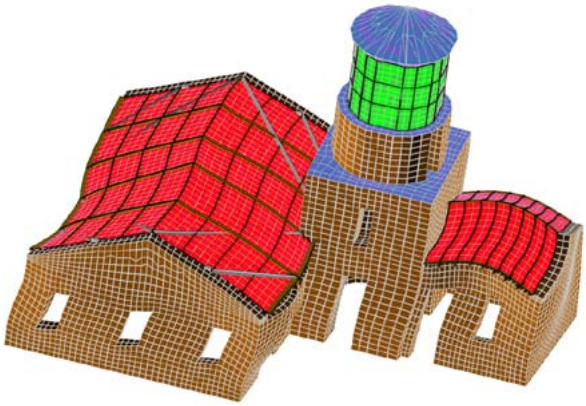

Diamond Braces Fund. Tower Mode

Figure 5.3-3a: Mode Shapes in Isometric View

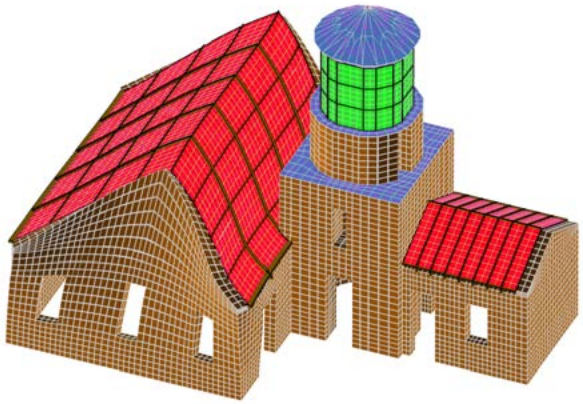

HSB Fund. Wall Mode

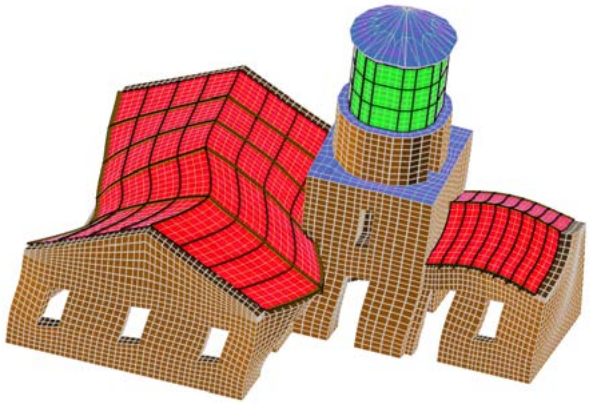

HSB Fund. Tower Mode

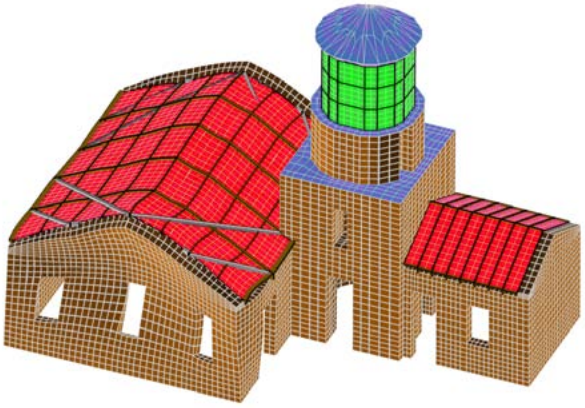

DB+HSB Fund. Wall Mode

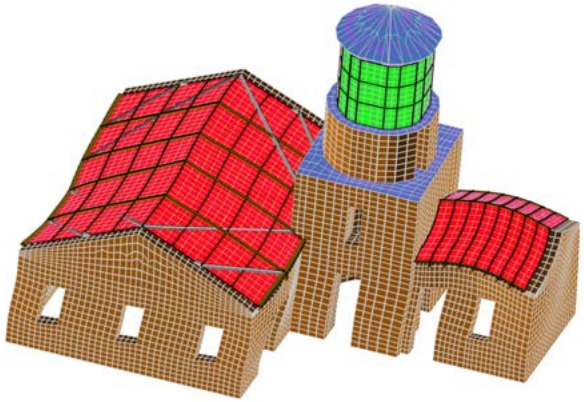

DB+HSB Fund. Tower Mode

Figure 5.3-3b: Mode Shapes in Isometric View

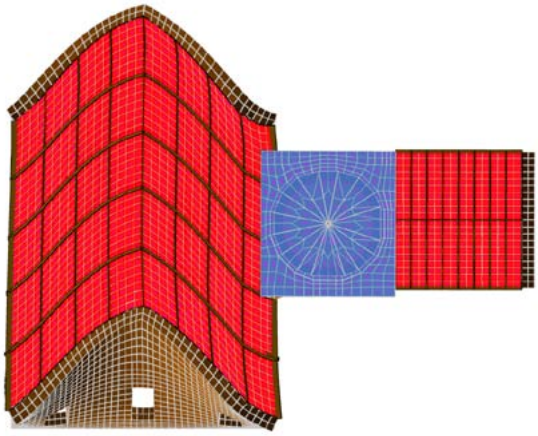

Connections Fund. Wall Mode

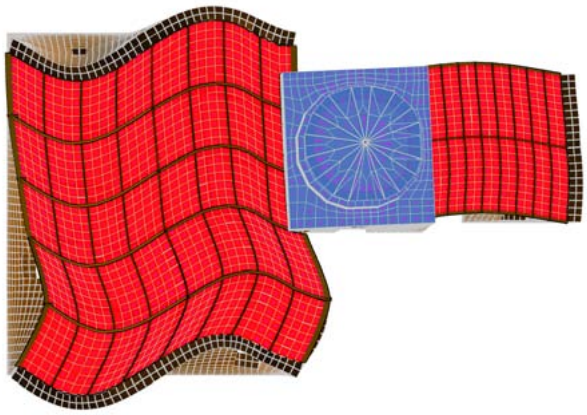

Connections Fund. Tower Mode

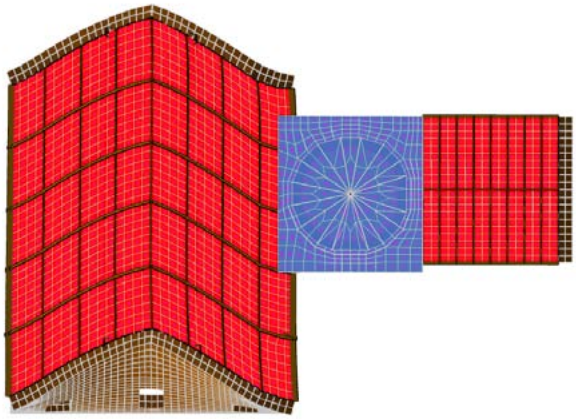

Strong-Backs Fund. Wall Mode

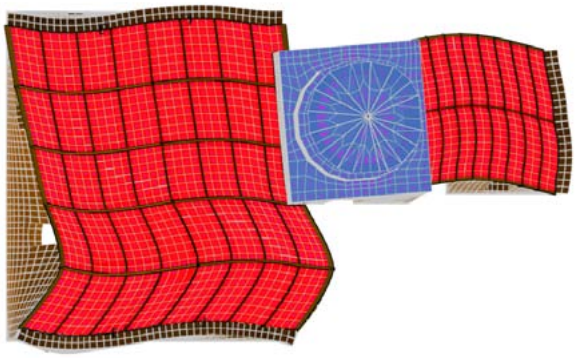

Strong-Backs Fund. Tower Mode

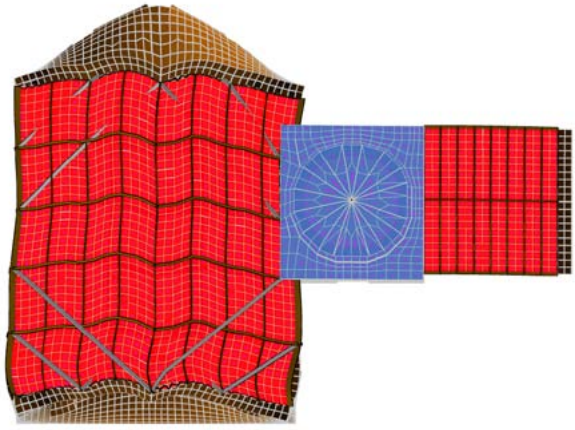

Diamond Braces Fund. Wall Mode

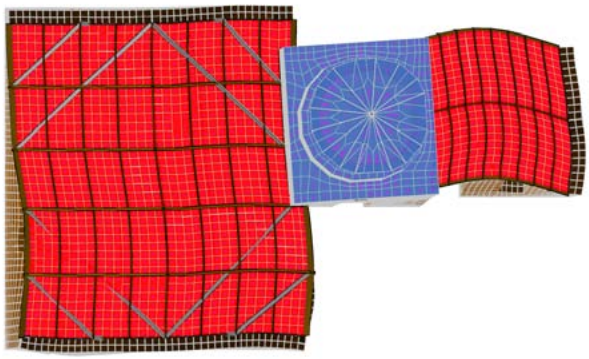

Diamond Braces Fund. Tower Mode

Figure 5.3-4a: Mode Shapes in Plan

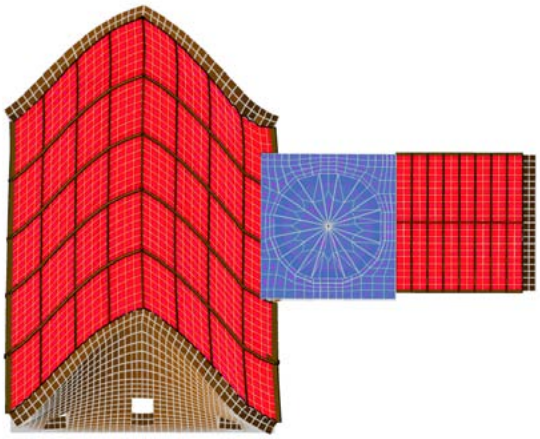

HSB Fund. Wall Mode

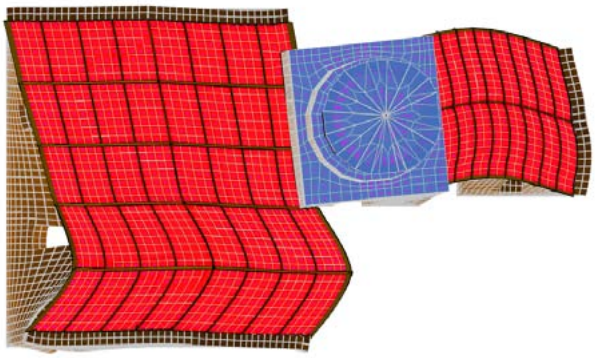

HSB Fund. Tower Mode

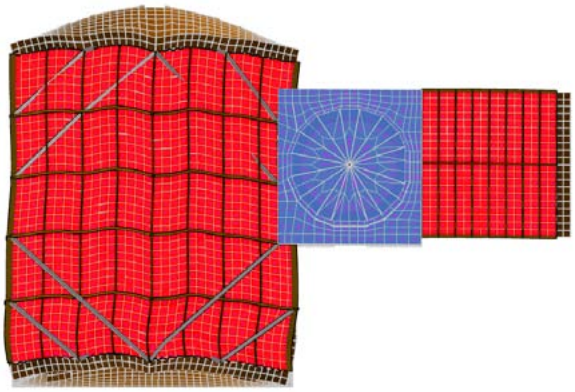

DB+HSB Fund. Wall Mode

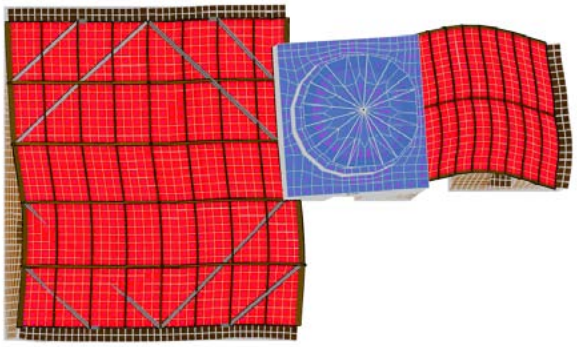

DB+HSB Fund. Tower Mode

Figure 5.3-4b: Mode Shapes in Plan

In order to get a closer look at the mode shapes of smaller sections of the lighthouse with each of the retrofit schemes, the modal displacements for the fog room gabled wall and rectangular wall, radio room gabled wall and rectangular wall, and tower are shown in Figures 5.3-5 through 5.3-9 for the fundamental wall mode out-of-plane and the fundamental tower mode in the east-west direction. The modal displacements of the walls were plotted in "heat map" style, where the larger displacements are in the lighter yellow and the smaller, sometimes negative, displacements are in darker blue. The modal displacements for the tower were drawn in wireframe and scaled for visualization. The maximum and minimum modal displacements in each section are noted as a percentage of the maximum displacements in the lighthouse but can only be used for a general idea of the retrofit scheme effects because of their relative nature.

5.3.3 Fog Room Gabled Wall

The fog room's gabled wall modal displacements out-of-plane changed the most between retrofit schemes, but this was expected because the retrofit schemes were designed to target the major deficiencies in the gabled walls first. The fundamental wall modal displacements out-of-plane in the gabled wall were very similar between the Connections, Strong-Backs, and HSB schemes, where the largest displacement occurred at the very highest peak of the wall. However, the HSB scheme decreased displacements of the fog room gabled wall in the tower mode over the Connections and Strong-Backs scheme. The retrofit schemes with diamond braces restrained the top edges of the gabled walls so much that the largest displacements occurred near the mid-height of the walls rather than the peak in both the wall and tower modes. The horizontal strong-backs in the DB+HSB scheme increased the portion of the gabled wall with the largest displacements in the fundamental wall mode over the Diamond Braces scheme. However, the

horizontal strong-backs in the DB+HSB scheme decreased the portion of the gabled wall with the largest displacements in the fundamental tower mode over the Diamond Braces scheme. The mode shapes gave a clear picture of the diamond brace configuration's ability to restrain the gabled walls in both fundamental modes.

5.3.4 Fog Room Rectangular Wall

The retrofit schemes without diamond braces had little effect on the modal displacements of the fog room rectangular wall, while the schemes that included diamond braces increased modal displacements. The reason for increased displacements with diamond braces is not because the displacements from the gabled walls were shifting to the rectangular walls, but rather the diamond braces increased rotation at the intersection of the walls causing larger displacements out-of-plane.

5.3.5 Radio Room Gabled Wall

The modal displacements in the radio room gabled wall were very small in the wall mode though their pattern did change with the addition of diamond braces in the fog room, engaging more of the wall. The pattern of the displacements in the tower mode changed very little with the retrofit scheme since the displacements in the tower itself changed very little.

5.3.6 Radio Room Rectangular Wall

Similarly, in the radio room rectangular wall, the displacements were small in the wall mode but diamond braces in the fog room engaged more of the wall and increased the displaced area. The displacements in the tower mode also changed very little.

5.3.7 Tower

The enormous stiffness of the tower allowed it to displace very little in both the fundamental tower and wall modes compared to the gabled walls in the fog room. The tower had a small amount of twist in both modes, most likely due to the differences in stiffness of the adjoining walls. No retrofit scheme had any large effect on the displacements in the tower except for the diamond braces in the wall mode, which are effective at reducing the tower's twisting.

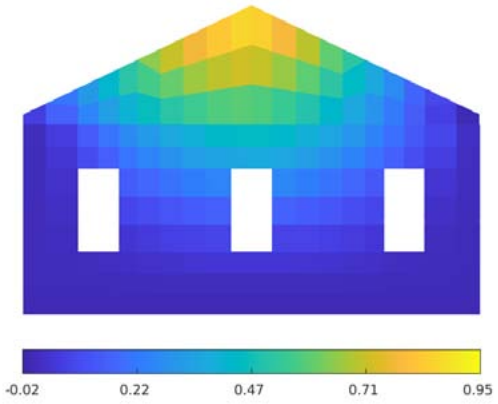

Connections Fund. Wall Mode (-2/+95)

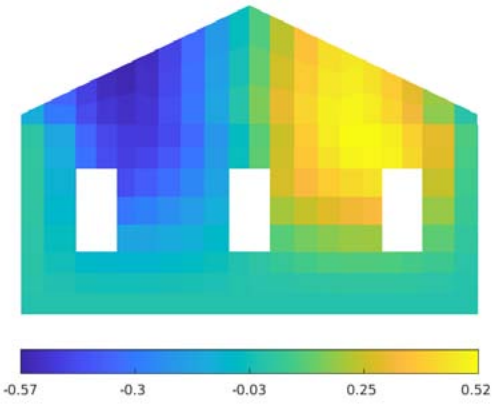

Connections Fund. Tower Mode (-57/+52)

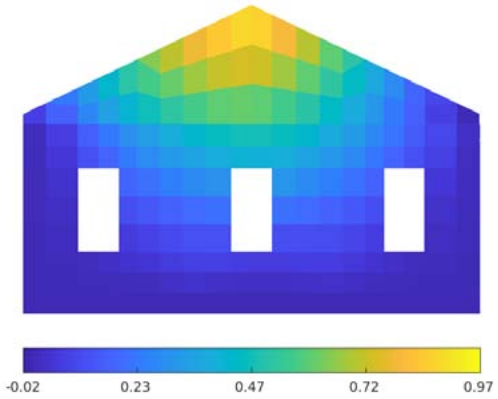

Strong-Backs Fund. Wall Mode (-2/+97)

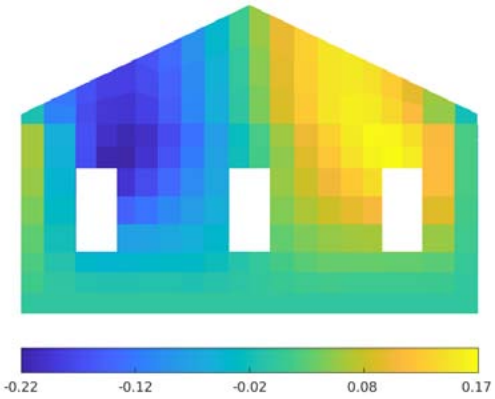

Strong-Backs Fund. Tower Mode (-22/+17)

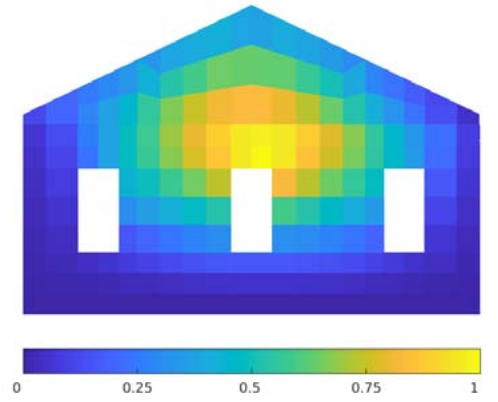

Diamond Braces Fund. Wall Mode (0/+100)

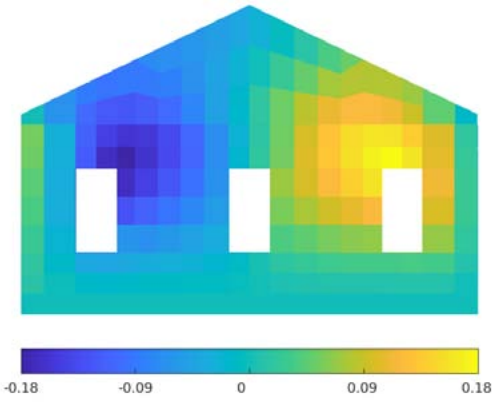

Diamond Braces Fund. Tower Mode (-18/+18)

Figure 5.3-5a: Fog Room Gabled Wall Modal Displacements
(% of Maximum Displacement in Lighthouse)

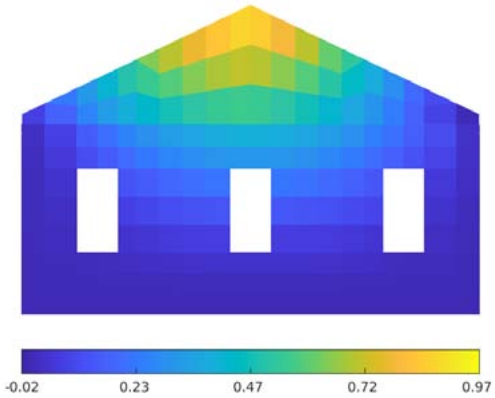

HSB Fund. Wall Mode (-2/+97)

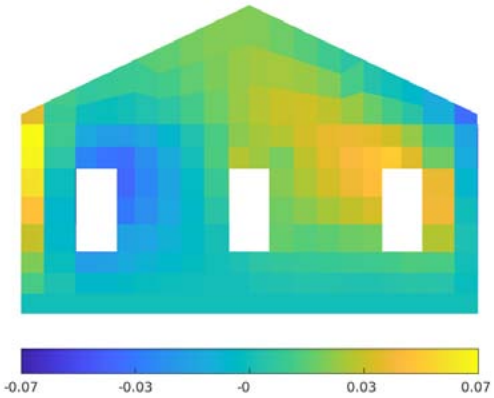

HSB Fund. Tower Mode (-7/+7)

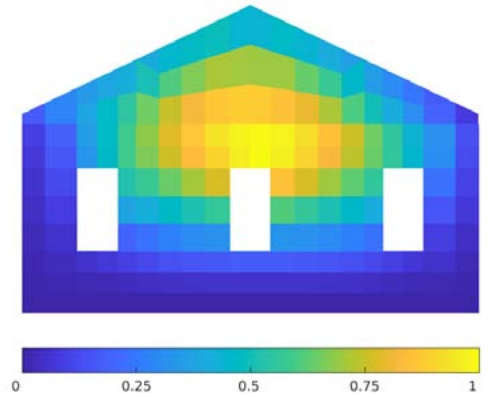

DB+HSB Fund. Wall Mode (0/+100)

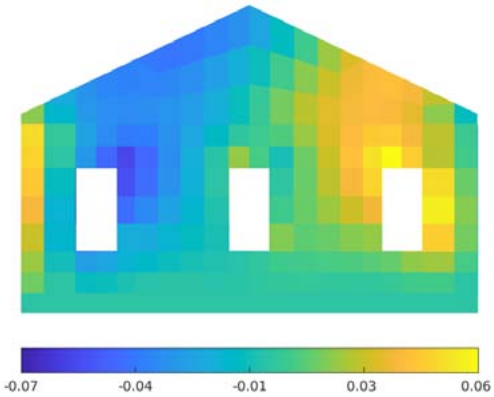

DB+HSB Fund. Tower Mode (-7/+6)

Figure 5.3-5b: Fog Room Bageled Wall Modal Displacements
(% of Maximum Displacement in Lighthouse)

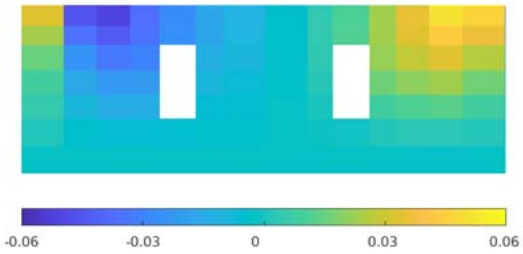

Connections Fund. Wall Mode (-6/+6)

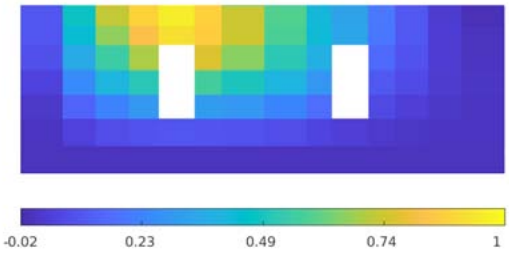

Connections Fund. Tower Mode (-2/+100)

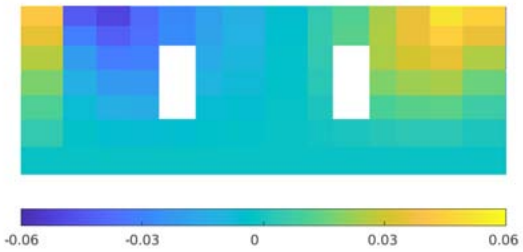

Strong-Backs Fund. Wall Mode (-6/+6)

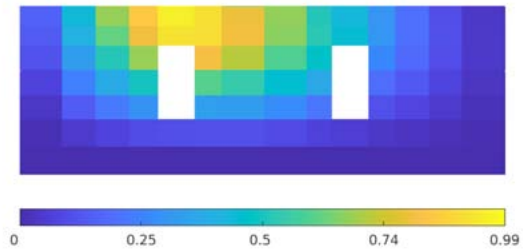

Strong-Backs Fund. Tower Mode (0/+99)

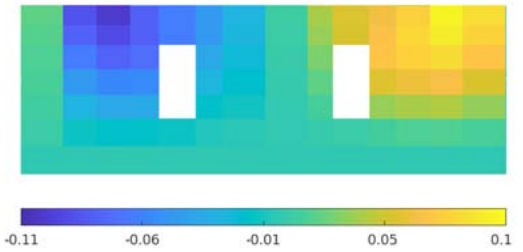

Diamond Braces Fund. Wall Mode (-11/+10)

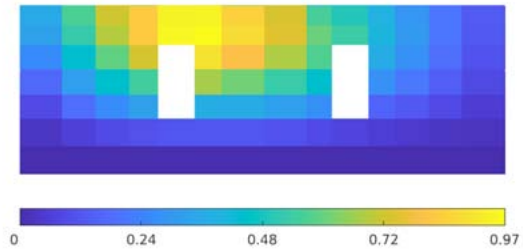

Diamond Braces Fund. Tower Mode (0/+97)

Figure 5.3-6a: Fog Room Rectangular Wall Modal Displacements
(% of Maximum Displacement in Lighthouse)

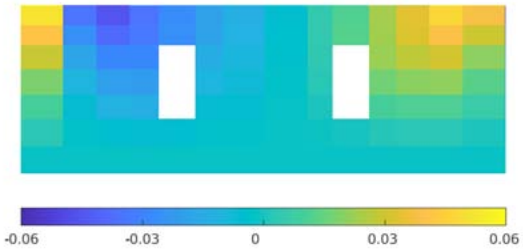

HSB Fund. Wall Mode (-6/+6)

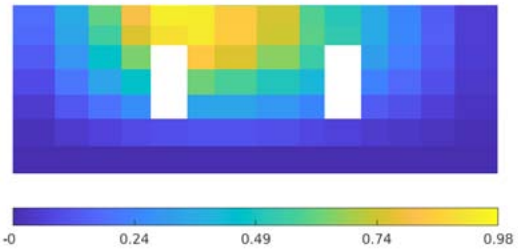

HSB Fund. Tower Mode (0/+98)

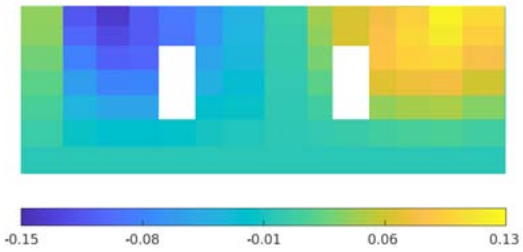

DB+HSB Fund. Wall Mode (-15/+13)

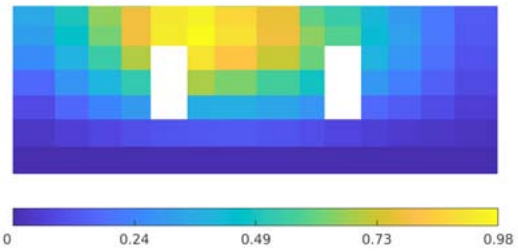

DB+HSB Fund. Tower Mode (0/+98)

Figure 5.3-6b: Fog Room Rectangular Wall Modal Displacements
(% of Maximum Displacement in Lighthouse)

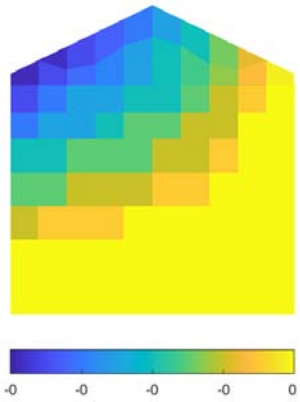

Connections Fund. Wall Mode (0/0)

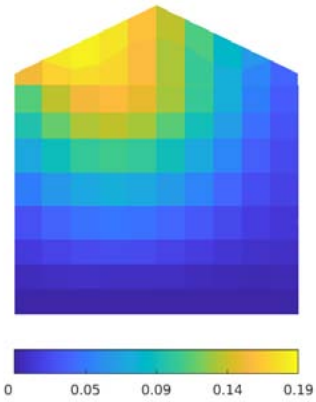

Connections Fund. Tower Mode (0/+19)

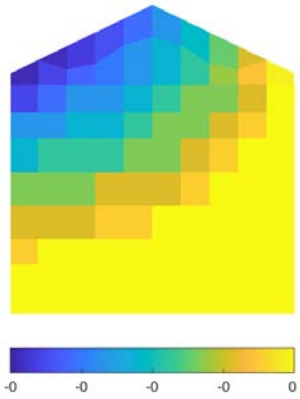

Strong-Backs Fund. Wall Mode (0/0)

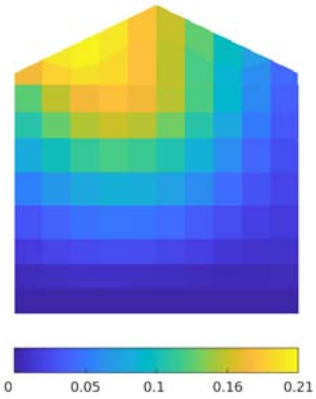

Strong-Backs Fund. Tower Mode (0/+21)

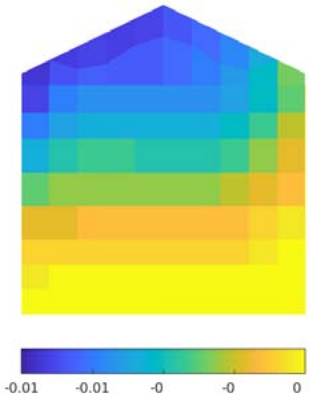

Diamond Braces Fund. Wall Mode (-1/0)

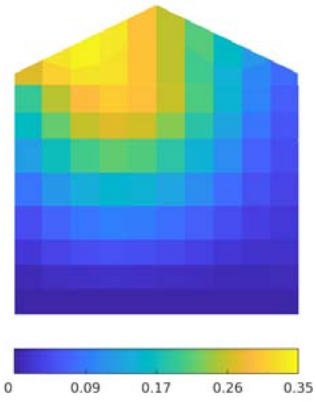

Diamond Braces Fund. Tower Mode (0/+35)

Figure 5.3-7a: Radio Room Gabled Wall Modal Displacements
(% of Maximum Displacement in Lighthouse)

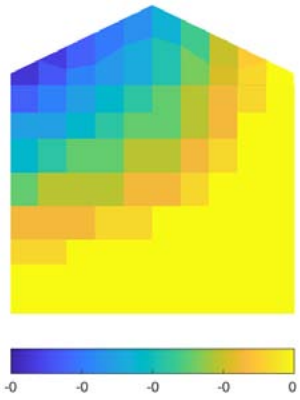

HSB Fund. Wall Mode (0/0)

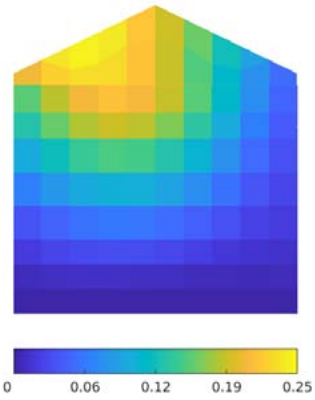

HSB Fund. Tower Mode (0/+25)

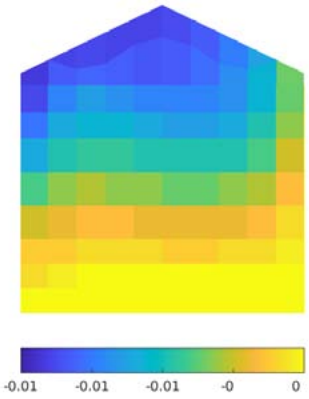

DB+HSB Fund. Wall Mode (-1/0)

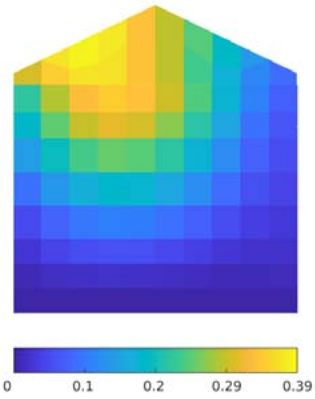

DB+HSB Fund. Tower Mode (0/+39)

Figure 5.3-7b: Radio Room Gabled Wall Modal Displacements
(% of Maximum Displacement in Lighthouse)

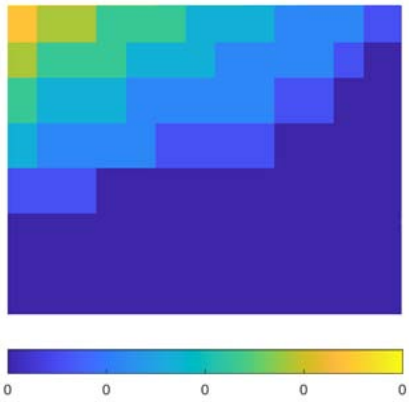

Connections Fund. Wall Mode (0/0)

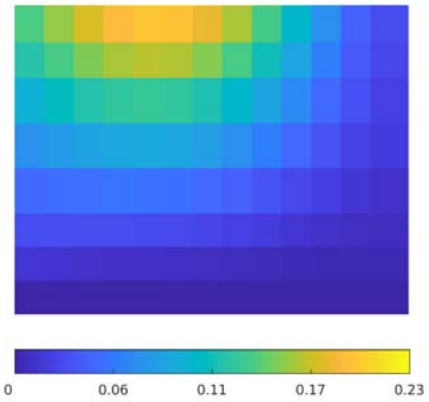

Connections Fund. Tower Mode (0/+23)

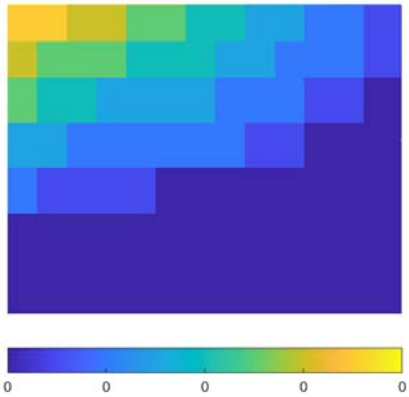

Strong-Backs Fund. Wall Mode (0/0)

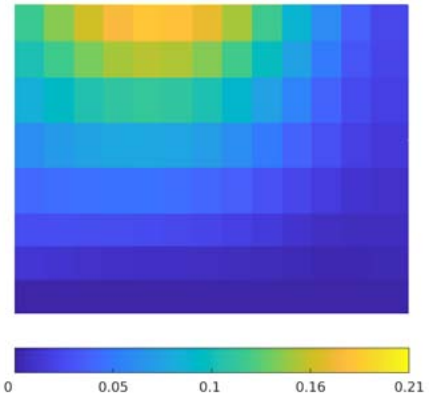

Strong-Backs Fund. Tower Mode (0/+21)

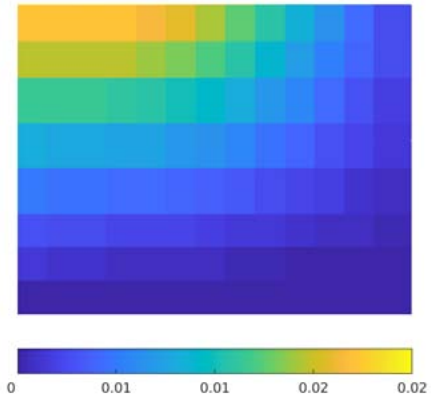

Diamond Braces Fund. Wall Mode (0/+2)

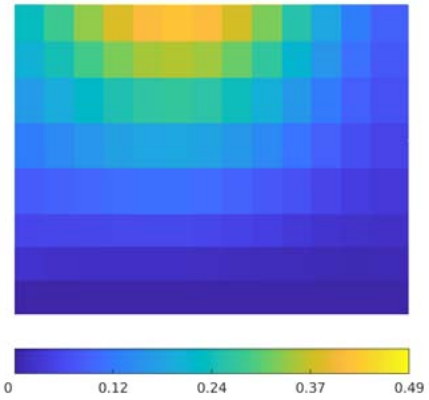

Diamond Braces Fund. Tower Mode (0/+49)

Figure 5.3-8a: Radio Room Rectangular Wall Modal Displacements
(% of Maximum Displacement in Lighthouse)

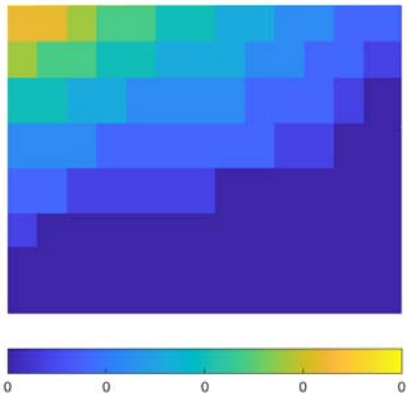

HSB Fund. Wall Mode (0/0)

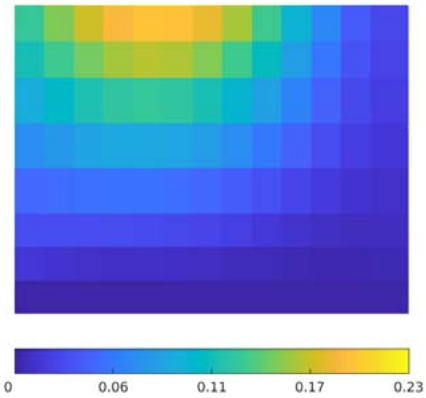

HSB Fund. Tower Mode (0/+23)

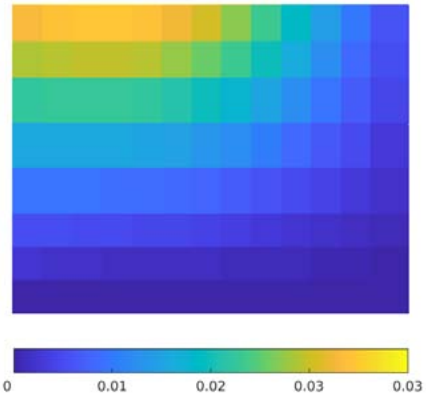

DB+HSB Fund. Wall Mode (0/+3)

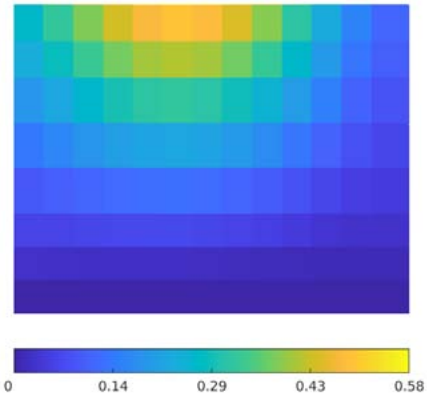

DB+HSB Fund. Tower Mode (0/+58)

Figure 5.3-8b: Radio Room Rectangular Wall Modal Displacements
(% of Maximum Displacement in Lighthouse)

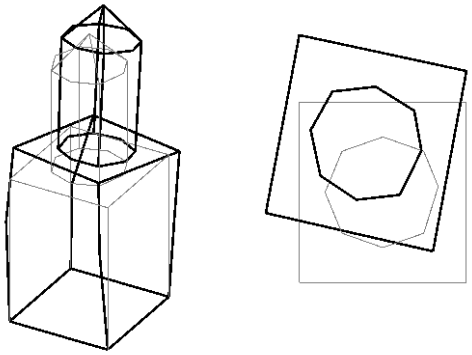

Connections Fund. Wall Mode (1)

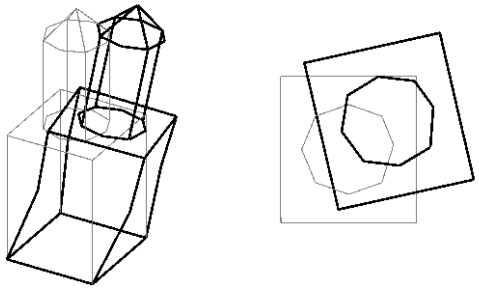

Connections Fund. Tower Mode (31)

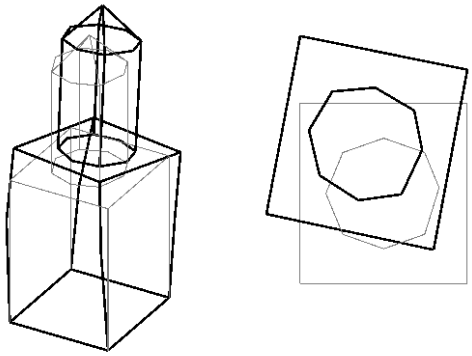

Strong-Backs Fund. Wall Mode (1)

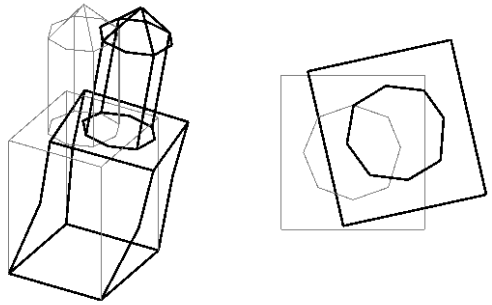

Strong-Backs Fund. Tower Mode (33)

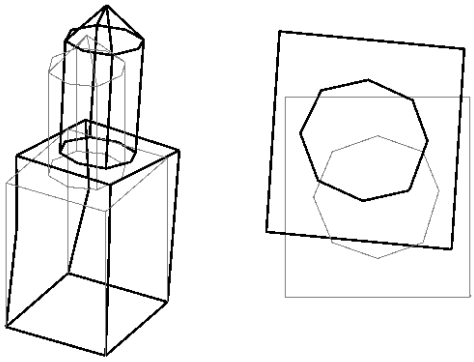

Diamond Braces Fund. Wall Mode (7)

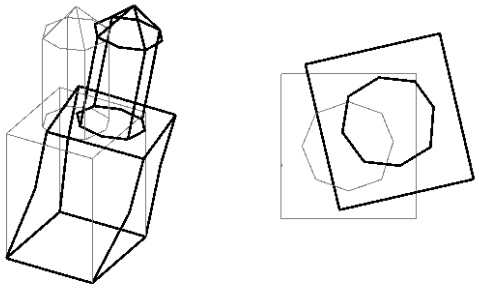

Diamond Braces Fund. Tower Mode (53)

Figure 5.3-9a: Tower Modal Displacements
(% of Maximum Displacement in Lighthouse)

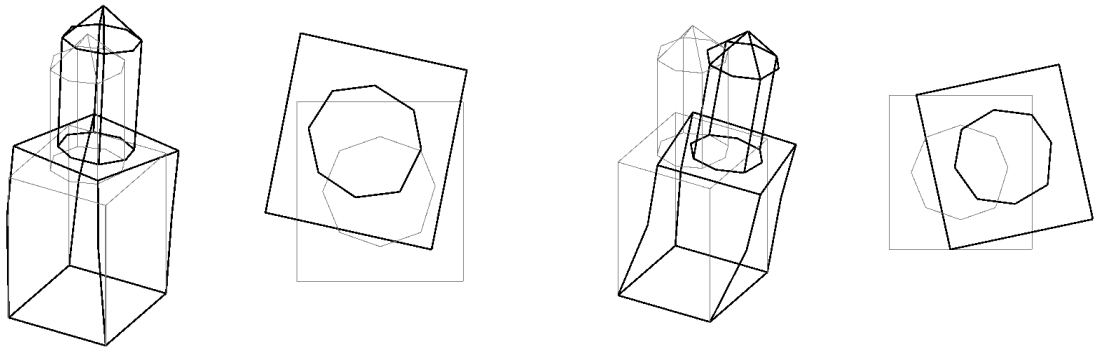

HSB Fund. Wall Mode (1)

HSB Fund. Tower Mode (39)

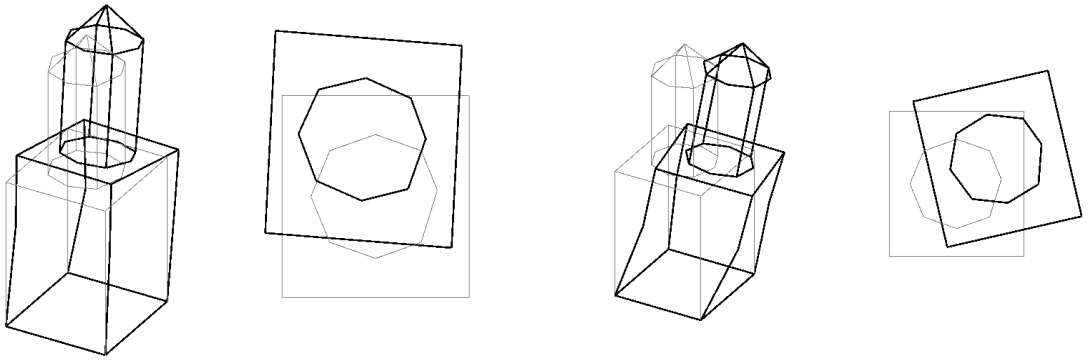

DB+HSB Fund. Wall Mode (10)

DB+HSB Fund. Tower Mode (60)

Figure 5.3-9b: Tower Modal Displacements
(% of Maximum Displacement in Lighthouse)

5.4 Equivalent Lateral Force Procedure

5.4.1 Full Lighthouse

The displacements from the equivalent lateral force analysis in the lighthouse model with each of the retrofit schemes are shown in isometric view in Figure 5.4-1 and in plan in Figure 5.4-2. The displacements were strikingly similar to the mode shapes, where the results of the ELFP analysis in the east-west direction resembled the fundamental tower mode shape and the results in the north-south direction resembled the fundamental wall mode shape. The displacements of the gabled walls were again the largest at the top edge without diamond braces providing restraint, and when diamond braces were included, the largest displacements occurred near the mid-height of the wall. It was difficult to compare the exact displacements in isometric and plan views, but it was clear that the retrofit schemes aided in reducing the displacements of the gabled walls. The large stiffness of the tower kept its displacements relatively constant between retrofit schemes.

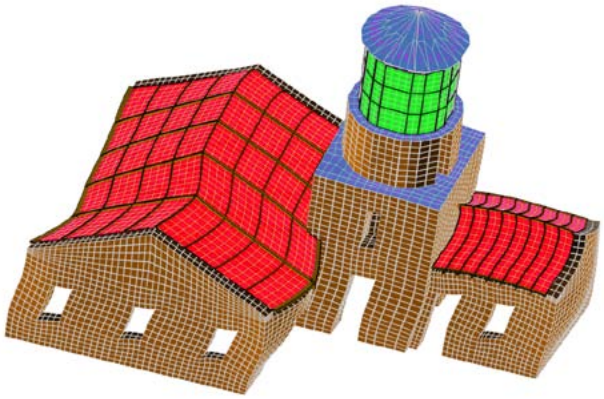

Connections E/W

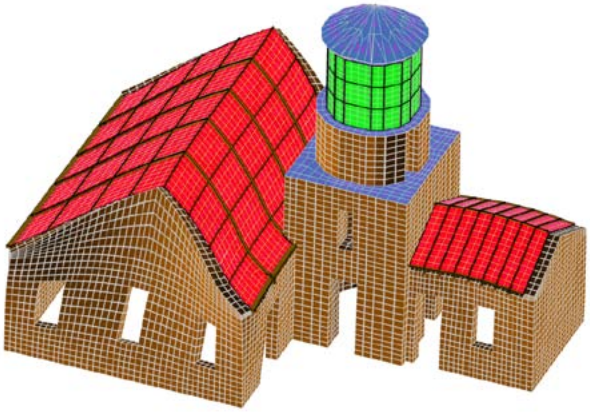

Connections N/S

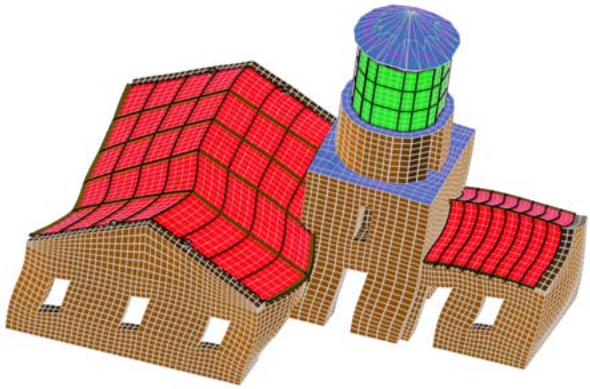

Strong-Backs E/W

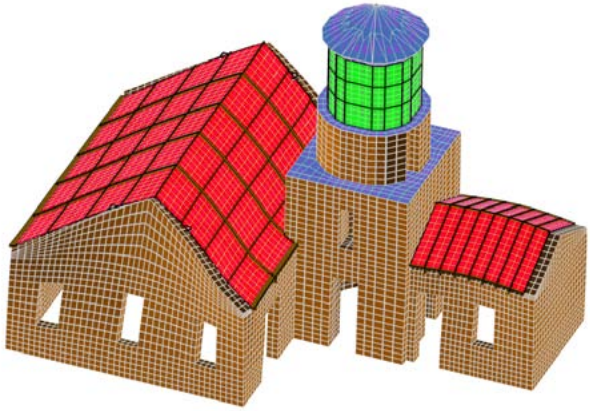

Strong-Backs N/S

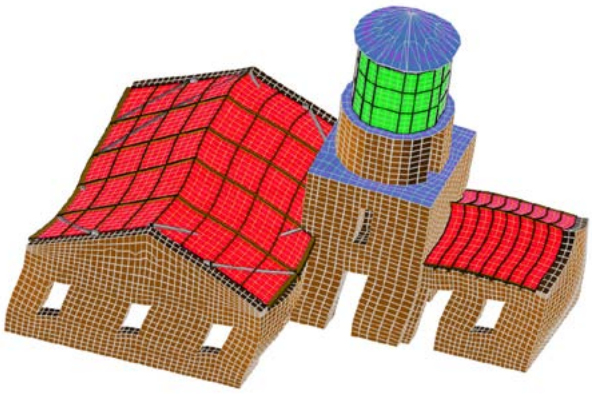

Diamond Braces E/W

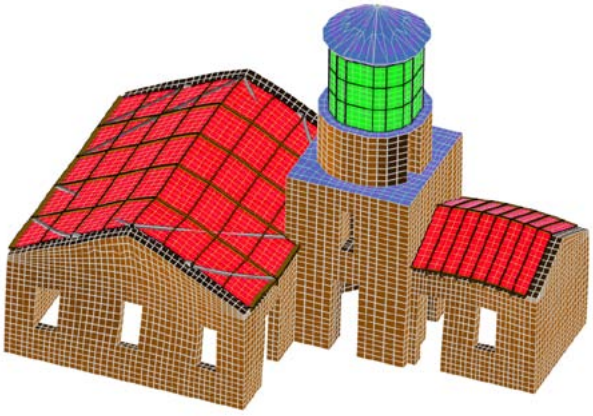

Diamond Braces N/S

Figure 5.4-1a: ELFP Displacements in Isometric View

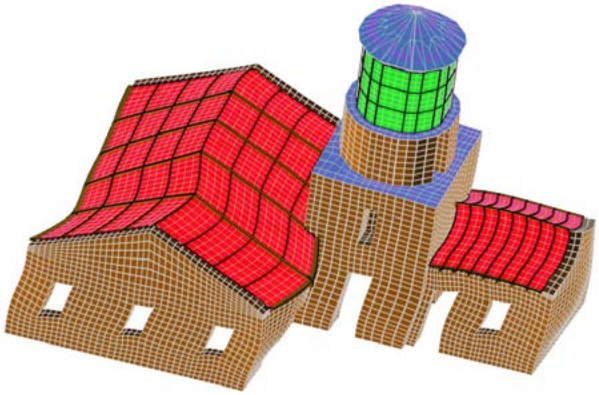

HSB E/W

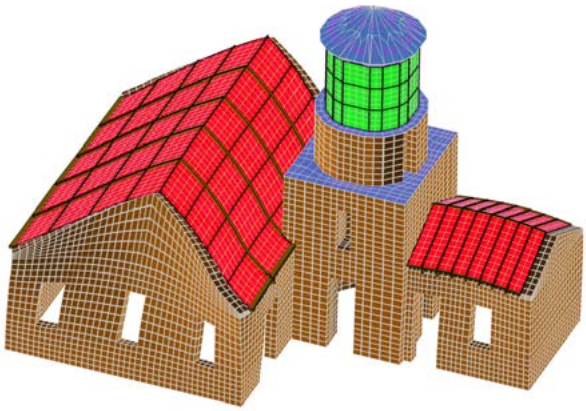

HSB N/S

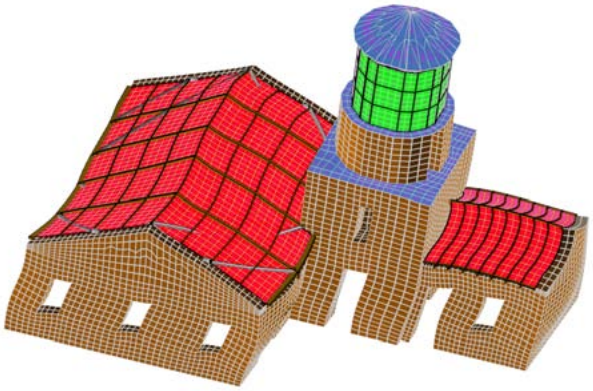

DB+HSB E/W

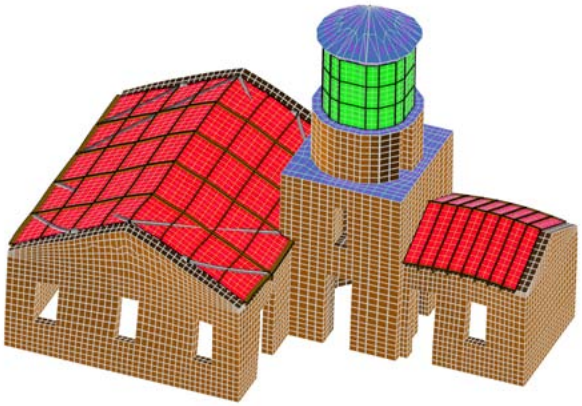

DB+HSB N/S

Figure 5.4-1b: ELFP Displacements in Isometric View

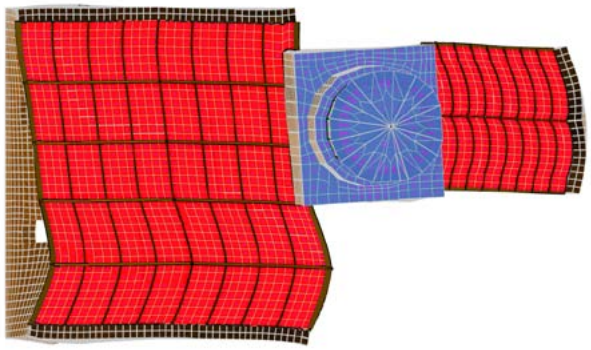

Connections E/W

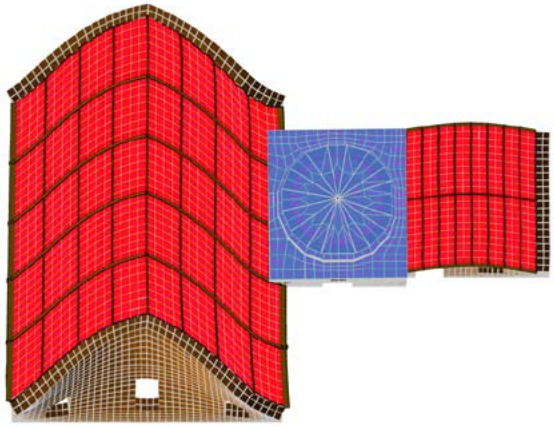

Connections N/S

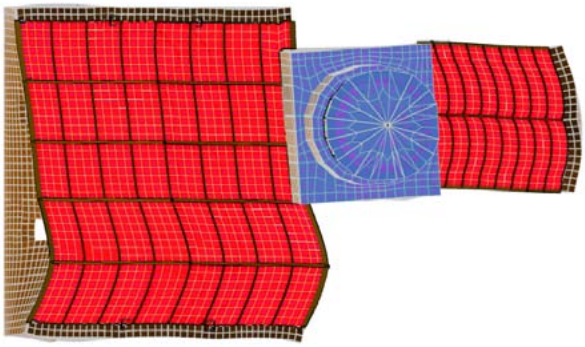

Strong-Backs E/W

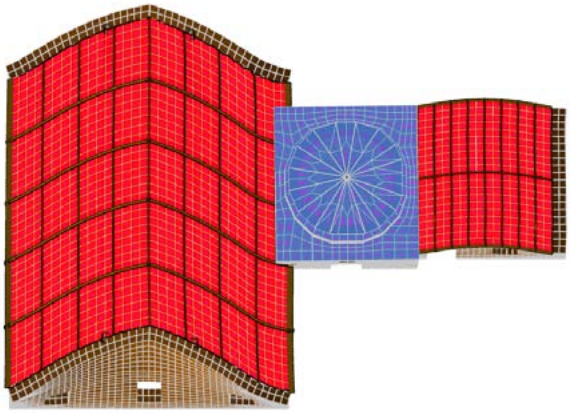

Strong-Backs N/S

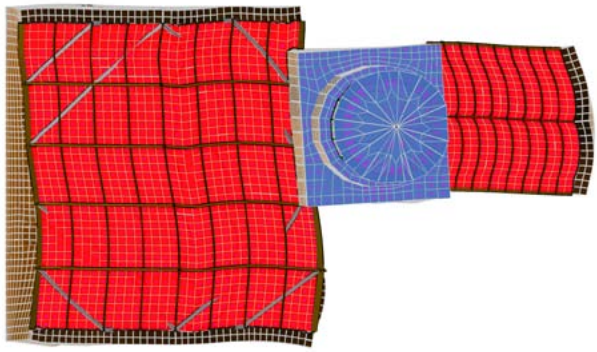

Diamond Braces E/W

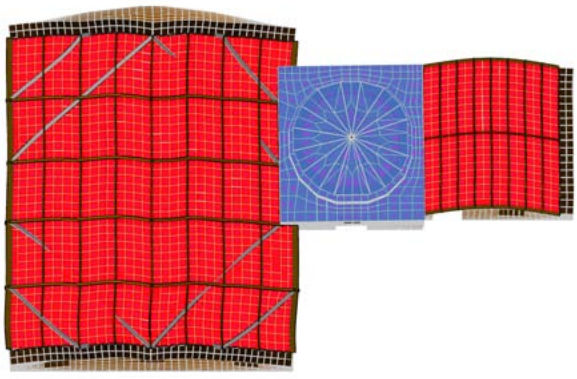

Diamond Braces N/S

Figure 5.4-2a: ELFP Displacements in Plan

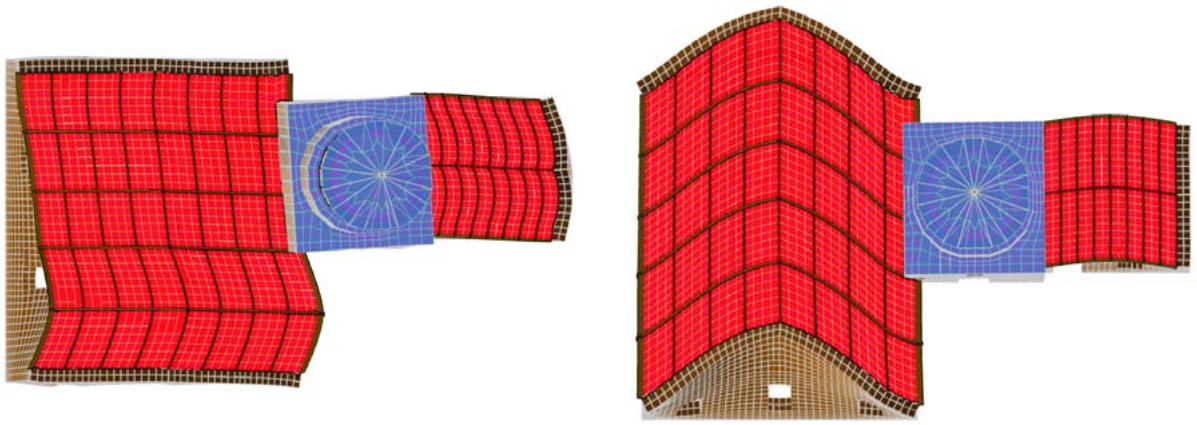

HSB E/W HSB N/S

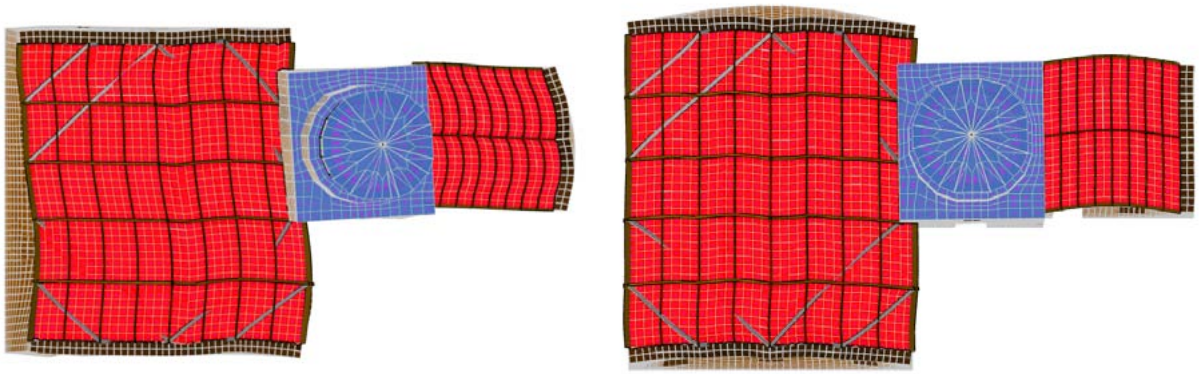

DB+HSB E/W DB+HSB N/S

Figure 5.4-2b: ELFP Displacements in Plan

The displacements from the ELFP analyses in the east-west and north-south directions for the fog room gabled wall, fog room rectangular wall, radio room gabled wall, radio room rectangular wall, and tower are shown in Figures 5.4-4 through 5.4-8 in order to provide a clearer picture of the smaller sections of the lighthouse with each of the retrofit schemes. The displacements of the walls were plotted in "heat map" style, where the larger displacements are in the lighter yellow and the smaller, sometimes even negative, displacements are in darker blue. The displacements for the tower were drawn in wireframe and scaled up for visualization. The maximum displacement for each section of the lighthouse is noted in inches. The displacements of the fog room gabled wall are also shown in Figure 5.4-3 in section.

5.4.2 Fog Room Gabled Wall

The fog room's gabled wall displacements were decreased with the addition of strong-backs or horizontal strong-backs, but those retrofit schemes were ineffective in restraining the top edge of the wall. Figure 5.4-3 clearly shows just how effective the retrofit schemes with diamond braces were at reducing the maximum displacements in the wall as well as restraining the wall out-of-plane. The "heat map" figures show that the Strong-Backs and HSB schemes were effective at reducing the displacements nearest the strong-back members themselves when loading in the east-west direction but did not change the displacement pattern of the wall like the retrofit schemes with diamond braces did. One of the reasons why the schemes with diamond braces were so effective at reducing the displacement of the walls is because the connection to the tower provided both restraint and stiffness out-of-plane to all of the walls in the fog room, especially the gabled walls.

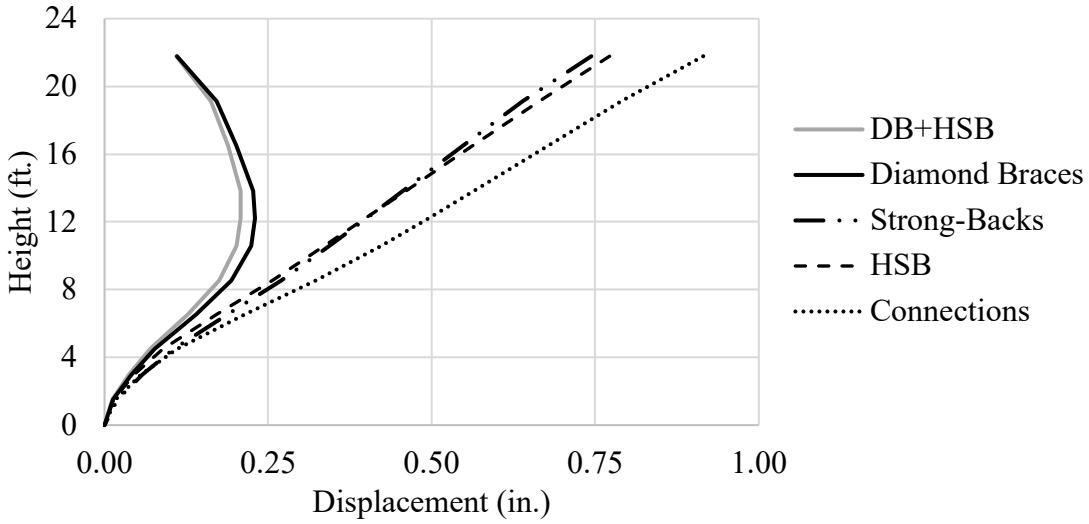

Figure 5.4-3: Fog Room Gabled Wall ELFP Displacements in Section

5.4.3 Fog Room Rectangular Wall

The retrofit schemes with diamond braces had the largest effect on the fog room rectangular wall displacements out-of-plane due to their ability to transfer the applied load to the adjacent gabled walls and tower when loading in the east-west direction out-of-plane. The schemes involving strong-backs had more of an effect on the ELFP displacements than they did on the modal displacements in the fog room rectangular wall because of the relative stiffness of the walls with and without the added members as well as the effects of the strong-backs on the rotation of the junction of the walls. The strong-backs reduced displacements significantly.

5.4.4 Radio Room Gabled Wall

The displacements in the radio room gabled wall due to the ELFP analysis were negligible and even the displacement patterns were affected very little by the retrofit schemes. The main reason for this was that the wall is short in length and has a higher height to thickness ratio than some of the other walls, making it stiffer both in-plane and out-of-plane.

5.4.5 Radio Room Rectangular Wall

The displacements in the radio room rectangular wall were also negligible when applying the ELFP analysis in the east-west direction, in the plane of the wall. The wall displaced more when loaded in the north-south direction, but the displacement pattern and values were largely unaffected by the retrofit scheme. The radio room rectangular wall is also stiffer in-plane than some of the other walls in the lighthouse because of its lower length to thickness and height to thickness ratios.

5.4.6 Tower

The tower displacements were largely unaffected by the retrofit scheme installed in the fog room since the maximum displacements were the same for all schemes when applying the ELFP analysis in the east-west or north-south direction. The only irregularities in the tower's displacements were a small amount of counter-clockwise twist when displacing in the east-west or north-south directions. The twist can be explained by the doorways in the base of the tower section that decrease the lateral stiffness of the south and east sides of the tower section as well as by the stiffness of the adjoining walls.

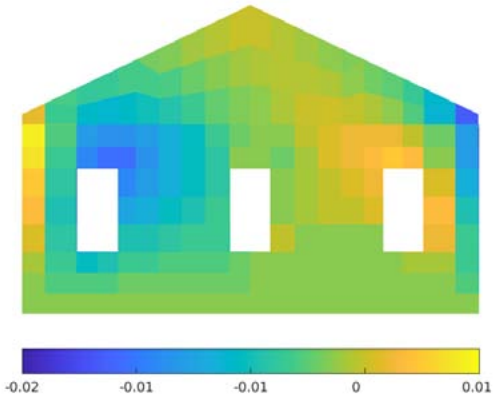

Connections E/W (0.02″)

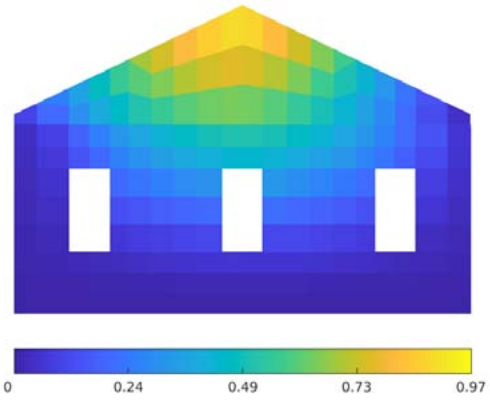

Connections N/S (0.97″)

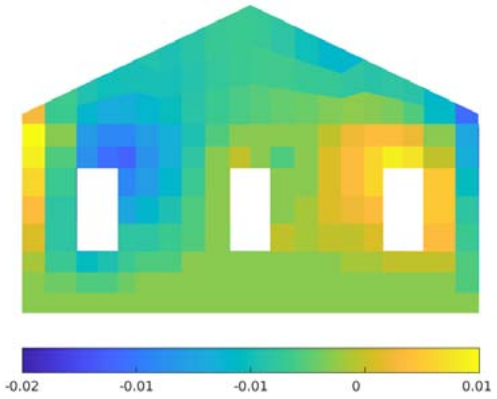

Strong-Backs E/W (0.02″)

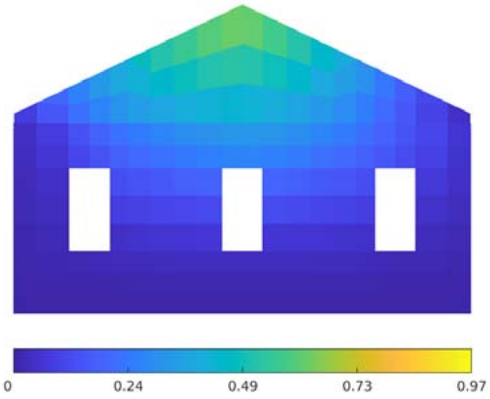

Strong-Backs N/S (0.69″)

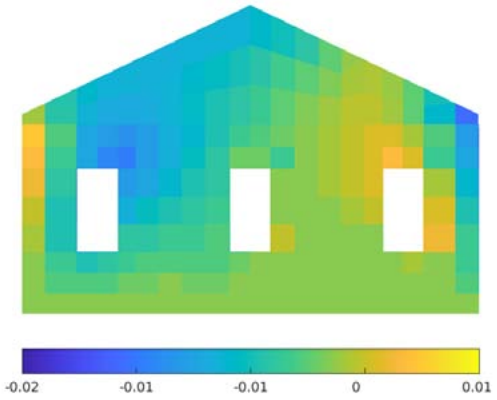

Diamond Braces E/W (0.02″)

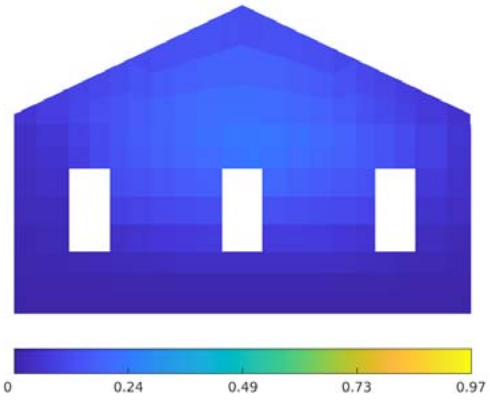

Diamond Braces N/S (0.23″)

Figure 5.4-4a: Fog Room Gabled Wall ELFP Displacements
(Maximum Displacement Out-of-Plane, in.)

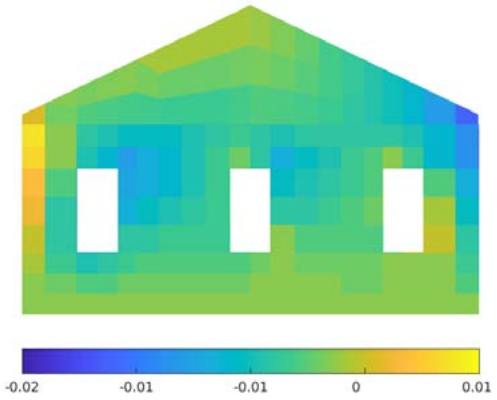

HSB E/W (0.02″)

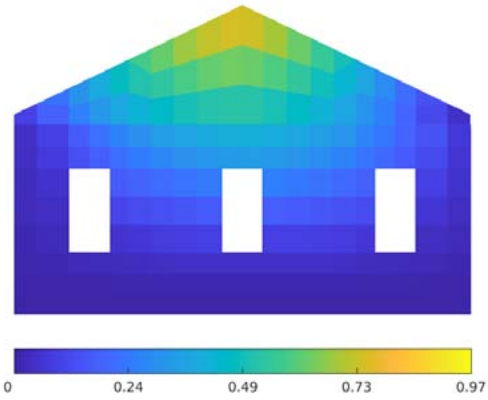

HSB N/S (0.82″)

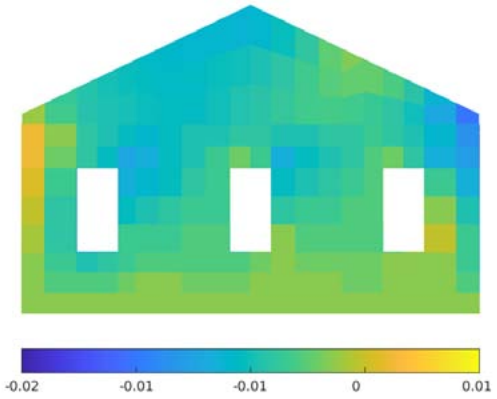

DB+HSB E/W (0.02″)

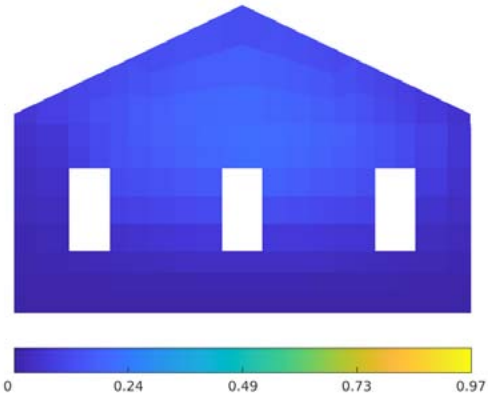

DB+HSB N/S (0.21″)

Figure 5.4-4b: Fog Room Gabled Wall ELFP Displacements
(Maximum Displacement Out-of-Plane, in.)

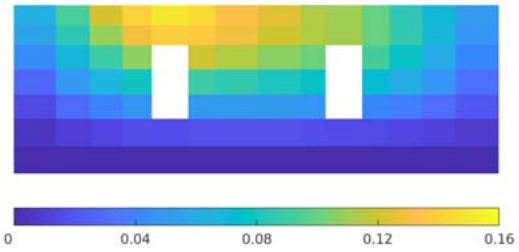

Connections E/W (0.16″)

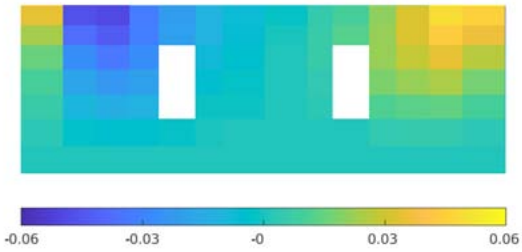

Connections N/S (0.06″)

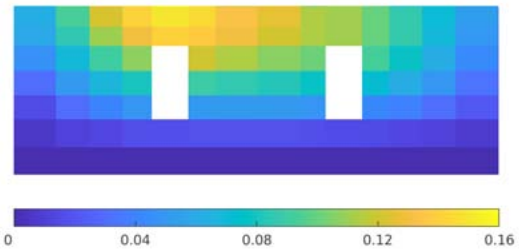

Strong-Backs E/W (0.16″)

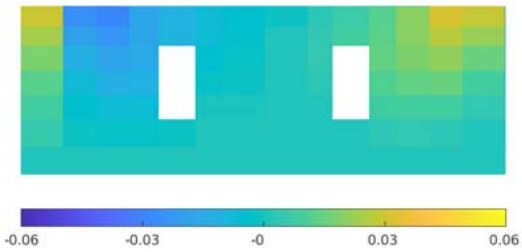

Strong-Backs N/S (0.04″)

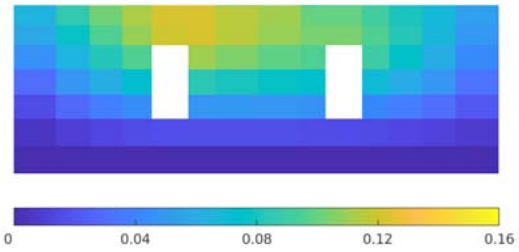

Diamond Braces E/W (0.13″)

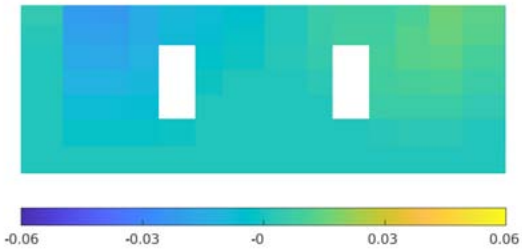

Diamond Braces N/S (0.03″)

Figure 5.4-5a: Fog Room Rectangular Wall ELFP Displacements
(Maximum Displacement Out-of-Plane, in.)

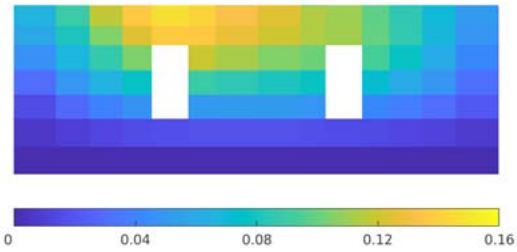

HSB E/W (0.16″)

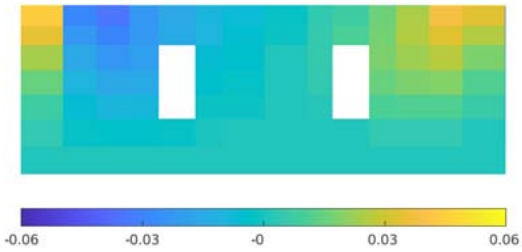

HSB N/S (0.05″)

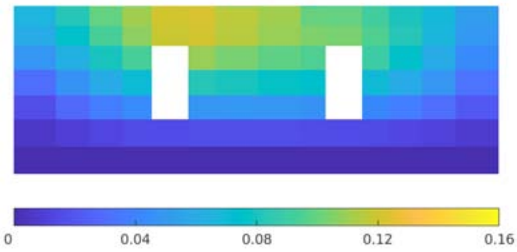

DB+HSB E/W (0.13″)

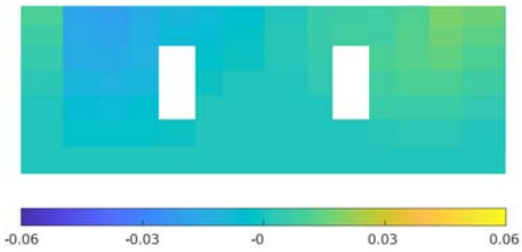

DB+HSB N/S (0.02″)

Figure 5.4-5b: Fog Room Rectangular Wall ELFP Displacements
(Maximum Displacement Out-of-Plane, in.)

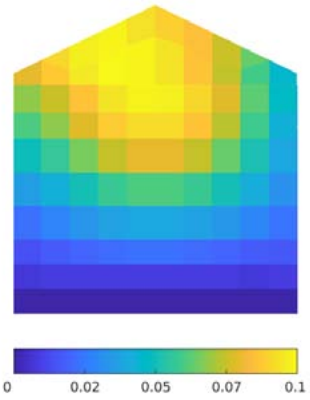

Connections E/W (0.01″)

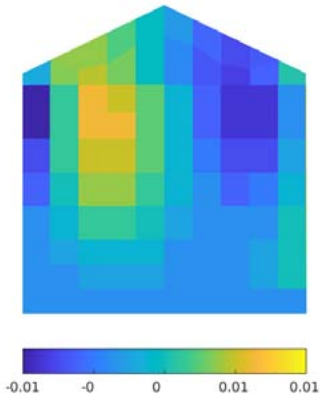

Connections N/S (0.01″)

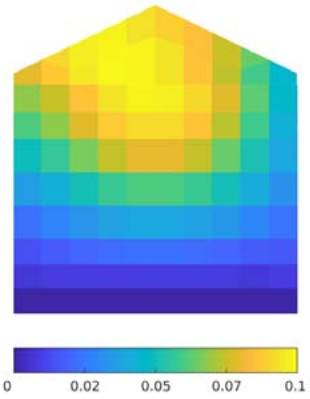

Strong-Backs E/W (0.01″)

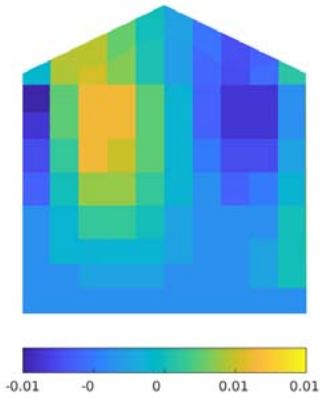

Strong-Backs N/S (0.01″)

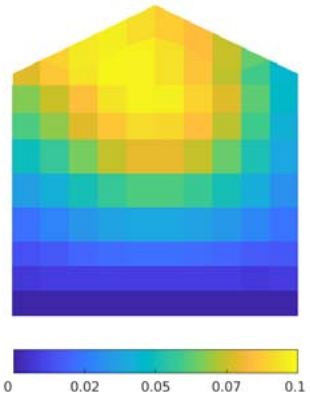

Diamond Braces E/W (0.01″)

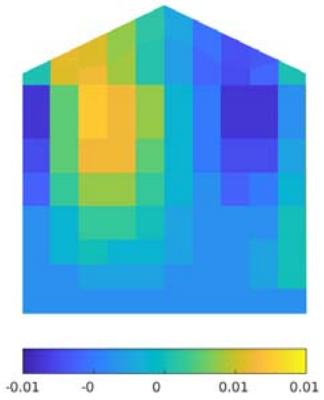

Diamond Braces N/S (0.01″)

Figure 5.4-6a: Radio Room Gabled Wall ELFP Displacements
(Maximum Displacement Out-of-Plane, in.)

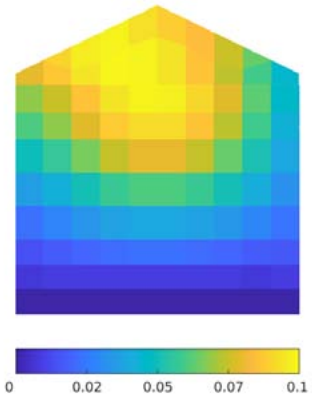

HSB E/W (0.01″)

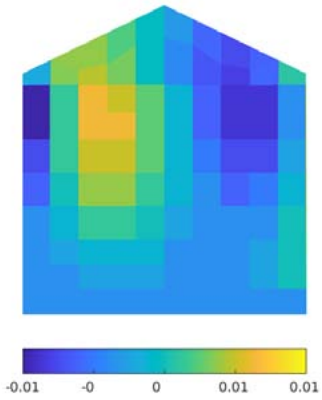

HSB N/S (0.01″)

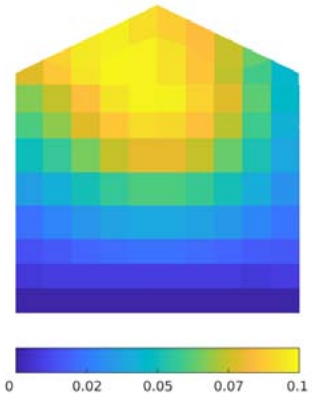

DB+HSB E/W (0.01″)

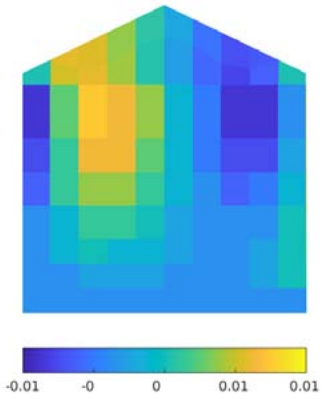

DB+HSB N/S (0.01″)

Figure 5.4-6b: Radio Room Gabled Wall ELFP Displacements
(Maximum Displacement Out-of-Plane, in.)

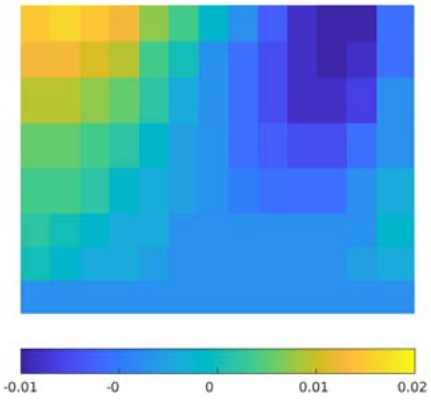

Connections E/W (0.02″)

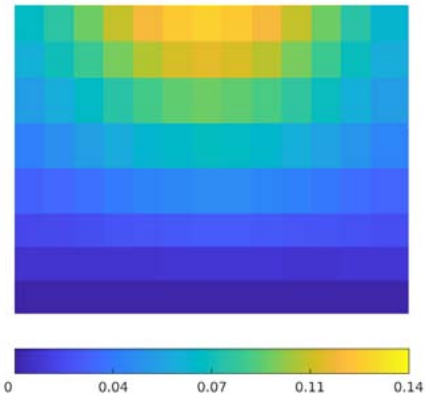

Connections N/S (0.14″)

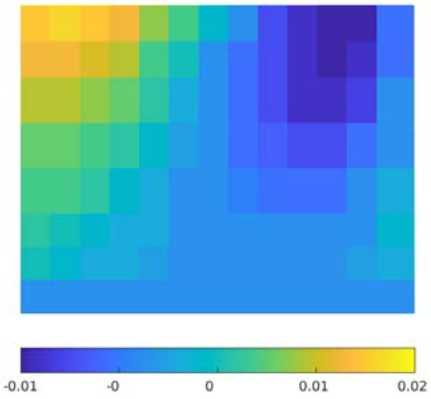

Strong-Backs E/W (0.02″)

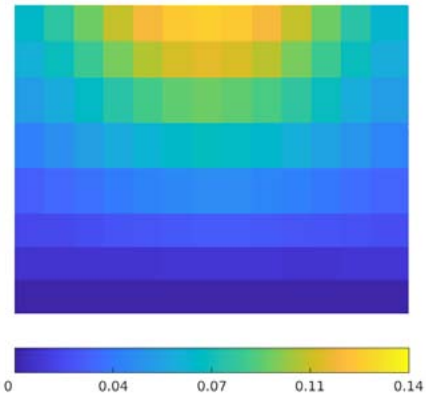

Strong-Backs N/S (0.14″)

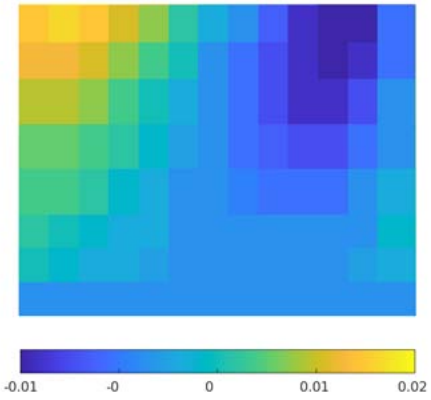

Diamond Braces E/W (0.02″)

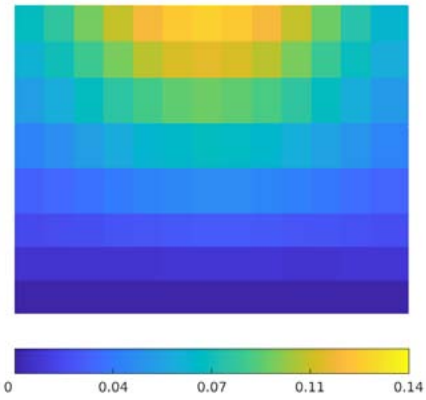

Diamond Braces N/S (0.14″)

Figure 5.4-7a: Radio Room Rectangular Wall ELFP Displacements
(Maximum Displacement Out-of-Plane, in.)

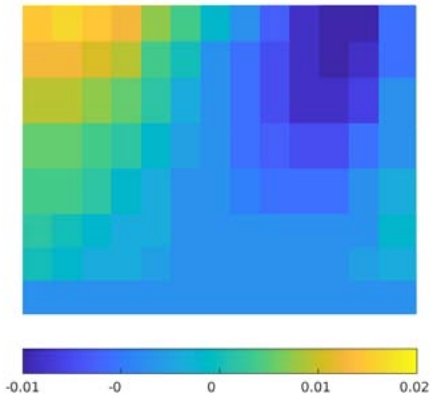

HSB E/W (0.02″)

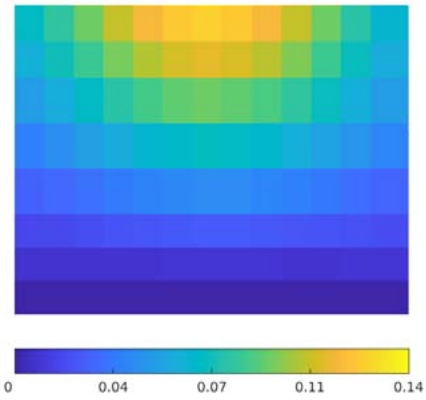

HSB N/S (0.14″)

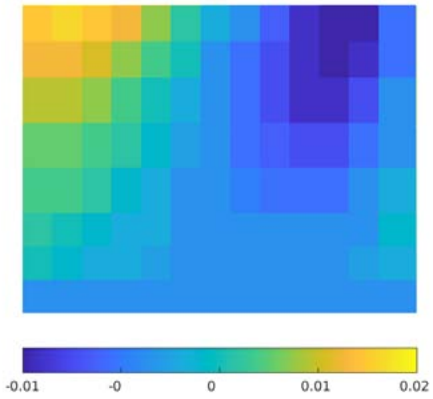

DB+HSB E/W (0.02″)

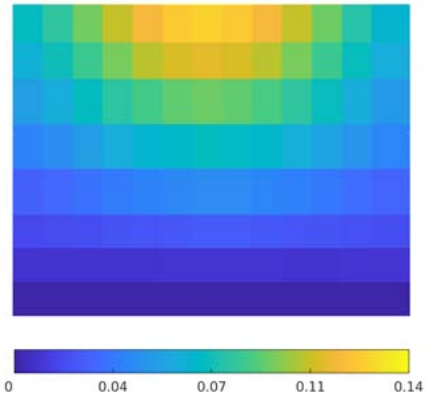

DB+HSB N/S (0.14″)

Figure 5.4-7b: Radio Room Rectangular Wall ELFP Displacements
(Maximum Displacement Out-of-Plane, in.)

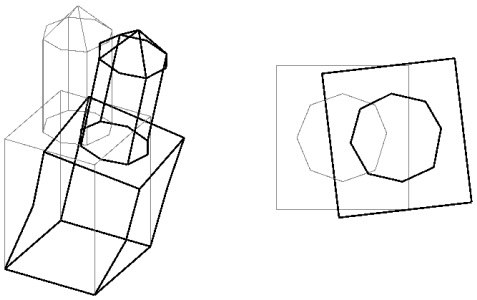

Connections E/W (0.16″)

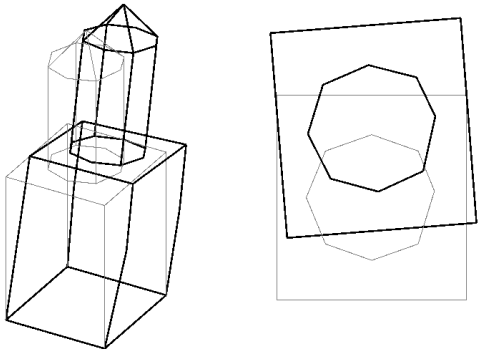

Connections N/S (0.14″)

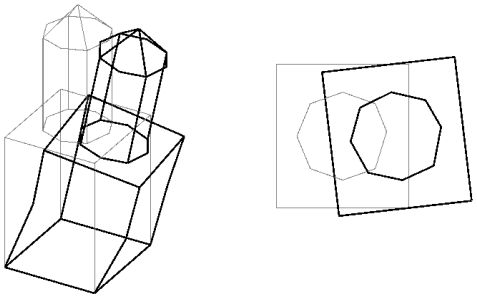

Strong-Backs E/W (0.16″)

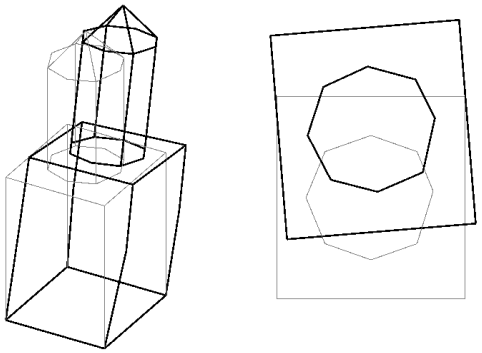

Strong-Backs N/S (0.14″)

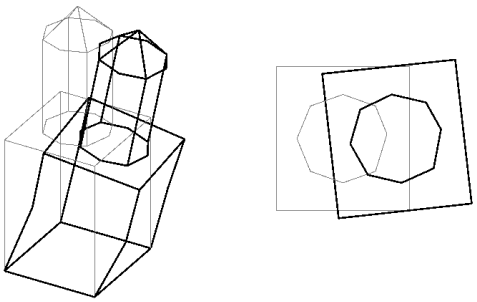

Diamond Braces E/W (0.16″)

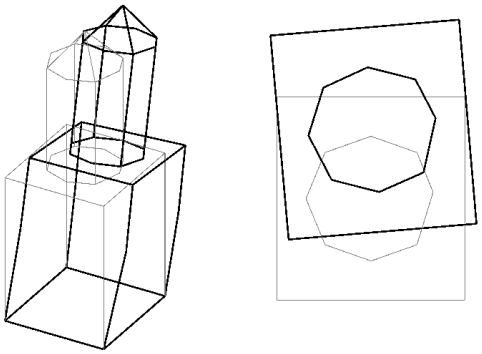

Diamond Braces N/S (0.14″)

Figure 5.4-8a: Tower ELFP Displacements
(Maximum Displacement at Peak, in.)

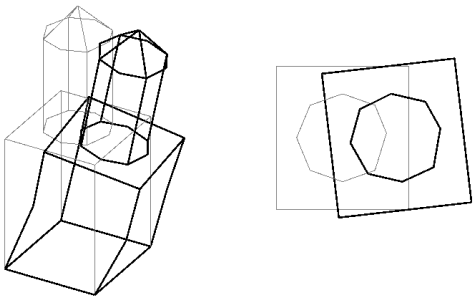

HSB E/W (0.16″)

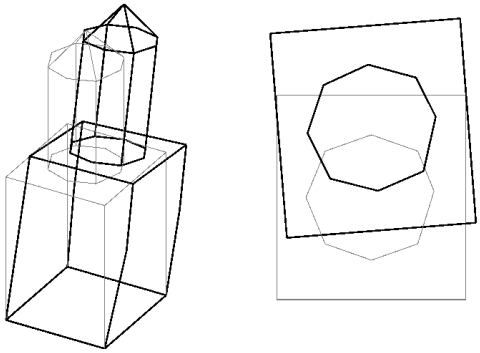

HSB N/S (0.14″)

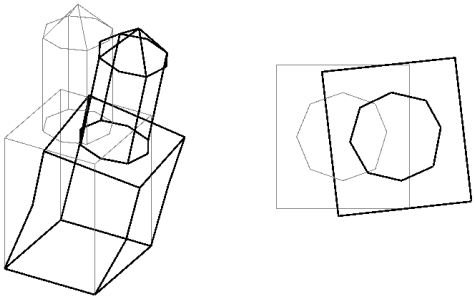

DB+HSB E/W (0.16″)

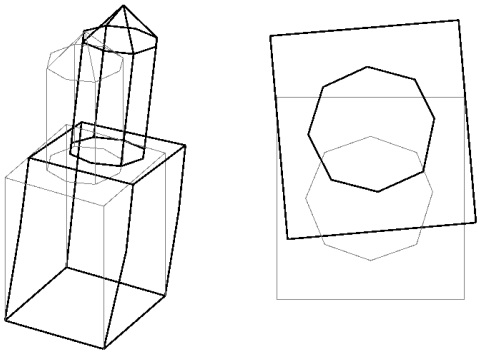

DB+HSB N/S (0.14″)

Figure 5.4-8b: Tower ELFP Displacements
(Maximum Displacement at Peak, in.)

5.5 Modal Response Spectrum Analysis

5.5.1 Full Lighthouse

The displacements from the modal response spectrum analysis in the lighthouse model with each of the retrofit schemes are shown in isometric view in Figure 5.5-1 and in plan in Figure 5.5-2. All displacements were plotted as their absolute values because of limitations in RISA-3D, but it was still clear the displacement patterns would have been similar to the displacement patterns from the ELFP analysis as well as the modal analysis had the displacements retained their original signs. The largest displacements when analyzing the lighthouse in the north-south direction were found in the gabled walls of the fog room, whether they were at the peak of the wall or near the mid-height when the retrofit scheme included diamond braces. The diamond braces were successful at restraining the top edges of all the walls in the fog room by providing a connection to perpendicular walls and ultimately the tower for support. It was difficult to compare the exact displacements in isometric and plan views, but it was apparent that the diamond braces were by far the most effective at restraining the gabled walls out-of-plane as well as supporting other portions of the fog room.

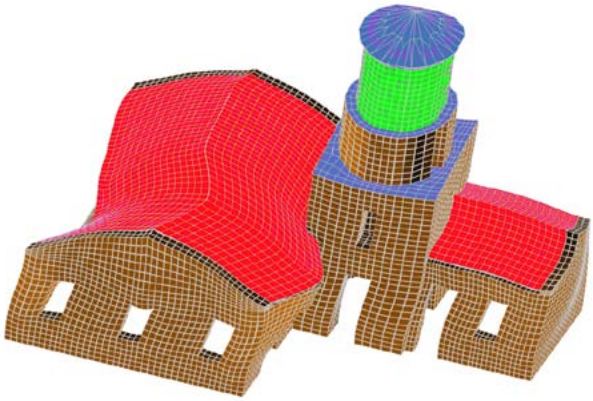

Connections E/W

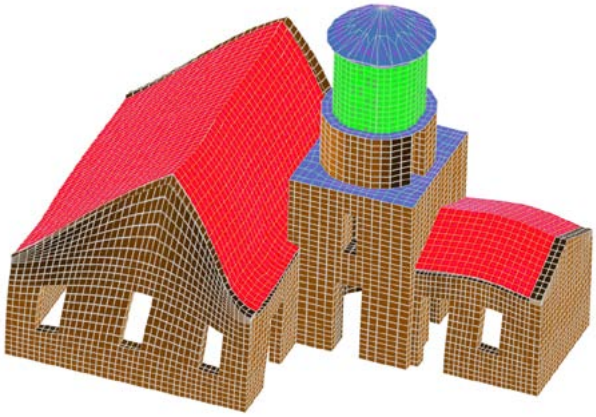

Connections N/S

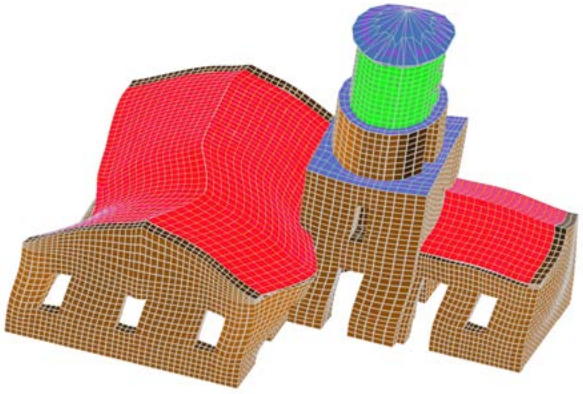

Strong-Backs E/W

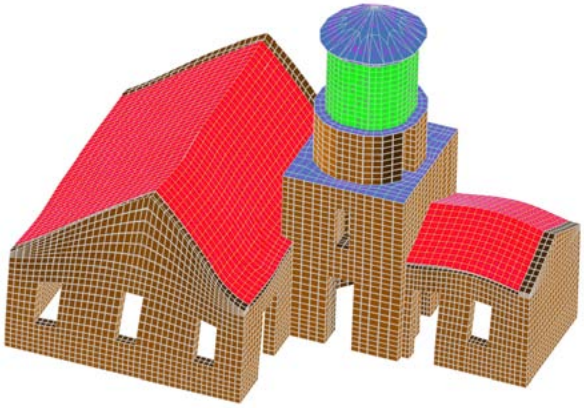

Strong-Backs N/S

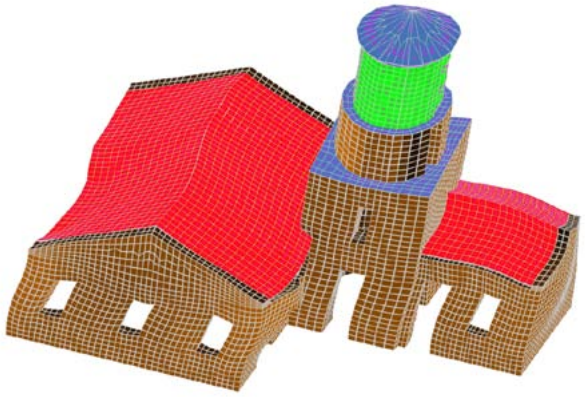

Diamond Braces E/W

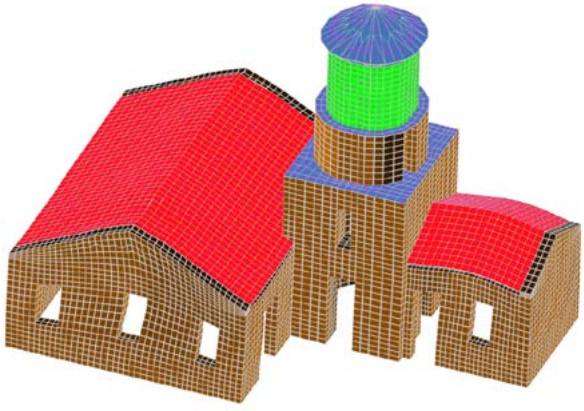

Diamond Braces N/S

Figure 5.5-1a: MRSA Displacements in Isometric View

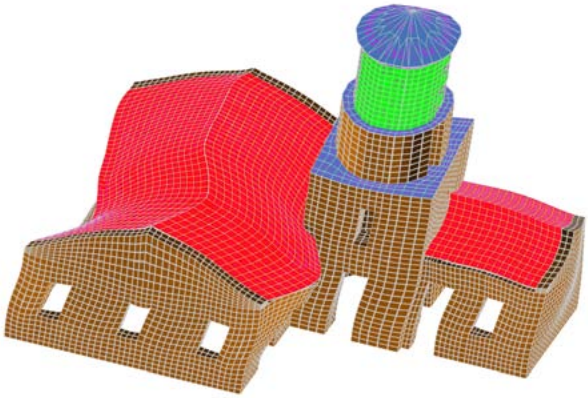

HSB E/W

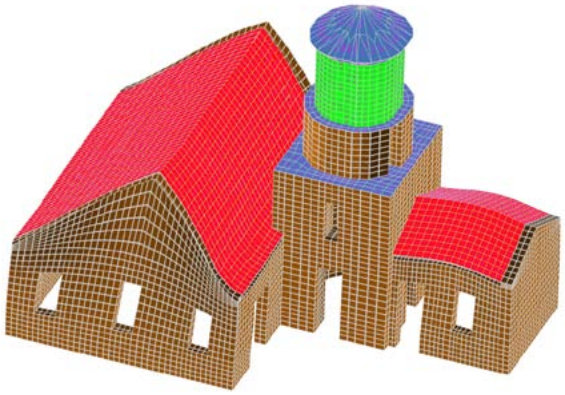

HSB N/S

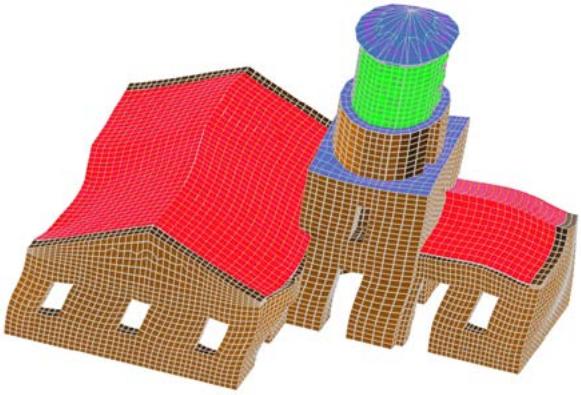

DB+HSB E/W

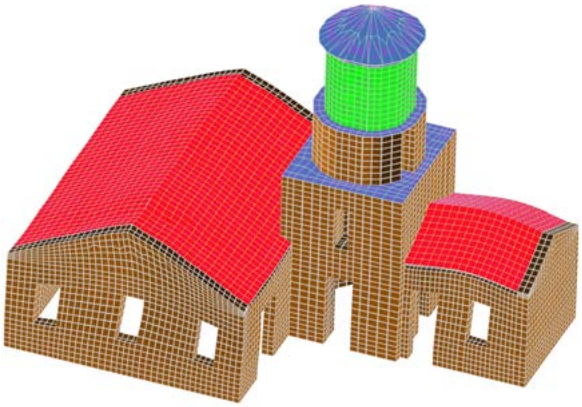

DB+HSB N/S

Figure 5.5-1b: MRSA Displacements in Isometric View

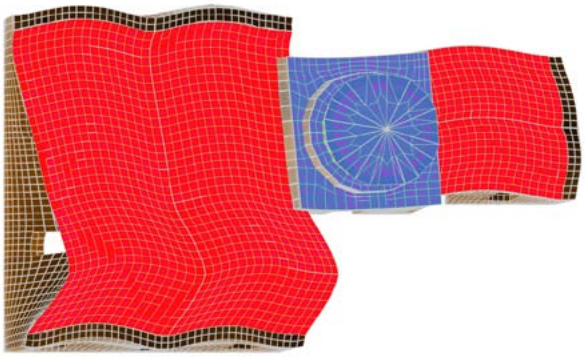

Connections E/W

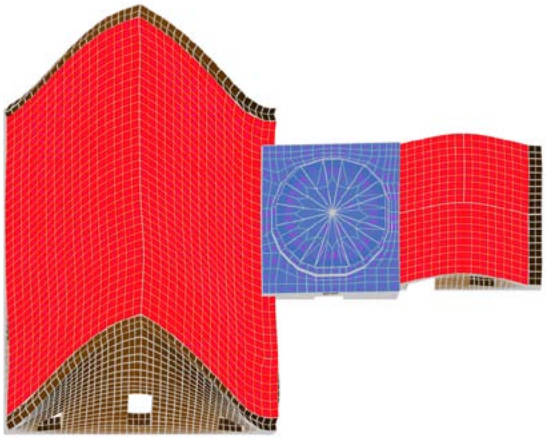

Connections N/S

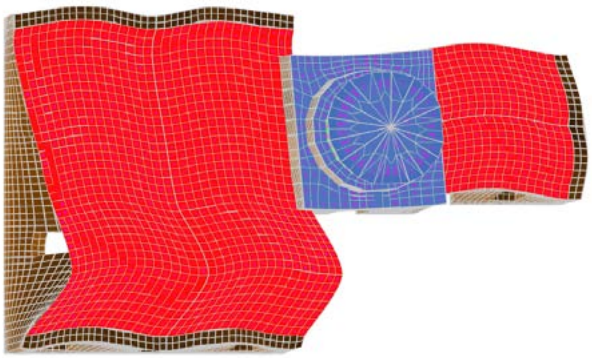

Strong-Backs E/W

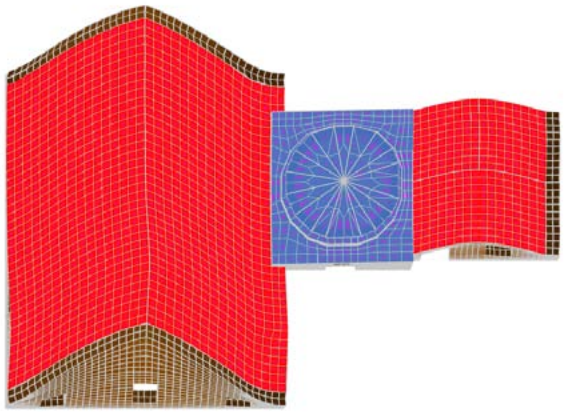

Strong-Backs N/S

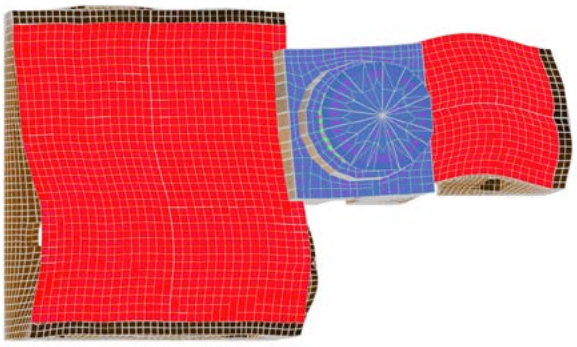

Diamond Braces E/W

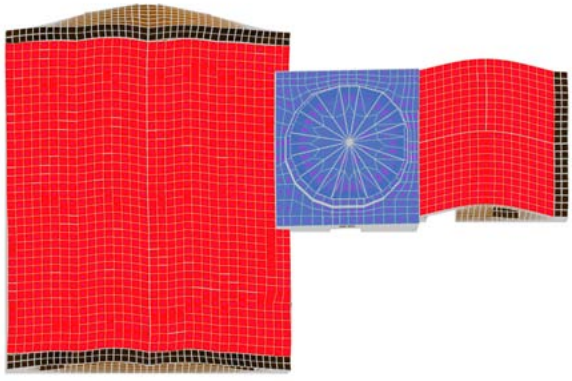

Diamond Braces N/S

Figure 5.5-2a: MRSA Displacements in Plan

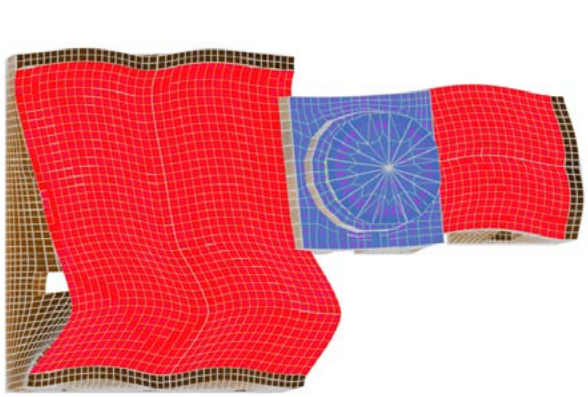

HSB E/W

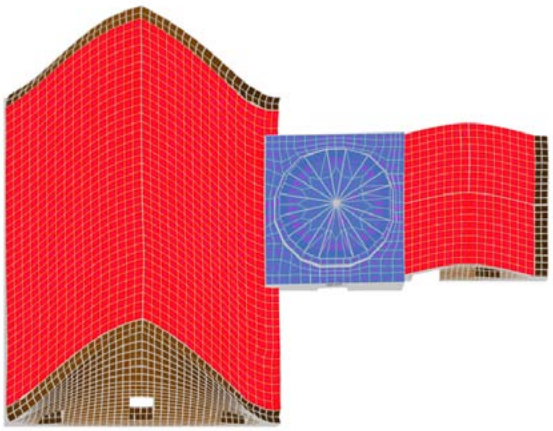

HSB N/S

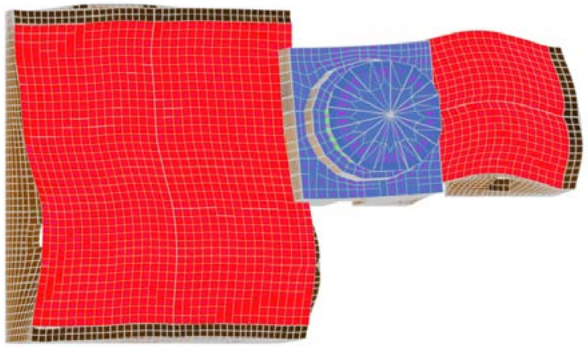

DB+HSB E/W

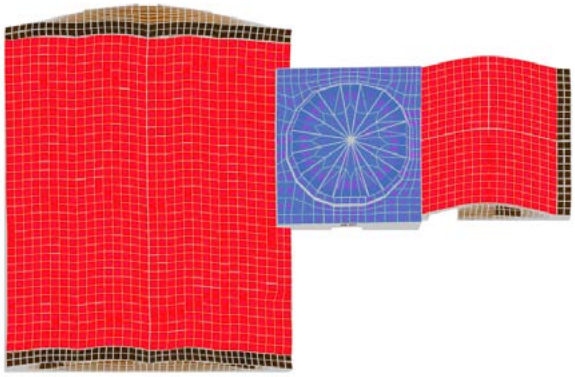

DB+HSB N/S

Figure 5.5-2b: MRSA Displacements in Plan

The displacements from the MRSA analyses in the east-west and north-south directions for the fog and radio rooms' walls of interest and the tower are shown in elevation in Figures 5.5-4 through 5.5-8 in order to get a clearer look at smaller sections of the lighthouse with each of the retrofit schemes. The fog room gabled wall displacements are also shown in Figure 5.5-3 in section. The displacements of the walls were plotted in "heat map" style, with the larger displacements in lighter yellow and smaller displacements in darker blue. The displaced tower was drawn in wireframe and its displacements were scaled up for visualization. The maximum displacement for each section of the lighthouse is noted in inches.

5.5.2 Fog Room Gabled Wall

The resulting displacements of the fog room's gabled wall due to the MRSA analysis followed a similar pattern as those of the ELFP analysis, where the diamond braces restrained the top edge of the wall and the strong-backs reduced deflection over the Connections scheme. The main differences between the MRSA and ELFP displacements were that the MRSA displacements were slightly larger and there was a clearer separation in performance of the Strong-Backs and HSB schemes even though they were designed to the same criteria. The reason for the clearer separation between the schemes involving strong-backs is because there is a difference in the effects that each of the schemes has on the higher modes of the gabled wall, and the MRSA analysis can capture that difference while the ELFP analysis cannot. The "heat map" figures show that the HSB scheme was less effective than the Strong-Backs scheme at limiting the out-of-plane displacements of the gabled walls for both directions of the MRSA analysis, and the retrofit schemes with diamond braces were the most effective at limiting deflections overall.

The MRSA analysis showed that the diamond braces were similarly effective at improving the stiffness of the gabled walls in-plane as the horizontal strong-backs, which was not evident from other analyses. The diamond braces and horizontal strong-backs allowed similar deflections in the wall but in different patterns, where the displacement with the horizontal strong-backs was more concentrated and the displacement with the diamond braces was more widespread. The maximum displacement in the gabled walls with diamond brace retrofit schemes was concentrated at the top of the two areas between the three windows, where the maximum modal displacement was above the middle window. The main reason for this difference is the contribution of other modes that the MRSA analysis captured.

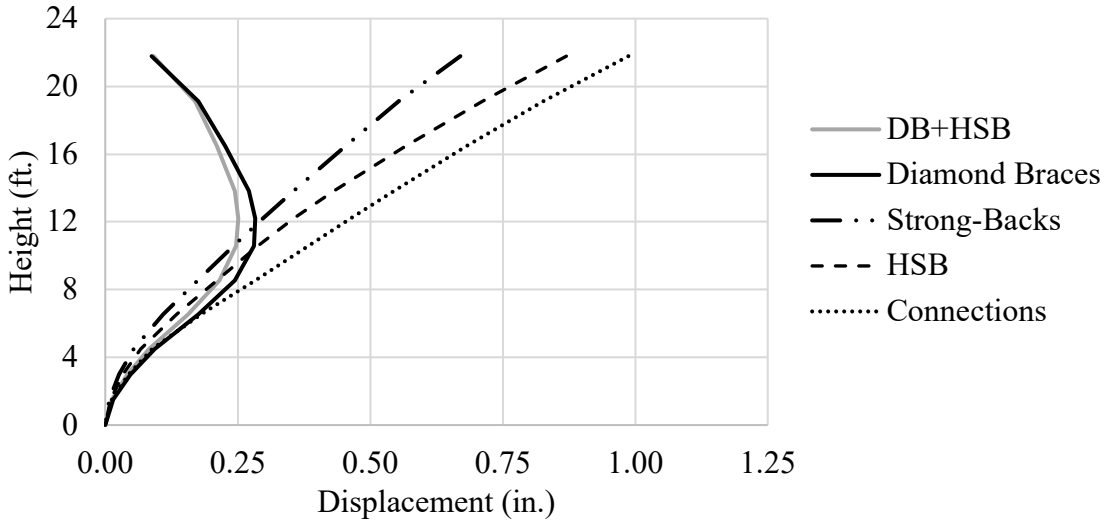

Figure 5.5-3: Fog Room Gabled Wall MRSA Displacements in Section

5.5.3 Fog Room Rectangular Wall

The displacement patterns in the fog room rectangular wall were very similar between the two MRSA analysis directions and it was clear that the retrofit schemes with diamond braces were also effective at reducing displacements in the fog room rectangular walls. The retrofit

schemes with strong-backs had little to no effect on the fog room rectangular walls though the HSB scheme had a larger effect than the Strong-Backs scheme at reducing the displacements at the top of the walls.

5.5.4 Radio Room Gabled Wall

Both the displacement magnitudes and displacement patterns from the MRSA analysis in the radio room gabled wall were affected very little by the retrofit scheme in the fog room. Previous analyses showed changes in the displacement pattern in the radio room gabled wall, but that was not the case for the MRSA analysis because the MRSA analysis showed that the stiffness characteristics unfairly highlighted by other analyses do not have as large of an effect in higher modes.

5.5.5 Radio Room Rectangular Wall

Unlike other analyses, the MRSA analysis on the radio room rectangular wall showed that retrofit schemes with diamond braces actually increased displacements out-of-plane in the east-west direction. The increase was small, but it was a good example of the MRSA analysis highlighting nuances that the other analyses could not. In general, the displacements in the radio room rectangular wall were largely unaffected by the retrofit scheme in the fog room.

5.5.6 Tower

The MRSA displacement results for the tower showed the differences of the retrofit schemes better than the ELFP analysis, though the differences in displacement were still small. The MRSA analysis showed a large amount of counter-clockwise distortion in the tower section from its original square shape into a diamond shape when loading in both directions. The distortion in the tower is the MRSA equivalent of the twist that was evident in the tower from the

ELFP results, and the reason for the distortion is the irregular stiffness at the base of the tower due to the doorways and adjoining walls. The tower distorted in the MRSA analysis rather than twisted because the distortion is a combination of the effects of more than one mode. The diamond braces alone reduced displacements in the tower when loading in the north-south direction but when coupled with the horizontal strong-backs, the displacements in the tower actually increased. As shown in other analyses, the retrofit scheme did not have a large effect outside of the fog room, especially in the tower.

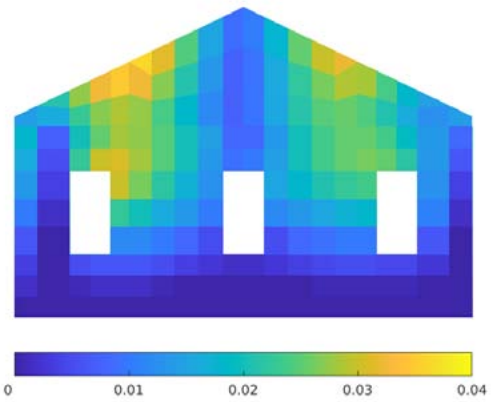

Connections E/W (0.04″)

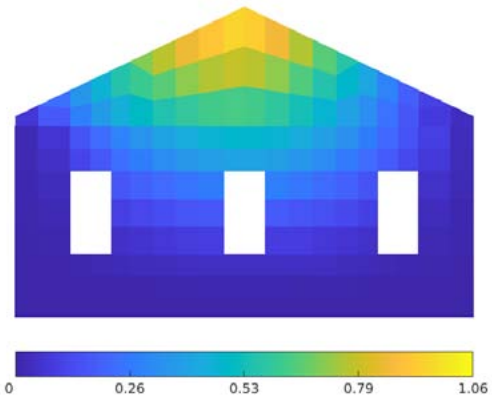

Connections N/S (1.06″)

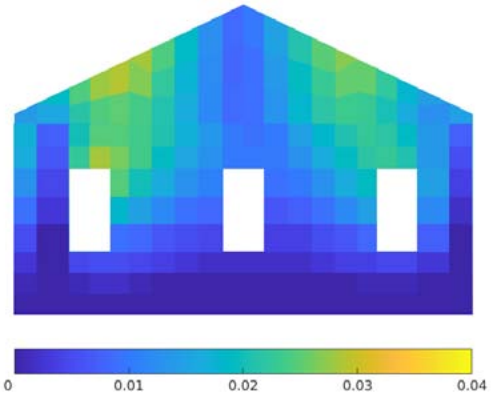

Strong-Backs E/W (0.04″)

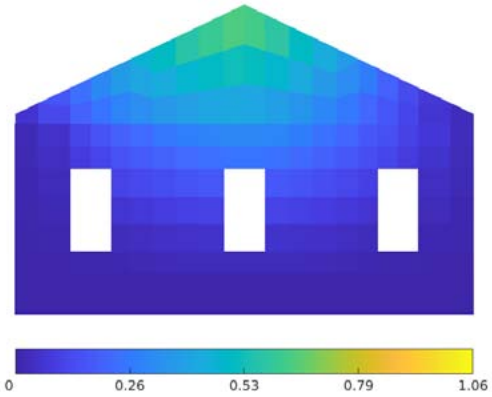

Strong-Backs N/S (0.72″)

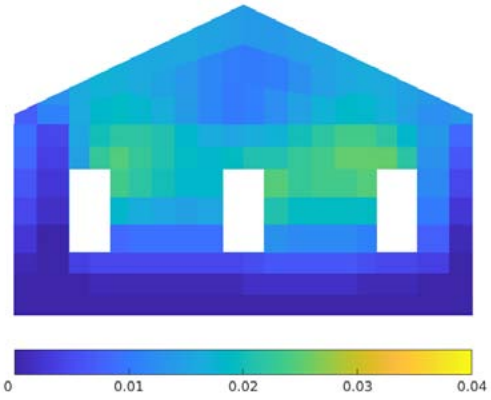

Diamond Braces E/W (0.03″)

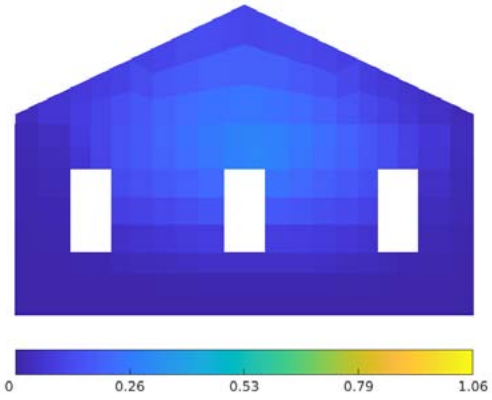

Diamond Braces N/S (0.30″)

Figure 5.5-4a: Fog Room Gabled Wall MRSA Displacements
(Maximum Displacement Out-of-Plane, in.)

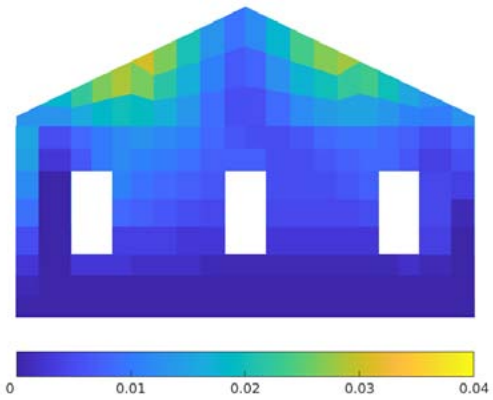

HSB E/W (0.04″)

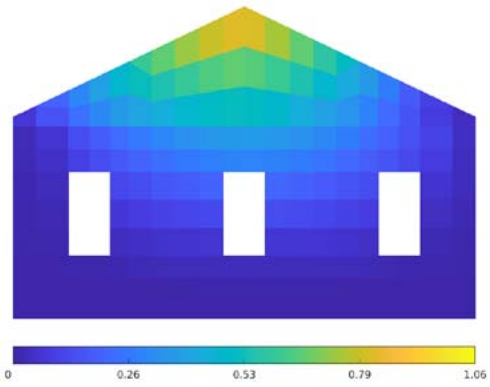

HSB N/S (0.93″)

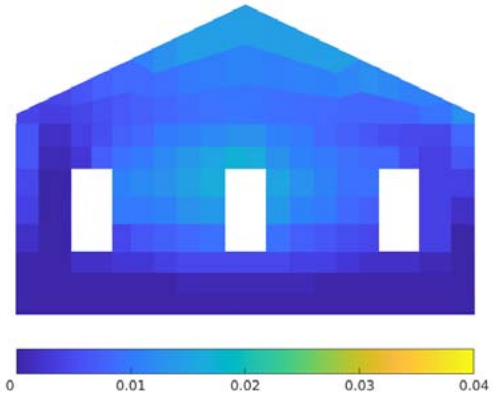

DB+HSB E/W (0.02″)

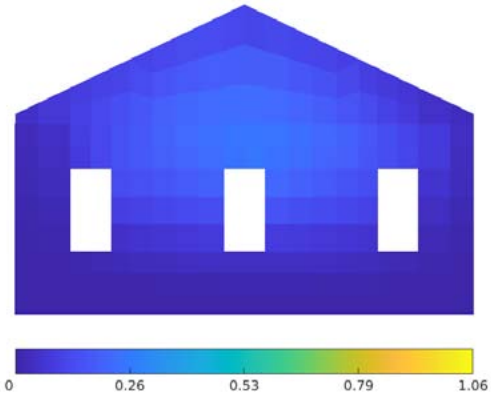

DB+HSB N/S (0.26″)

Figure 5.5-4b: Fog Room Gabled Wall MRSA Displacements
(Maximum Displacement Out-of-Plane, in.)

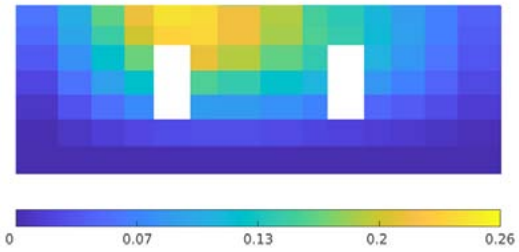

Connections E/W (0.25″)

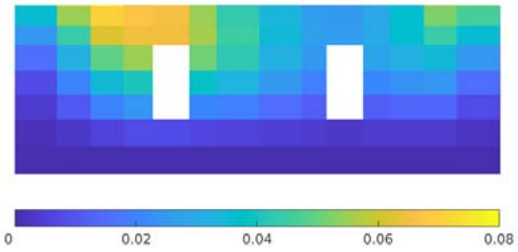

Connections N/S (0.08″)

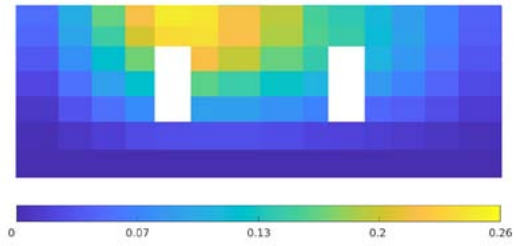

Strong-Backs E/W (0.26″)

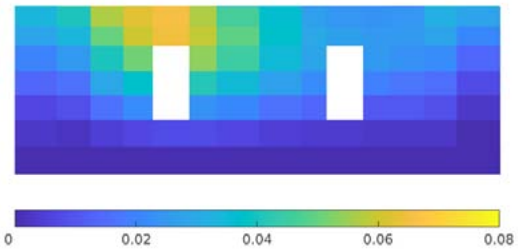

Strong-Backs N/S (0.07″)

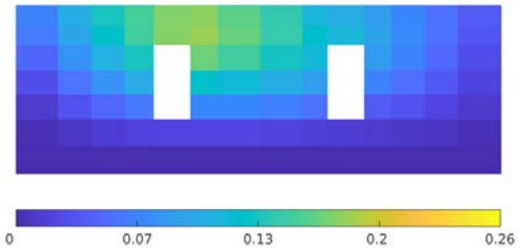

Diamond Braces E/W (0.18″)

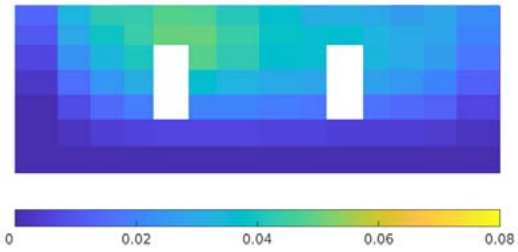

Diamond Braces N/S (0.05″)

Figure 5.5-5a: Fog Room Rectangular Wall MRSA Displacements
(Maximum Displacement Out-of-Plane, in.)

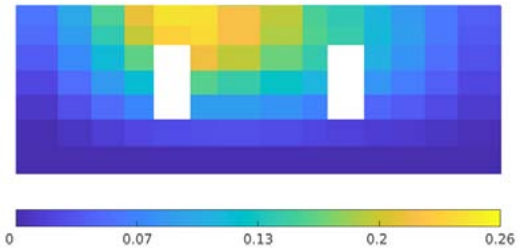

HSB E/W (0.25″)

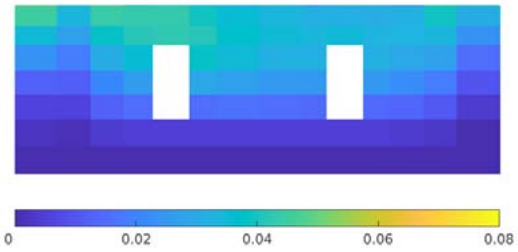

HSB N/S (0.06″)

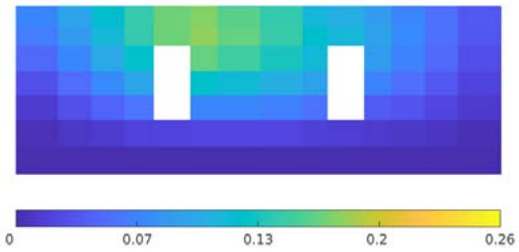

DB+HSB E/W (0.18″)

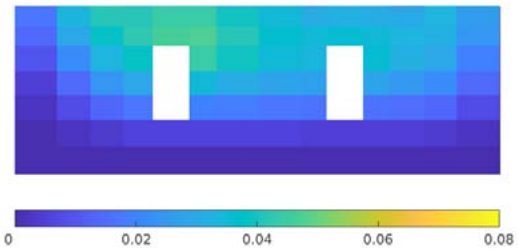

DB+HSB N/S (0.05″)

Figure 5.5-5b: Fog Room Rectangular Wall MRSA Displacements
(Maximum Displacement Out-of-Plane, in.)

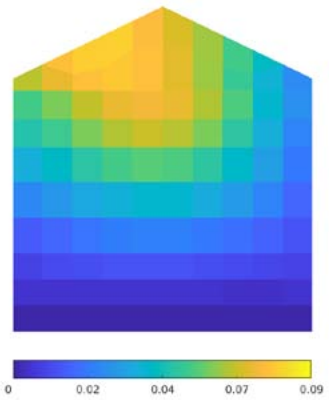

Connections E/W (0.08″)

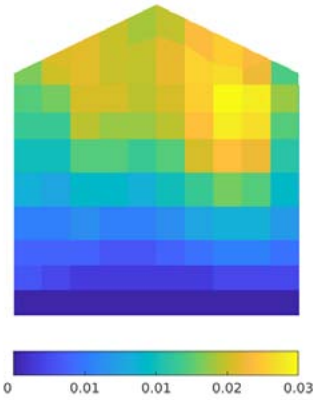

Connections N/S (0.03″)

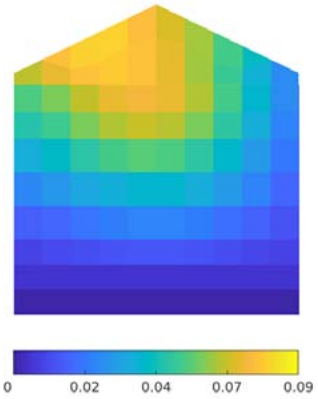

Strong-Backs E/W (0.08″)

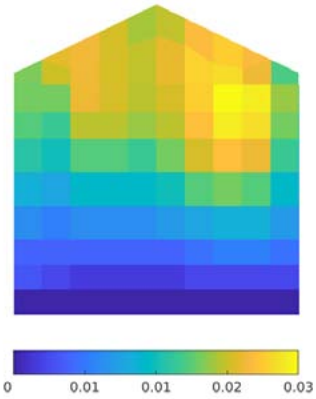

Strong-Backs N/S (0.03″)

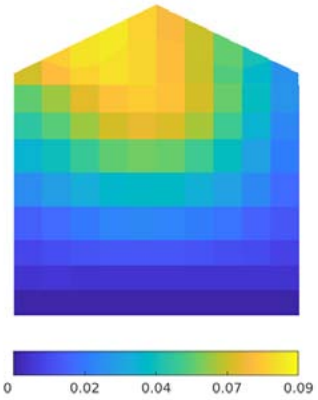

Diamond Braces E/W (0.09″)

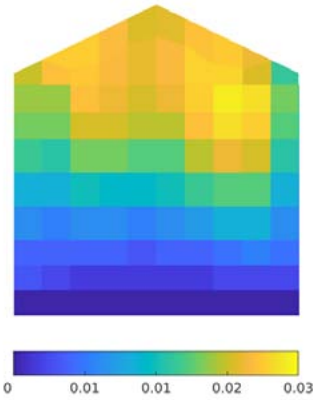

Diamond Braces N/S (0.03″)

Figure 5.5-6a: Radio Room Gabled Wall MRSA Displacements
(Maximum Displacement Out-of-Plane, in.)

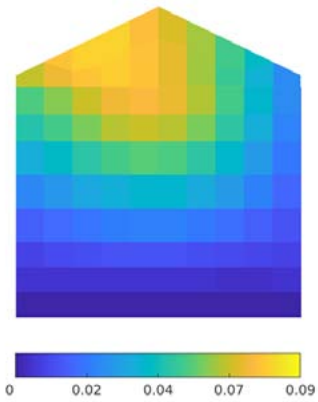

HSB E/W (0.08″)

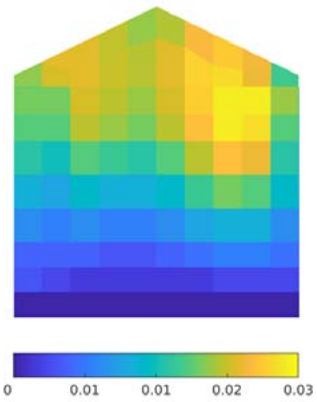

HSB N/S (0.03″)

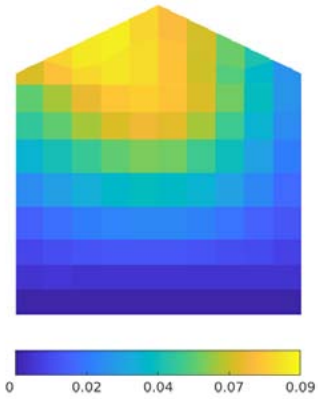

DB+HSB E/W (0.09″)

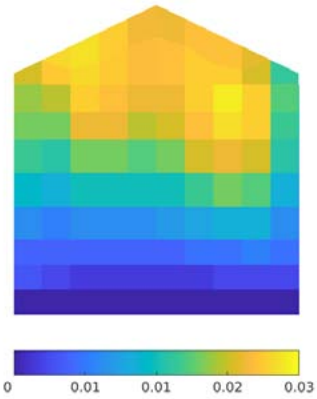

DB+HSB N/S (0.03″)

Figure 5.5-6b: Radio Room Gabled Wall MRSA Displacements
(Maximum Displacement Out-of-Plane, in.)

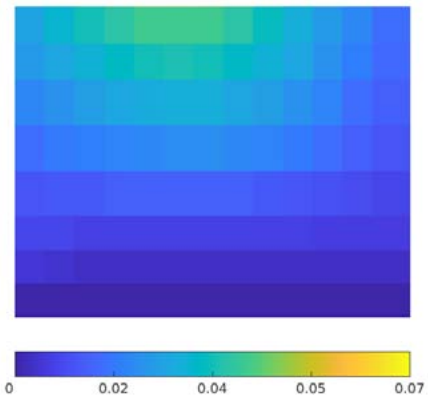

Connections E/W (0.05″)

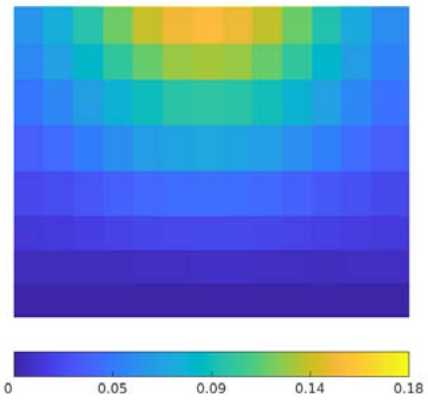

Connections N/S (0.18″)

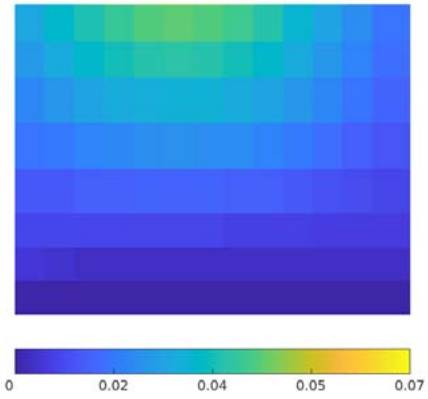

Strong-Backs E/W (0.05″)

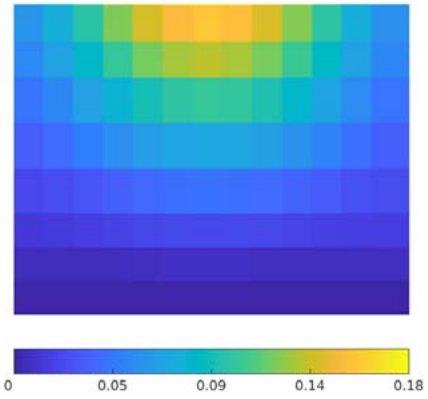

Strong-Backs N/S (0.18″)

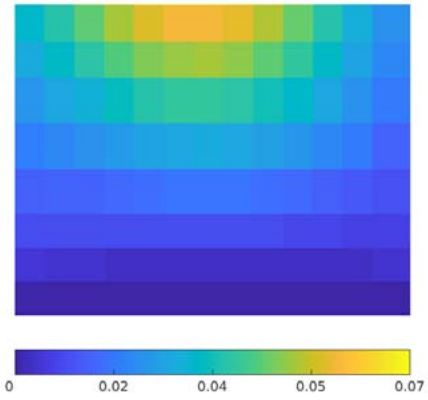

Diamond Braces E/W (0.07″)

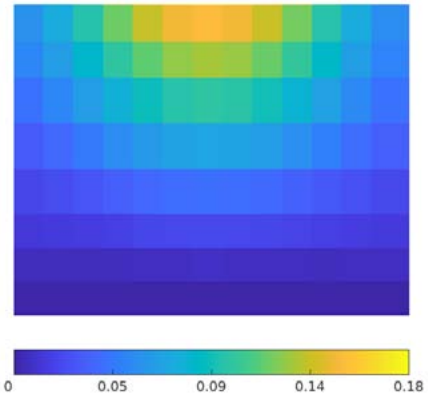

Diamond Braces N/S (0.18″)

Figure 5.5-7a: Radio Room Rectangular Wall MRSA Displacements
(Maximum Displacement Out-of-Plane, in.)

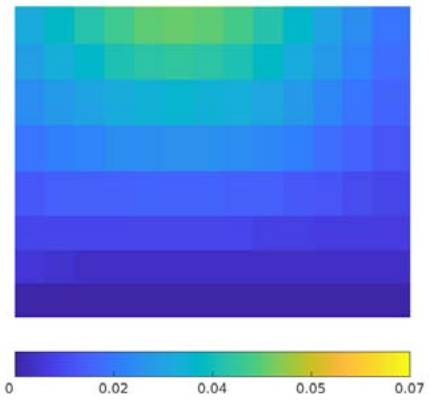

HSB E/W (0.05″)

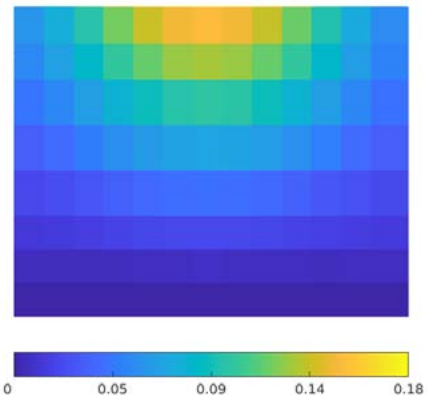

HSB N/S (0.18″)

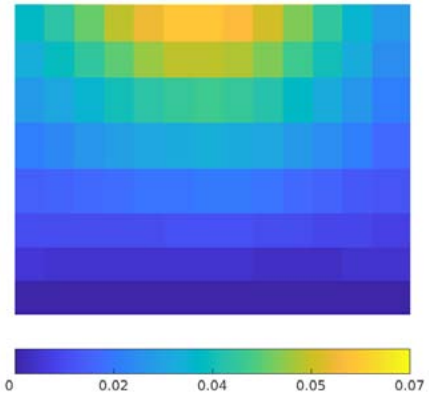

DB+HSB E/W (0.07″)

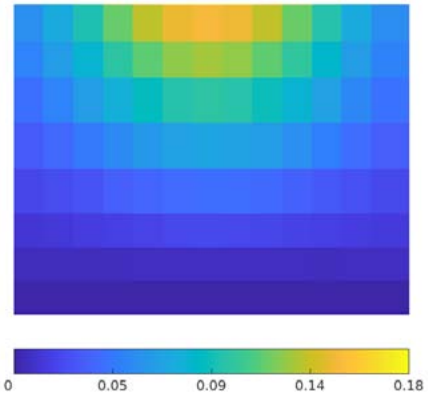

DB+HSB N/S (0.17″)

Figure 5.5-7b: Radio Room Rectangular Wall MRSA Displacements
(Maximum Displacement Out-of-Plane, in.)

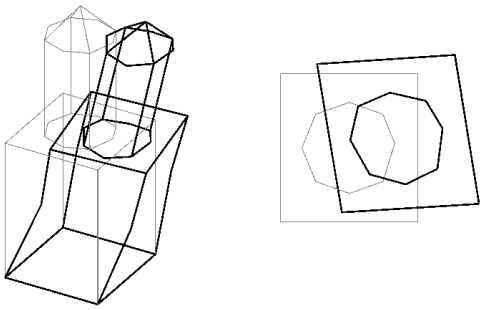

Connections E/W (0.15″)

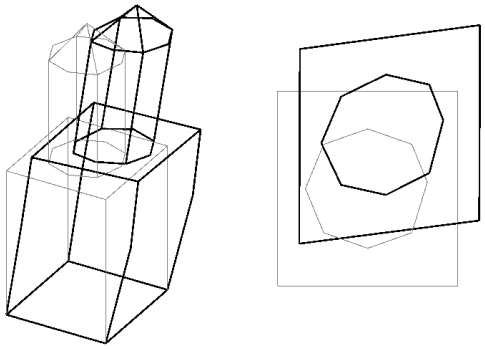

Connections N/S (0.13″)

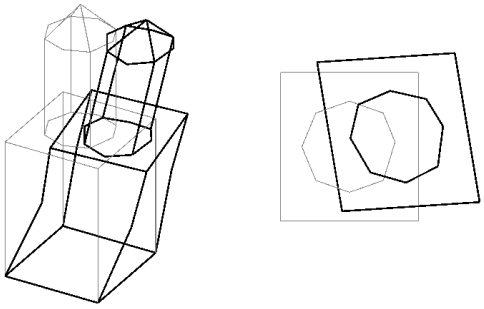

Strong-Backs E/W (0.15″)

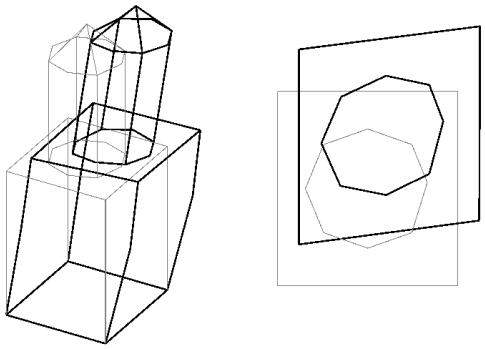

Strong-Backs N/S (0.13″)

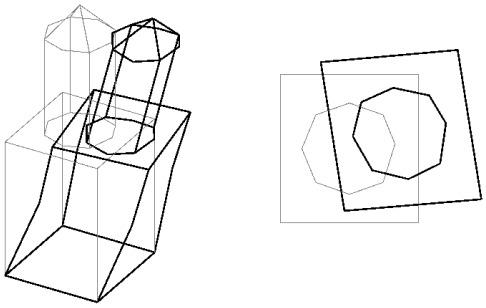

Diamond Braces E/W (0.15″)

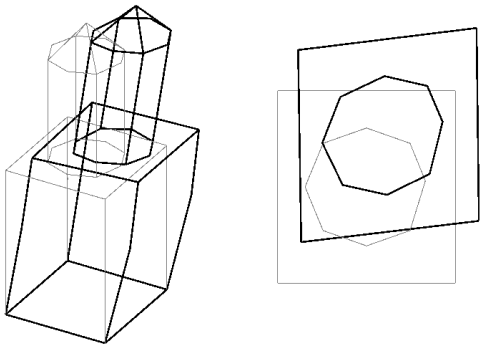

Diamond Braces N/S (0.12″)

Figure 5.5-8a: Tower MRSA Displacements
(Maximum Displacement at Peak, in.)

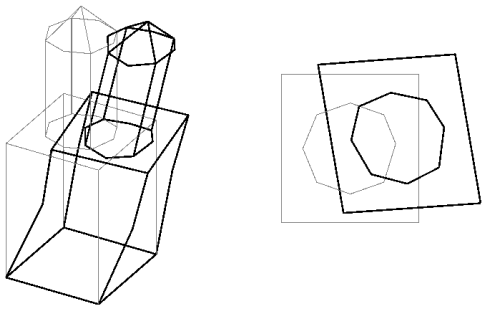

HSB E/W (0.15″)

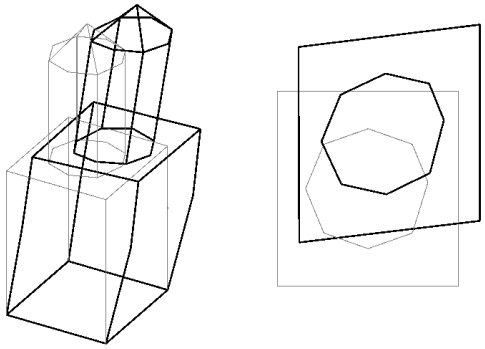

HSB N/S (0.13″)

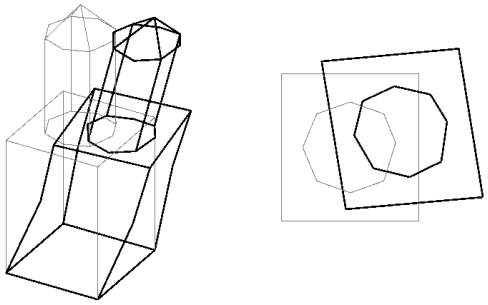

DB+HSB E/W (0.16″)

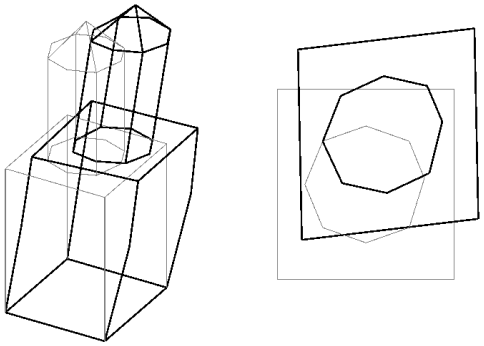

DB+HSB N/S (0.12″)

Figure 5.5-8b: Tower MRSA Displacements
(Maximum Displacement at Peak, in.)

5.6 Addition of Lens

5.6.1 Natural Frequencies, Periods, and Mass Participation

The retrofit scheme that had the largest change in any of the modal properties due to the addition of the lens into the finite element model was the Connections scheme, where the mass participation of the first fundamental tower mode increased by 7%. This change was larger than expected and may be due to an error in the analysis, since it is significantly larger than the percentage of mass added by the lens even though the lens was added to the top of the tower which would amplify its effects. The change in the mass participation for the other fundamental tower mode and decreases in natural frequency for both tower modes were closer to what was expected. The changes in modal properties for the Connections scheme due to the addition of the lens are summarized in Table 5.6-1, shown as percentages.

Table 5.6-1: Modal Property Changes from Added Lens, Connections Scheme (%)

Mode	ΔFreq. (Hz)	ΔPeriod (s)	ΔMP E/W (%)	ΔMP N/S (%)
1	-	-	-	-0.1
3	-0.7	0.9	7.0	0.8
5	-1.5	1.0	-	1.0

The largest change to any of the modal properties for the Strong-Backs scheme due to the addition of the lens came to the mass participation for the fundamental tower modes. The changes in mass participation were close to what was expected based on the added mass of the lens, as were the decreases in natural frequency. The changes in modal properties for the Strong-Backs scheme due to the addition of the lens are summarized in Table 5.6-2, shown as percentages.

Table 5.6-2: Modal Property Changes from Added Lens, Strong-Backs Scheme (%)

Mode	ΔFreq. (Hz)	ΔPeriod (s)	ΔMP E/W (%)	ΔMP N/S (%)
1	-	-	-	0.2
3	-1.1	1.9	0.8	1.0
4	-1.1	1.0	2.9	1.3

The Diamond Braces scheme is the only retrofit scheme to have a change in modal properties for the fundamental wall mode out-of-plane with the addition of the lens, though the change was relatively small and close to what was expected. The main reason for the change in the properties for the wall mode was the connection between the fog room gabled walls, rectangular walls, and the tower section where the lens was added. One unexpected change in modal properties for the Diamond Braces scheme was at the mass participation of the second fundamental tower mode, which decreased with the addition of the lens. The changes in modal properties for the Diamond Braces scheme due to the addition of the lens are summarized in Table 5.6-3, shown as percentages.

Table 5.6-3: Modal Property Changes from Added Lens, Diamond Braces Scheme (%)

Mode	ΔFreq. (Hz)	ΔPeriod (s)	ΔMP E/W (%)	ΔMP N/S (%)
1	-1.9	1.9	-	0
2	-1.1	0.9	0.7	0.1
3	-1.5	1.9	0.3	-3.1

The largest change to any of the modal properties for the HSB scheme with the addition of the lens came to the mass participation of the second fundamental tower mode. This change was unexpected due to the lack of connection between the gabled walls and tower section where the lens was added. Other changes in modal properties due to the addition of the lens were close

to what was expected based on the percentage of added mass with the lens. The changes in modal properties for the HSB scheme due to the addition of the lens are summarized in Table 5.6-4, shown as percentages.

Table 5.6-4: Modal Property Changes from Added Lens, HSB Scheme (%)

Mode	ΔFreq. (Hz)	ΔPeriod (s)	ΔMP E/W (%)	ΔMP N/S (%)
1	-	-	-	-0.1
3	-1.0	0.9	1.9	0.6
4	-0.9	1.0	1.5	6.2

The largest changes in natural frequency of any of the retrofit schemes by the addition of the lens were in the DB+HSB scheme, where the natural frequencies of the fundamental tower modes decreased by more than 2%. This change was on the same order of the changes in natural frequency for the fundamental tower modes that whole retrofit schemes had on the lighthouse model. This change in modal properties was close to what was expected since it is the approximate sum of the changes due to the addition of the lens for the individual retrofit schemes that make up the DB+HSB scheme. The changes in modal properties for the DB+HSB scheme due to the addition of the lens are summarized in Table 5.6-5, shown as percentages.

Table 5.6-5: Modal Property Changes from Added Lens, DB+HSB Scheme (%)

Mode	ΔFreq. (Hz)	ΔPeriod (s)	ΔMP E/W (%)	ΔMP N/S (%)
1	-	-	-	0.8
3	-2.3	1.9	0.3	1.0
4	-2.4	3.0	4.0	1.2

5.6.2 Mode Shapes

The addition of the lens had a negligible effect on the modal displacements of the fundamental wall mode around the lighthouse and the modal displacements of the fundamental tower mode changed minimally. The largest and most consistent changes in the modal displacements occurred in the tower and radio room rectangular wall, and this was expected since the lens was added to the tower and the radio room rectangular wall is directly adjacent to the tower. The changes in modal displacement were almost always positive, which was consistent with adding more mass to the tower. The changes in modal displacements of the tower mode for the retrofit schemes due to the addition of the lens are summarized in Table 5.6-6, shown as percentages. Two values in one cell represent the changes to the upper and lower limits of the section's displacements, respectively.

Table 5.6-6: Modal Disp. Changes in Tower Mode from Added Lens, All Schemes (%)

Scheme	Fog Gable	Fog Rect.	Radio Gable	Radio Rect.	Tower
Connections	-10 / 13	- / -2	4 / -	2 / -	8
Strong-Backs	-1 / 2	-	3 / -	2 / -	6
Diamond Braces	-1 / -	-	-	4 / -	-4
HSB	-1 / -	-	3 / -	2 / -	7
DB+HSB	-	-	10 / -	7 / -	22

5.6.3 Equivalent Lateral Force Procedure

The addition of the lens had a negligible effect on the displacements from the ELFP analysis for all five of the retrofit schemes. Adding the simplified lens into the lighthouse model increased the mass of the lighthouse by less than 1% and increased the mass of the tower by less than 1.5%. The total pseudo seismic force applied to the model increased the same amount the

mass increased because it is directly proportional to the mass of the building. The negligible increase in displacements around the lighthouse is expected with a small increase in lateral load.

5.6.4 Modal Response Spectrum Analysis

Even though the MRSA and ELFP analyses induced a lateral load on the lighthouse model in a similar way, the changes in the displacement results due to the addition of the lens into the model were notable for the MRSA analysis. The largest changes in displacement for the Connections scheme occurred in the radio room's gabled wall and in the tower, where the radio room's gabled wall displacements decreased by almost 8% for the analysis in the north-south direction, and the displacements in the tower increased by about 7% in both analysis directions. The changes in displacement for the tower were expected because the lens was added to the tower itself and the tower had multiple modes with significant mass participation that the MRSA analysis can capture. The changes in MRSA displacements for the Connections scheme due to the addition of the lens are summarized in Table 5.6-7, shown as percentages.

Table 5.6-7: MRSA Disp. Changes from Added Lens, Connections Scheme (%)

Direction	Fog Gable	Fog Rect.	Radio Gable	Radio Rect.	Tower
E/W	-2.3	1.2	3.7	-	6.9
N/S	3.9	-	-7.7	-1.7	6.3

The largest change in MRSA displacements for the Strong-Backs scheme was in the fog room's gabled wall, though significant changes in displacements also occurred in the radio room and tower. One explanation for the large change in displacements for the fog room's gabled wall is that the MRSA analysis revealed a connection between the wall and the tower that other analyses could not, or the change could be due to an error. Almost all of the MRSA analysis

displacements decreased around the lighthouse except for those in the tower, showing that the effect of adding the lens was more widespread than expected. The changes in MRSA displacements for the Strong-Backs scheme due to the addition of the lens are summarized in Table 5.6-8, shown as percentages.

Table 5.6-8: MRSA Disp. Changes from Added Lens, Strong-Backs Scheme (%)

Direction	Fog Gable	Fog Rect.	Radio Gable	Radio Rect.	Tower
E/W	-11	-6.5	4.8	-3.8	9.0
N/S	-3.1	-	-7.7	-9.9	7.9

The largest changes in the MRSA displacements for the Diamond Braces scheme were in the tower and significant changes in displacement occurred in the fog room's rectangular wall as well. The displacements in the fog room's rectangular wall and other walls in the lighthouse usually decreased in both directions while the displacements in the tower increased. The reason for the trends in the displacement results could be the connection the diamond braces provided between sections of the tower or the ability of the MRSA analysis to uncover characteristics of the building that other analyses could no. The changes in MRSA displacements for the Diamond Braces scheme due to the addition of the lens are summarized in Table 5.6-9, shown as percentages.

Table 5.6-9: MRSA Disp. Changes from Added Lens, Diamond Braces Scheme (%)

Direction	Fog Gable	Fog Rect.	Radio Gable	Radio Rect.	Tower
E/W	-3.6	-5.1	3.4	-4.4	7.8
N/S	0.7	-5.8	-	-6.2	7.3

The changes in MRSA displacements for the HSB scheme due the addition of the lens followed a similar trend as the changes for the Strong-Backs scheme. The largest changes in displacement were the increase to the tower's displacement and decreases to the fog room's gabled wall and radio room's rectangular wall. Even though the horizontal strong-backs themselves had been shown to provide only minimal improvement to the dynamic behavior of the gabled walls, the MRSA analysis showed that they had a larger effect than previously thought. The changes in MRSA displacements for the HSB scheme due to the addition of the lens are summarized in Table 5.6-10, shown as percentages.

Table 5.6-10: MRSA Disp. Changes from Added Lens, HSB Scheme (%)

Direction	Fog Gable	Fog Rect.	Radio Gable	Radio Rect.	Tower
E/W	-5.4	-2.8	3.6	-	6.8
N/S	0.1	-1.8	-	-5.1	8.5

Similar to the results of other analyses, the effects of the combination of individual retrofit schemes were roughly equal to the sum of the effects of the individual schemes, even in slightly different scenarios such as the addition of the lens. The largest change in displacements due to the addition of the lens occurred in the tower and the rectangular walls of the fog and radio rooms. The displacements increased in the tower and decreased in the walls, which was consistent with the results of other retrofit schemes. In general, the changes in displacement for the DB+HSB were the largest of any retrofit scheme because the scheme had the largest impact on the stiffness of the walls in the fog room and their connection to the tower. The changes in MRSA displacements for the DB+HSB scheme due to the addition of the lens are summarized in Table 5.6-11, shown as percentages.

Table 5.6-11: MRSA Disp. Changes from Added Lens, DB+HSB Scheme (%)

Direction	Fog Gable	Fog Rect.	Radio Gable	Radio Rect.	Tower
E/W	-	-8.0	2.2	-9.7	9.0
N/S	1.2	-8.2	-4.0	-8.0	7.4

5.6.5 Summary

The changes in modal properties for each of the retrofit schemes were close to what was expected based on the percentage of the total mass that was added with the lens. The natural frequencies always decreased and the mass participation almost always increased, which was consistent with the addition of mass. The Diamond Braces scheme was effective at using the tower and fog room rectangular walls to engage the fog room gabled walls, indicated by the change in modal properties in the fundamental wall mode based on the addition of the lens in the tower. The DB+HSB scheme had the greatest amount of change in all categories due to the addition of the lens, which was consistent with previous findings that showed the effects of the scheme were the approximate sum of each of the individual retrofit schemes. In general, however, the addition of the lens had very little effect on the modal properties of the lighthouse.

The changes in modal displacements for the fundamental tower mode were also approximately what was expected; the majority of the changes in modal displacements occurred in the tower and the walls directly adjacent to the tower in the radio room. The DB+HSB retrofit scheme showed an unexpectedly large change in modal displacements which may be due to the scheme's effective connection and stiffening of a variety of sections in the lighthouse. The change in modal displacements for the fundamental wall mode were negligible, though this was expected because a majority of the mass participation and displacement in the wall mode

occurred in the fog room's gabled walls, away from the tower and added lens. The changes in displacement due to addition of the lens from the ELFP analysis were also negligible for all retrofit schemes because the small change in mass resulted in an equally small change in the applied lateral load.

The results of the MRSA analysis showed the most consistent changes in displacement due to the addition of the lens, though the changes were generally minimal. The displacements in the walls of the fog and radio rooms always decreased, except for the radio gabled wall during the analysis in the east-west direction and the fog room gabled wall during the analysis in the north-south direction. The tower displacements always increased with the addition of the lens regardless the retrofit scheme, though the amount the displacements increased was more than expected since the addition of the lens had no effect in the ELFP analyses. These trends in the changes in displacement would not have been recognized had the MRSA analysis not been conducted. Though the magnitude of the change in displacements in the MRSA analysis was larger than in other analyses, the change was still small enough to conclude that the addition of the lens will not have a significant effect on the dynamic of the behavior of the lighthouse, whether a retrofit scheme is installed or not.

5.7 Analysis Comparison

Though each of the analyses conducted on the lighthouse finite element model showed differences between the retrofit schemes, the differences were used to identify trends in the overall effectiveness of the retrofit scheme and were not used as specific criteria to determine which retrofit scheme was definitively better than the others. The reason the retrofit schemes could not be compared directly was because they were not all developed to meet the same

criteria. The schemes involving strong-backs were designed to the same deflection criteria, but the diamond braces were only designed to restrain the top edge of the fog room's gabled wall. For this reason, the analysis results of the schemes involving strong-backs could be compared directly, but their results were generalized for comparison with retrofit schemes with diamond braces. For example, the Strong-Backs scheme and HSB scheme showed similar reductions in out-of-plane displacement for the fog room's gabled wall in the ELFP analysis, so those two retrofit schemes could be compared to each other. However, when including the schemes with diamond braces in the comparison, a fair comparison only considered the ability of the retrofit scheme to improve the dynamic behavior of the wall overall, in which case the results of more than one analysis were be considered.

Another condition that was considered in a general comparison of the retrofit schemes was that the performance of the retrofit scheme could change with a modification in the members' cross sections. For example, a strong-back section may be overdesigned to exceed the code-allowed deflection limit, and this may cause a much different result on the dynamic behavior of the lighthouse as a whole than if the section were only designed to satisfy the deflection criteria. The last condition that was considered in the retrofit scheme comparison was that it was very difficult to compare the modal displacements even generally without a concrete datum. The datum used in this research, the maximum modal displacement anywhere in the lighthouse, only gave insight into the mode shape of a single retrofit scheme since the maximum modal displacement changed significantly between retrofit schemes.

6.0 CONCLUSIONS

6.1 Overview

This research used an uncommon combination of analysis methods to provide an in-depth seismic evaluation of a historic unreinforced masonry lighthouse. The two main analysis methods, ultra-low forced vibration testing and finite element modeling, worked in conjunction to determine dynamic properties of the lighthouse that other analysis methods could not. Several retrofit schemes were proposed for the lighthouse and evaluated according to their effects on the dynamic behavior of the structure based on the results of multiple analyses on the finite element model. The repatriation of the lighthouse's massive first-order Fresnel lens was also considered in the evaluation in order to determine if it was safe for the lens to return to its original setting.

6.2 Retrofit Procedure

The combination of ultra-low forced vibration testing and finite element modeling proved successful for the thorough seismic evaluation of the Point Sur Lighthouse. Though the analysis methods were time and labor intensive, the work was justified for the historic lighthouse because it resulted in the identification of structural characteristics, such as strength and stiffness, and dynamic properties, such as natural frequency and mode shapes. Other analysis methods would have been incapable of producing the same information. The results of the ultra-low forced vibration testing laid the foundation for understanding the dynamic behavior of the lighthouse that the finite element modeling results expanded on, and the two methods gave a sufficiently thorough picture of the dynamic behavior as a whole for the purposes of this research. The combination of the two methods was what made each of them so effective for this research; the ultra-low forced vibration testing was important for calibrating the finite element model and the

finite element model was needed to supplement the limited amount of ultra-low forced vibration testing data. The creation of a finite element model that accurately represented the lighthouse's construction and dynamic behavior will be advantageous when the time comes for the full design of the retrofit scheme of the lighthouse because it will give confidence in the intended effects of the retrofit solution.

Other analysis methods would not have been able to capture some of the most important structural characteristics or dynamic properties of the lighthouse because many analysis methods rely on inspection of plans or the building itself in order to obtain information. For example, even though the ASCE 41-17 tiered screening procedures are a common and reliable method of designing seismic retrofit schemes for existing buildings, the screening procedures rely on visual inspection of a building's construction drawings or the building itself. In the case of the Point Sur Lighthouse, the ASCE 41-17 screening procedures were unable to identify the fact that the fog room's gabled walls behaved closer to a cantilever than a simply supported beam because the screening procedures assumed a restraining connection between the roof diaphragm and the masonry walls for lack of sufficient information. Only with in-depth finite element modeling was the true behavior of the fog rooms' gabled walls fully understood.

This research aimed to prove and develop state-of-the-art seismic retrofitting procedures on a simple and typical structure. The work on the lighthouse was justified because of the lighthouse's historic character and value as well as the safety of the rare and valuable first-order Fresnel lens if repatriated. The retrofitting procedures explored in this research may become more feasible for typical structures with advancements in the necessary technology and equipment or the growing need for comprehensive analysis of any structure.

6.3 Analysis Results

The results of the analyses conducted in this research provided several valuable points of comparison for the retrofit schemes, both qualitative and quantitative. The natural frequencies, periods, and mass participation from the modal analyses of the lighthouse with each of the retrofit schemes were used to understand the changes in dynamic behavior in a very general sense since those values could only describe the dynamic behavior of the lighthouse as a whole. A broader view of the dynamic behavior of the lighthouse was beneficial because a retrofit scheme should be evaluated on multiple scales, but additional analysis was needed to understand the local effects of the retrofit schemes. The mode shapes provided a closer look at the local effects of the retrofit schemes as well as the lighthouse as a whole, but it was difficult to directly compare the mode shapes between retrofit schemes because of their unitless nature. In general, the results of the modal analysis were the best basis for a qualitative comparison of the proposed retrofit schemes.

The results of the equivalent lateral force procedure analysis were used to make more quantitative comparisons than the modal analysis results, but they were still not the best basis for a final decision on which retrofit scheme is best. The results of the equivalent lateral force procedure analysis for a retrofit scheme largely depended on the specific member sections used so the displacements could be compared directly between retrofit schemes but were subject to change with future design iterations. For example, the HSS14x14x7/8 steel section used for the Strong-Backs scheme may be changed to an HSS16x20x7/8 and the displacements in the gabled wall would also change in an equivalent lateral force procedure analysis.

One reason why the equivalent lateral force procedure analysis was not the best to compare the effects of a retrofit scheme on the lighthouse as a whole was because the analysis unrealistically targets vulnerabilities of some sections while neglects the vulnerabilities in other sections. The analysis was used to compare local effects of the retrofit schemes, but not overall effects on the lighthouse. For example, the application of the same equivalent lateral acceleration in the north-south direction over the entire lighthouse produces a larger response in the fog room's gabled walls relative to its strength and stiffness than it does in the tower. The 210 modes that were required to exceed 90% mass participation also confirmed the need for a more comprehensive analysis that a single equivalent lateral force procedure analysis could not provide. Another reason why the results of the equivalent lateral force procedure analysis was not the best basis for the comparison of the retrofit schemes was because the analysis is not technically allowed by code to be used for the real design of a retrofit scheme. The lighthouse's irregular plan and large differences in stiffness between the tower and rooms disqualify it from analysis by the equivalent lateral force procedure so other analysis methods must be used.

The results of the modal response spectrum analysis were used to make the most quantitative comparisons of the proposed retrofit schemes since the results represented the most comprehensive analysis of all the analyses conducted. The modal response spectrum analysis used both the dynamic properties of the lighthouse found in the modal analysis and the site-specific seismic parameters used in the equivalent lateral force procedure analysis to identify dynamic properties of the lighthouse that the other analyses could not. The results of the modal response spectrum analysis were used to quantitatively compare the effects of the retrofit schemes for the lighthouse as a whole as well as for smaller sections of the lighthouse because

the analysis fairly targets the vulnerabilities of each of the sections of the lighthouse through its inclusion of the number of modes required to reach approximately sufficient mass participation.

The addition of the simplified lumped mass model of the lens into the finite element model of the lighthouse had very little effect on the dynamic behavior. The largest changes in dynamic behavior were in the tower and the changes in the dynamic behavior of the walls were minimal. The retrofit schemes with diamond braces increased the changes in displacements for the fog room walls because the diamond braces provided an effective means of uniting more sections of the lighthouse than other retrofit schemes. The changes in displacements from each of the analyses were almost always increases for the tower and were always close to the expected magnitude. Based on the results of the analyses with and without the lens in the model of the lighthouse, the lens should be safe in the lantern room upon its repatriation to the lighthouse. The main concern for the lens repatriation is the connection of the lens stand to the floor of the watch room, and any connection that is designed in the future should be designed to remain elastic.

6.4 Final Recommendations

The retrofit schemes with diamond braces were the most effective at restraining the top edge of the fog room's gabled walls, allowing the walls to behave more closely to simply supported or fixed-pinned beams rather than cantilevers out-of-plane. The diamond braces were also effective at limiting the in-plane response and decreasing displacements in each of the analyses conducted for this research. The horizontal strong-backs were beneficial for reducing the out-of-plane response for the fog room gabled wall's second mode and in-plane loading, for example in the fundamental tower mode in the east-west direction and when the equivalent lateral acceleration was applied in the east-west direction. Even though the strong-backs and

horizontal strong-backs provided the gabled walls with additional stiffness, they did not increase the fundamental wall mode's mass participation in the north-south direction because they did not provide a direct connection to the tower in the north-south direction. The horizontal strong-backs added minimal additional benefits to the fog room gabled walls when diamond braces were also present. The diamond braces alone were therefore sufficient in mitigating the most prominent deficiencies in the fog room gabled walls under all analysis scenarios. The diamond braces also intruded the least on the historic character of the interior of the lighthouse of all the proposed retrofit schemes with structural members.

With any retrofit scheme, it was important that the additional demands to the lighthouse foundation were carefully considered and minimized wherever possible. The foundation provides sufficient stability for the lighthouse, but the overall condition of the foundation is unknown. Providing proper restraint to the top edge of the fog room gabled walls not only improves the dynamic behavior of the walls themselves but also reduces the demands on the foundation at the base of the wall because the wall behaves closer to a fixed-pinned beam, which has reduced demands at the fixed connection over a cantilevered wall.

7.0 FUTURE RESEARCH

7.1 Overview

The evaluations performed in this research did not constitute a complete evaluation of the Point Sur Lighthouse, and they were the neither the beginning nor the end of the evaluation process. This research can continue with additional evaluations of the lighthouse using both additional ultra-low forced vibration testing and finite element modeling. The lighthouse could be subjected to another UL-FVT test to record more data and better understand its real dynamic behavior, especially the behavior of the walls in the fog room out-of-plane. More UL-FVT data would allow a closer comparison between the lighthouse and the unretrofitted lighthouse model and continued finite element modeling could provide the means for a better comparison of the retrofit schemes. Continued finite element modeling could also potentially provide design criteria for a future retrofit scheme.

7.2 UL-FVT "Re-shake"

One way this research could continue is with additional ultra-low forced vibration testing on the lighthouse in order to better understand the response of the walls between their junctions. Additional data would be useful for a more complete description of the mode shape of the existing lighthouse as well as a better comparison to the finite element model's mode shapes. The data recorded in the first UL-FVT tests gives no indication of the out-of-plane behavior of the fog room walls, which are the walls most at risk of damage due to poor out-of-plane behavior in a large seismic event. The new accelerometer locations are shown in Figure 7.2-1 and a majority of them are at the midspan of their respective walls. The gabled walls in the fog room will be equipped with accelerometers at the top and midheight of the wall's midspan where

possible in order to capture a more complete profile of their response. The few that are not at the midspan of a wall are either in the tower or at the junction of two of the radio room's walls. The accelerometers in the tower are necessary to identify the natural frequency of the mode and this is done best with an accelerometer close to the shaker.

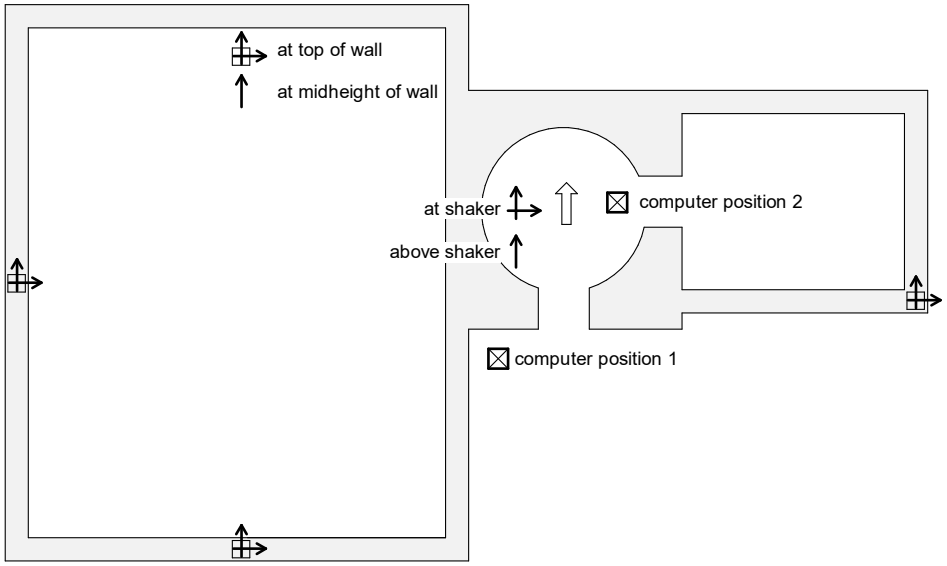

Figure 7.2-1: 12 Accelerometer Locations in Plan for UL-FVT Re-Shake

Another important consideration in the re-shake is the location of the laptop computer used to view and record the accelerometer data. The addition of accelerometers, especially accelerometers spaced farther apart around the building, also adds constraints to the possible locations of the laptop computer used in the test. Two possible locations for the computer are the ground level adjacent to the fog room entrance or in the watch room near the shaker, labeled in Figure 7.2-1. No matter the location of the laptop, great care must be taken in the preparations for another ultra-low forced vibration test because of the limited resources at the lighthouse and other constraints due to its remote location.

Additional UL-FVT tests may also be conducted when a retrofit scheme is installed. If the installed retrofit is not one that was studied in this research, it can be easily implemented in the finite element model and the same variety of comparisons may be made. The dynamic behavior of the lighthouse with and without a retrofit can be compared both in the real lighthouse and in the finite element model.

7.3 Finite Element Model Adjustments

Another way this research can be continued is by making adjustments to the components of the finite element model and running additional analyses. The goal of making adjustments to the finite element model is to make the model a more accurate representation of the lighthouse as well as increase the usability of the model on a computer with standard processing power. Most of the adjustments that could be made to the lighthouse model are not expected to have a significant impact on the results that renders the analyses conducted in this research invalid. Remodeling portions of the lighthouse to use fewer elements would increase the usability of the model and relieve some of the burden placed on the computer's graphics and computational abilities during modeling and analyses.

The goal of running additional analyses is to provide additional points of comparison for the finite element model versus the lighthouse as it stands, as well as between retrofit schemes. A better comparison of the finite element model and current lighthouse would allow the finite element model to be better calibrated and to more accurately reflect the dynamic behavior of the lighthouse. A more accurate finite element model would in turn be better at predicting the behavior of the lighthouse with the various retrofit schemes installed, and this would aid in a more complete design of the retrofit schemes as well as a better basis for a final retrofit decision.

7.3.1 Model Improvements

The following adjustments can be made to improve the RISA-3D model:

1. Changing the material of the solid elements at the watch room level from brick to sandstone would allow the model to be a more accurate representation of the lighthouse's true construction. This change is not expected to have a significant impact on the results since a majority of the tower's section is already sandstone and the solid elements in question are at the top of the tower rather than at the base.
2. Increasing the shear modulus of the diaphragm material to reflect the stiffness of a modern diaphragm may change the out-of-plane modal properties and stiffness of the walls measurably. The shear modulus of the diaphragm material represents a stiffness of 2,000 lb./in., the default expected value found in ASCE 41-17 for the diaphragm type in the lighthouse. Overlaying wood structural panels on the existing straight sheathing and adding blocking and chords brings the default expected value up to 18,000 lb./in. This strengthening may not be possible in the lighthouse for constructability reasons, and it is potentially too large of an intrusion on the architectural features of the building.
3. Remodeling the walls in the lighthouse using a single layer of plate elements instead of two layers of solid elements may increase the usability of the model without compromising the accuracy of the results. Both the graphics and computational power of standard computer hardware are bogged down significantly simply due to the number of elements contained in the model. Reducing the number of elements would allow for easier manipulation and viewing of the model as well as faster run times for complex analyses such as large modal analyses and time history loads.

4. Adding a number of minor elements would allow the model to more accurately represent the lighthouse's true construction, though this would counteract the effects of the previous recommendation. If the usability of the model is deemed to be acceptable, then the following elements may be added to the model: steel stairs and landings in the tower, steel plates on the interior and exterior of the watch room level, and glass windows in the fog and radio rooms. The displacements and accelerations resulting from the model analyses may be compared to the allowable limits for glass in order to predict if the windows would break under loading.

7.3.2 Simulated UL-FVT

One additional and very useful analysis that may be conducted on the finite element model of the lighthouse is a simulated UL-FVT test because it would provide much better grounds for comparison between the finite element model and the real lighthouse than comparing the mode shapes. The mode shapes found in the real UL-FVT testing of the lighthouse are believed to be a combination of multiple mode shapes while the mode shape from the finite element model is a pure mode shape from just one natural frequency. Simulating the ultra-low forced vibration test in the finite element model with the same "accelerometer" and "shaker" setup would produce a combination of mode shapes and provide a more direct apples-to-apples comparison. Even though the exact shaker and accelerometer locations used in the real test are unknown, their locations in the finite element model can be closely approximated to yield accurate results.

The simulation can be executed as a time history load in RISA-3D and the following steps outline the procedure from creation of the loading scenario to analysis of the results. The

steps are not meant to be exhaustive, so a general knowledge of RISA-3D is recommended. Special care should be taken when adjusting the advanced settings described in Step 3b because those settings have a large effect on the results.

1. Generate and modify a new time history function.
    a. In RISA-3D Version 17, a new time history function may be generated by: *Modify > Time History Function Library > Generate*
    b. In RISA-3D Version 18, a new time history function may be generated by: *Advanced > Time History > Generate*
    c. *Base Function*: Name the function appropriately, select the function type, and enter a frequency or period for the shaker excitation with proper units. The duration of the function should be determined so that there is sufficient time for the transient response to reduce to 1% or less of the steady state response. This may be done using Equation 7.3-1, where ζ is the damping ratio of the mode and ω_n is the natural circular frequency of the mode.

$$t \geq \frac{ln(0.01)}{-\zeta\omega_n} \qquad \text{(Equation 7.3-1)}$$

    Damping values and natural circular frequencies resulting from UL-FVT tests of the lighthouse may be found in previous sections but should ultimately be determined by the user for simulations in RISA-3D. The option to complete the last cycle need not be applied, the scale factor may be left as 1, and the phase angle may be left as 0.

d. *Ramp Up* and *Coast Down*: The ramp up and coast down options may be included in the function but their durations should be added separately from the duration determined in Step 1d.

e. *Display Range*: Setting a display range may be useful for presentation purposes. An example time history function is shown in Figure 7.3-1.

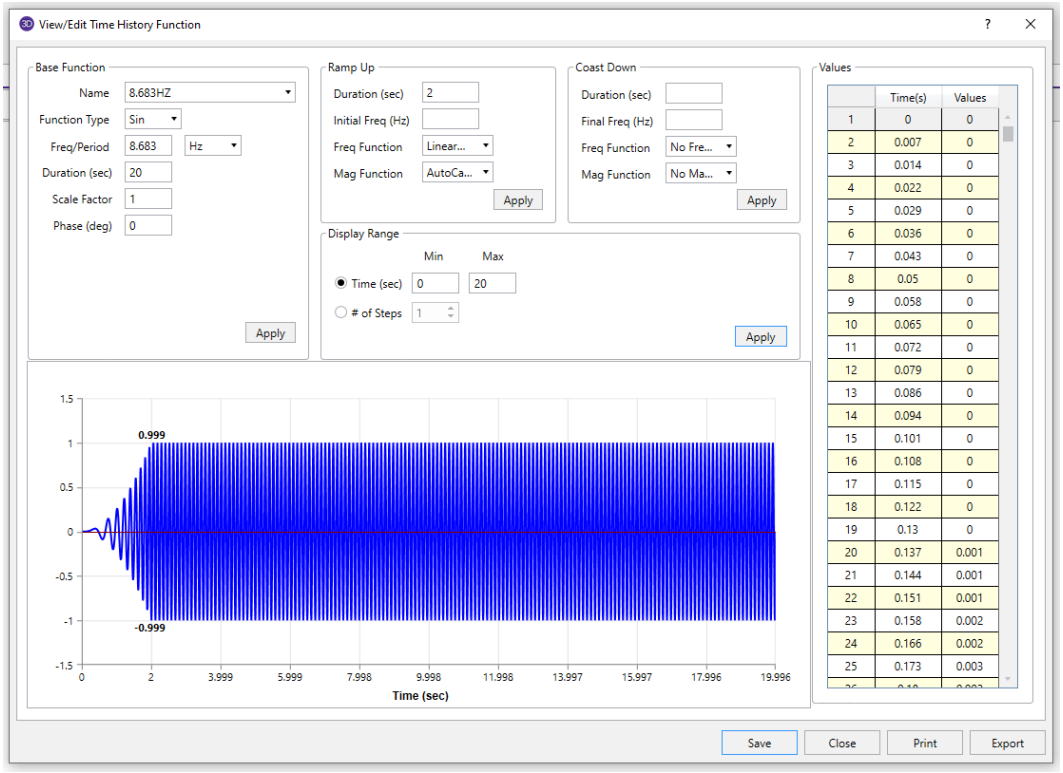

Figure 7.3-1: Example Time History Function in RISA-3D

2. Generate and modify a new time history load.

a. In RISA-3D Version 17, the time history load settings may be accessed by:

Spreadsheets > Loads > Time History Loads

b. In RISA-3D Version 18, the time history load settings may be accessed by:

Spreadsheets > Data Entry > Time History Loads

c. Create a new time history load by clicking within the spreadsheet area. Two rows for each time history load will appear in the spreadsheet and entries should be identical between rows.

d. *Tag* and *Label*: The tag for the load is determined by RISA-3D but the label may be edited by the user.

e. *Time Step*: According to the RISA-3D reference manual, the time step for a sinusoidal time history function should be $1/20^{th}$ or $1/24^{th}$ of the function's period which correspond to an integration step every 18 and 15 degrees of frequency rotation, respectively [27].

f. *Type*, *Function*, and *Node*: The load type should be set to *Force* and the function should be set to the function generated in Step 1. The node(s) to receive the load should reflect the shaker placement in the original UL-FVT test. Node N14273A is an approximate location for the shaker in the RISA-3D models created for this research and is compatible with all models regardless of the lens configuration.

g. *Direction*: The direction should correspond to the shaker direction of interest in the global axes and a direction that is not aligned with the global axes may be reproduced using orthogonal components. If this is the case, change the direction in one of the rows of the time history load to the desired orthogonal direction.

h. *F Factor*: If the shaking direction is aligned with the global axes, the F Factor for one of the rows should be set to the force induced by the shaker and the F Factor for the other row should be set to 0. If the shaker direction is not aligned with the global axes, the F Factors should represent the orthogonal components of the

force induced by the shaker in the desired direction. **Note:** The F Factor represents a force according to Step 2f and units are determined by the overall units of the model. More information on the shaker's force amplitude as a function of frequency and signal voltage can be found in Gerbo [4].

i. *T Factor*, *Arrival*, and *Run Out*: The T Factor, Arrival, and Run Out spaces may be left blank. An example time history load window is shown in Figure 7.3-2.

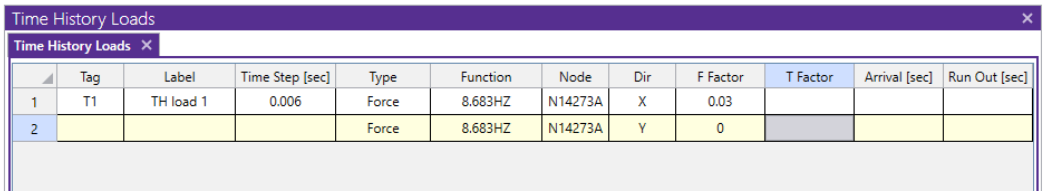

Figure 7.3-2: Example Time History Load in RISA-3D

3. Run the time history load analysis.
   a. Generate a new load combination that includes only self-weight and the time history load. Enter the time history load's tag as its basic load case and its load combination factor as 1. For simulating UL-FVT in RISA-3D, the time history function Scale Factor, time history load F Factor, and load combination Factor can all be used separately to define the force amplitude, but the method for defining the force amplitude outlined above is recommended.
   b. A Dynamics solution must be run before the load combination containing the time history load may be run. The required number of modes for the Dynamics solution depends on the integration method: the number of modes required for the Modal Superposition method is related to the time history function frequency but there is no requirement for the Direct Integration method. An investigation into

the effects of changing the advanced solution settings may be valuable. The advanced settings are shown in Figure 7.3-3 and can be accessed by:

Settings > Solution > Advanced

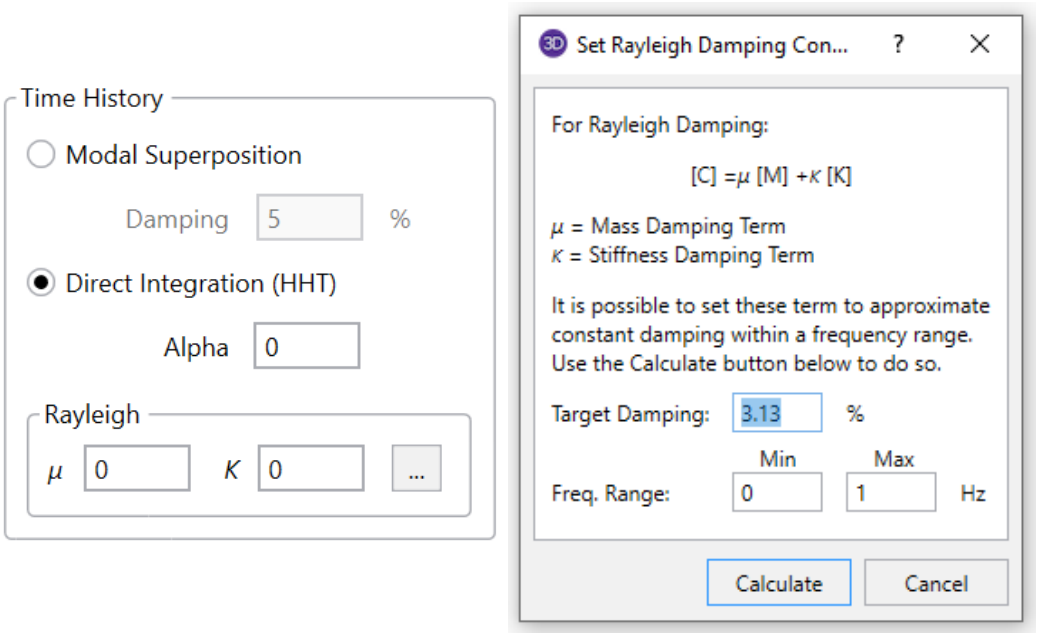

Figure 7.3-3: Advanced Solution Settings in RISA-3D

A preliminary simulated UL-FVT test was run without sufficient knowledge of the advanced settings and a sample of the results is shown in Figure 7.3-4. The results were considered invalid because the response never reached a constant steady state amplitude, the most likely reason being an error in the advanced damping settings. The forcing frequency and "shaker direction" for the simulation will also need to be considered carefully because the sample results suggest that one or both of those variables may not perfectly aligned with the natural frequency and modal axis of the tower, respectively.

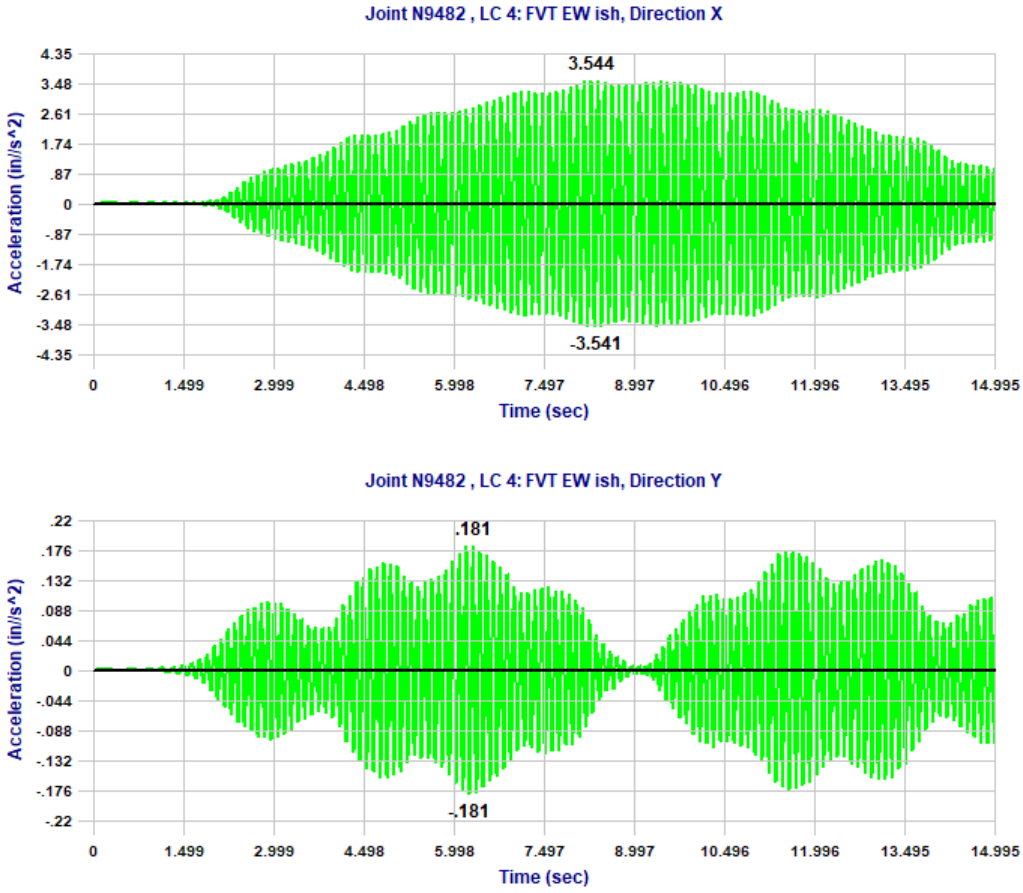

Figure 7.3-4: Simulated UL-FVT Sample Results

c. Run the load combination containing the time history load. The results of interest for the time history load in RISA-3D Versions 17 and 18 can be found by:

Results > TH (Joint) Trace

The maximum steady state amplitude of acceleration in a certain direction can be compared to the UL-FVT raw data found in the Appendix or plotted in the same format used in Section 5.2.1. The nodes in the RISA-3D model that most closely

correspond to the accelerometer locations in the original UL-FVT test of the lighthouse are given in Table 7.3-1.

Table 7.3-1: Node Labels for Accelerometer Locations

Accel.	Node Label
A	N14273A
B	N9537
C	N9482
D	N6057
E	N21365
F	N14177A

7.3.3 Linear Response History Analysis

A linear response history analysis is possible in RISA-3D and could be implemented in a similar way as the simulated UL-FVT, the only difference being the use of a ground motion instead of a sinusoidal function in the first step of the previous section. A linear response history analysis would provide the best comparison of the performance of the different retrofit schemes since it would provide demands from probable seismic events. The results from a linear response history analysis would provide the best means of choosing a retrofit scheme and could be used in the full design of the chosen retrofit scheme.

7.3.4 Direct Results from RISA-3D

Given the relationship between the responses in real and modal spaces described in Section 3.2.2, it is possible to draw the real results for the simulated UL-FVT and other analyses directly from RISA-3D without manipulation. However, an important condition must be satisfied before the direct results may be used. The mass matrix for the model must be normalized, but is impossible to tell if RISA-3D normalizes the matrix by default without further research.

BIBLIOGRAPHY

[1] McDaniel, C., Archer, G. (2011): Ultra-Low Forced Vibration Testing – NEESR Project Report 2011-1089. Architectural Engineering Department, California Polytechnic State University, San Luis Obispo. https://datacenterhub.org/resources/14520.

[2] Archer, G., McDaniel, C. (2011): Determination of Building Modal Parameters Using Low-Level Excitation. *2011 Architectural Engineering Conference (AEI)*, Oakland, California.

[3] California Coastal Records Project. Copyright © 2002-2020 Kenneth & Gabrielle Adelman. Photographs used with permission. www.californiacoastline.org.

[4] Gerbo, E. (2014): Structural Damage Detection Utilizing Experimental Mode Shapes. Master's thesis submitted to California Polytechnic State University, San Luis Obispo, Architectural Engineering Department.

[5] Ramos, P. (2013): System Identification of a Bridge-Type Building Structure. Master's thesis submitted to California Polytechnic State University, San Luis Obispo, Architectural Engineering Department.

[6] The Structural Engineering Institute of the American Society of Civil Engineers (2017). ASCE 41-17: Seismic Evaluation and Retrofit of Existing Buildings.

[7] McDaniel, C., Laursen, P., Archer, G., Elster, B. (2018): Experimental/Computational Exploration of Retrofit Strategies for the Piedras Blancas Light Station. *16th European Conference on Earthquake Engineering (16th ECEE),* Thessaloniki, Greece.

[8] Sourer, M.M., et al. (2009): Evaluation of Young's Modulus for Sandstone Masonry Walls Under Compression. *11th Canadian Masonry Symposium,* Toronto, Ontario.

[9] Furtmüller, T., Adam, C. (2011): Numerical Modeling of the In-Plane Behavior of Historical Brick Masonry Walls. Institute for Basic Sciences in Civil Engineering, Unit for Applied Mathematics, University of Innsbruck, Innsbruck, Austria.

[10] Vaculik, J. (2012): Unreinforced Masonry Walls Subjected to Out-of-Plane Seismic Actions. Doctoral thesis submitted to the University of Adelaide School of Civil, Environmental & Mining Engineering, Adelaide, Australia.

[11] Dekker, N., McDaniel, C., Laursen, P., Archer, G. (2020): Forced Vibration Testing and Retrofit of the Historic Unreinforced Masonry Point Sur Light Station. *17th World Conference on Earthquake Engineering (17th WCEE),* Sendai, Japan.

[12] California Historical Landmarks by County: Monterey. California State Parks Office of Historic Preservation website. Accessed 4/11/2020 http://ohp.parks.ca.gov/?page_id=21441.

[13] Google Maps. Accessed 6/24/2020. https://www.google.com/maps/.

[14] Relief Map of California, USA. Wikipedia Commons user Nzeemin. Accessed 4/28/2020. https://commons.wikimedia.org/wiki/File:Relief_map_of_California.png.

[15] United States Government Printing Office (1887): The Statutes at Large of the United States of America From December, 1885, to March, 1887, and Recent Treaties, Postal Conventions, and Executive Proclamations, Volume XXIV. Pages 225, 513.

[16] United States Government Printing Office (1891): The Executive Documents of the House of Representatives for the Second Session of the Fifty-First Congress. Page 112.

[17] United States Coast Guard Historic Light Station Information & Photography: California, Point Sur Light. United States Coast Guard History website. Accessed 4/28/2020. https://web.archive.org/web/20170501201850/http://www.uscg.mil/history/weblighthouses/LHCA.asp.

[18] Point Sur State Historic Park. Copyright © 2016 California State Parks. Informational brochure. www.parks.ca.gov.

[19] Big Sur Chamber of Commerce: Point Sur Lighthouse. Big Sur Chamber of Commerce website. Accessed 6/24/2020. https://www.bigsurcalifornia.org/pointsur.html.

[20] Bieber, D., Pfeiffer, J., Zorne, J. (2012): Geotechnical Investigation: Point Sur Bridges, Monterey, California. Technical report prepared by Geocon Consultants, Inc. for California State Parks.

[21] Rendon, A. (2011): Determination of the Modal Parameters of a Five Story Reinforced Concrete Structure Using Ultra-Low Level Excitation and Computational Analysis. Master's thesis submitted to California Polytechnic State University, San Luis Obispo, Architectural Engineering Department.

[22] Chopra, A. (2012): Dynamics of Structures: Theory and Applications to Earthquake Engineering (Fourth Edition). University of California at Berkeley. Prentice Hall Publishers.

[23] Fast Fourier Transformation FFT – Basics. NTi Audio website. Accessed 6/24/2020. https://www.nti-audio.com/en/support/know-how/fast-fourier-transform-fft.

[24] Simpson Strong-Tie Wood Construction Connectors: 2017-2018, C-C-2017. Simpson Strong-Tie Company, Inc. https://www.strongtie.com.

[25] Dizhur, D. et al. (2013): Performance of Posttensioned Seismic Retrofit of Two Stone Masonry Buildings During the Canterbury Earthquakes. *Australian Earthquake Engineering Society Conference,* Hobart, Tasmania, Australia.

[26] ATC Hazards by Location: Seismic hazards for coordinate 36.3064°N, 121.9017°W. Accessed 6/24/2020. https://hazards.atcouncil.org.

[27] RISA-3D General Refence Manual Version 17. 2018. RISA Tech, Inc. https://risa.com.

Table A.1-1: UL-FVT Frequency Sweep E/W Raw Data

Freq (Hz)	Acceleration (µg)			Average (µg)
9.20	281.4	278.5	280.1	280.0
9.30	366.6	368.8	368.4	368.0
9.40	449.9	448.5	448.0	448.8
9.50	483.6	484.7	478.2	482.2
9.60	525.6	522.0	521.2	522.9
9.65	539.2	536.0	534.9	536.7
9.70	544.9	543.6	545.9	544.8
9.80	497.9	498.6	499.7	498.8
9.90	451.2	448.5	446.2	448.6
10.00	392.6	389.7	392.2	391.5
10.10	333.1	334.8	332.9	333.6
10.20	282.0	281.6	281.0	281.5

Table A.1-2: UL-FVT Frequency Sweep N/S Raw Data

Freq (Hz)	Acceleration (µg)			Average (µg)
9.20	297.5	298.5	299.8	298.6
9.30	413.4	409.6	416.9	413.3
9.40	474.7	468.6	494.0	479.1
9.50	482.2	507.1	491.3	493.5
9.60	531.7	553.3	542.2	542.4
9.70	463.0	470.8	455.4	463.1
9.80	383.4	378.2	375.9	379.2
9.90	374.1	367.4	367.8	369.8
10.00	326.7	326.1	319.8	324.2

Table A.1-3: UL-FVT Frequency Sweep N/S Raw Data (unused)

Freq (Hz)	Acceleration (µg)			Average (µg)
9.50	476.0	482.2	472.1	476.7
9.55	480.8	482.4	472.5	478.6
9.58	475.8	479.5	483.4	479.6
9.60	483.3	482.9	483.3	483.2
9.62	474.3	475.7	475.3	475.1
9.65	471.6	469.9	472.9	471.5
9.70	443.8	446.4	446.9	445.7

Table A.1-4: UL-FVT Mode Shape E/W Raw Data

Accel. Location	Accel. Direction	Acceleration (μg)			Average (μg)
A	N/S	226.3	223.8	219.7	223.3
	E/W	690.8	689.0	688.8	689.6
B	N/S	176.3	176.7	173.7	175.5
	E/W	149.4	149.3	149.5	149.4
C	N/S	90.72	93.75	87.15	90.54
	E/W	124.2	122.9	121.6	122.9
D	N/S	96.88	96.36	96.41	96.55
	E/W	25.39	25.32	25.52	25.41
E	N/S	123.5	123.8	125.2	124.2
	E/W	44.40	44.72	43.99	44.37
F	N/S	144.8	146.1	143.6	144.9
	E/W	406.0	405.9	405.0	405.6

Table A.1-5: UL-FVT Mode Shape N/S Raw Data

Accel. Location	Accel. Direction	Acceleration (μg)			Average (μg)
A	N/S	698.5	696.5	696.4	697.1
	E/W	171.6	172.1	173.5	172.4
B	N/S	390.8	387.7	393.9	390.8
	E/W	82.09	68.43	81.72	77.41
C	N/S	178.2	184.1	185.8	182.7
	E/W	59.28	60.44	60.19	59.97
D	N/S	168.0	169.2	167.8	168.3
	E/W	11.31	11.82	11.27	11.47
E	N/S	366.8	375.9	373.6	372.1
	E/W	50.96	52.53	52.68	52.06
F	N/S	390.7	387.0	386.6	388.1
	E/W	109.8	110.8	111.6	110.7

Table A.2-1: Modal Properties for 210 Modes (≥90% Mass Participation E/W and N/S), Connections Scheme

Mode	Freq. (Hz)	Period (s)	MP E/W (%)	MP N/S (%)	MP Vert. (%)
1	3.635	0.275	0	11.40	0
2	7.286	0.137	0	0.025	0
3	8.735	0.114	24.08	4.326	0
4	8.939	0.112	18.00	0.521	0
5	9.438	0.106	0.054	7.521	0
6	9.562	0.105	0.073	20.04	0
7	9.902	0.101	3.837	11.43	0.014
8	10.52	0.095	0.129	1.135	0
9	10.60	0.094	6.042	0.843	0.024
10	11.72	0.085	2.570	0.119	0
11	11.92	0.084	3.169	0.054	0
12	12.88	0.078	0.353	0.022	0
13	13.47	0.074	6.345	0.485	0.013
14	13.84	0.072	0.092	4.005	0
15	14.54	0.069	0.022	1.199	0
16	14.80	0.068	0.137	1.423	0
17	15.40	0.065	0.615	0.684	0
18	15.65	0.064	0.302	0.069	0
19	16.01	0.062	0.297	0.024	0.011
20	16.25	0.062	0.024	0.525	0
21	17.77	0.056	0.013	0	0.259
22	18.44	0.054	0.113	0.763	0.049
23	19.59	0.051	0	0.263	0.133
24	20.04	0.050	0.025	0.070	0.051
25	20.93	0.048	0.086	0.195	0.924
26	21.12	0.047	0.011	2.061	0.040
27	21.39	0.047	0.403	0.779	0.019
28	21.52	0.046	0.711	0.219	1.012
29	22.03	0.045	0.190	0.374	0
30	22.52	0.044	0.423	0.109	1.080
31	22.92	0.044	0.024	0.295	3.781
32	23.48	0.043	0.625	0.018	0.115
33	23.75	0.042	0.697	0.515	0.143

Mode	Freq. (Hz)	Period (s)	MP E/W (%)	MP N/S (%)	MP Vert. (%)
34	24.13	0.041	0.013	0.135	0.017
35	24.28	0.041	1.890	0.107	2.175
36	24.35	0.041	0.152	0	1.618
37	24.86	0.040	0.101	0.254	0.029
38	24.98	0.040	0.398	1.479	0.059
39	25.58	0.039	1.265	0.500	0
40	26.18	0.038	0	0.284	0.044
41	26.46	0.038	0.240	0.062	3.490
42	26.95	0.037	0.011	0.305	0.196
43	27.29	0.037	0.649	2.503	1.443
44	27.44	0.036	0.157	0.390	0.324
45	27.65	0.036	0.397	0.017	0.136
46	28.02	0.036	2.994	1.112	1.498
47	28.77	0.035	0	0.653	0.321
48	28.92	0.035	0.396	0.195	0.471
49	29.16	0.034	0.313	0	0.452
50	29.49	0.034	0.390	0.655	2.190
51	29.81	0.034	0.044	0.208	0
52	30.00	0.033	0	0	2.486
53	30.38	0.033	0.353	0.503	0.021
54	30.93	0.032	1.131	0.381	2.536
55	31.12	0.032	0.117	0	6.374
56	31.58	0.032	0.276	0.145	1.463
57	32.17	0.031	0.013	0.201	1.011
58	32.23	0.031	0.018	0.033	0.266
59	32.67	0.031	0.059	0.019	2.573
60	32.97	0.030	0.245	0.079	29.71
61	33.17	0.030	0.040	0	0.218
62	33.31	0.030	0	0.232	0.823
63	33.49	0.030	0.263	0	0.458
64	33.81	0.030	0	0	4.486
65	34.03	0.029	0	0.200	0.373
66	34.25	0.029	0.035	0.013	0.556
67	34.46	0.029	0.074	0.023	0.673
68	34.63	0.029	0.048	0	0.979

Mode	Freq. (Hz)	Period (s)	MP E/W (%)	MP N/S (%)	MP Vert. (%)
69	35.04	0.029	0	0.206	0.010
70	35.63	0.028	0.012	0.058	0.143
71	35.78	0.028	0.712	0	0.058
72	36.12	0.028	0	0.058	0.064
73	36.83	0.027	0.011	0.025	0
74	36.93	0.027	0.105	0.025	0.048
75	37.85	0.026	0.262	0.014	0.028
76	37.90	0.026	0	0	0.011
77	38.52	0.026	0.273	0.149	0
78	38.99	0.026	0.025	0	0.068
79	39.10	0.026	0.025	0.014	0.018
80	39.65	0.025	0.011	0	0.036
81	39.71	0.025	0	0.126	0
82	40.17	0.025	0.109	0.017	0.157
83	40.36	0.025	0.054	0	0.016
84	40.82	0.024	0.042	0.142	0.032
85	40.84	0.024	0	0.151	0.337
86	41.03	0.024	0.055	0.010	0.035
87	41.17	0.024	0	0.082	0.151
88	41.50	0.024	0	0.057	0.193
89	41.90	0.024	0.031	0.021	0.054
90	42.06	0.024	0.208	0	0.016
91	42.70	0.023	0.473	0	0
92	42.99	0.023	0.028	0.059	0
93	43.20	0.023	0	0.351	0
94	43.55	0.023	0	0.053	0.061
95	43.71	0.023	0.032	0.041	0
96	43.86	0.023	0.013	0.202	0.108
97	43.91	0.023	0.037	0.122	0
98	44.17	0.023	0.014	0.109	0
99	44.46	0.022	0	0.029	0.010
100	45.01	0.022	0.017	0	0.010
101	45.34	0.022	0.029	0	0.039
102	45.45	0.022	0.154	0.019	0.021
103	45.57	0.022	0.235	0.015	0

Mode	Freq. (Hz)	Period (s)	MP E/W (%)	MP N/S (%)	MP Vert. (%)
104	45.68	0.022	0.051	0.335	0
105	46.08	0.022	0.354	0	0.084
106	46.12	0.022	0	0.068	0.081
107	46.85	0.021	0.133	0.108	0.020
108	47.20	0.021	0.149	0.176	0.010
109	47.48	0.021	0.047	0.184	0
110	47.73	0.021	0.070	0.053	0.077
111	48.17	0.021	0.098	0.544	0
112	48.37	0.021	0.308	0	0.027
113	48.97	0.020	0	0	0.019
114	49.03	0.020	0.483	0.087	0
115	49.48	0.020	0	0.014	0
116	49.68	0.020	0.102	0.391	0
117	49.97	0.020	0.045	0.307	0
118	50.13	0.020	0.036	0	0
119	50.31	0.020	0	0	0.024
120	50.71	0.020	0.020	0.017	0
121	50.89	0.020	0.193	0.266	0.059
122	51.16	0.020	0.019	0.011	0
123	51.31	0.019	0.035	0	0
124	51.57	0.019	0.015	0.058	0
125	52.30	0.019	0.213	0.146	0
126	52.36	0.019	0.029	0	0
127	52.61	0.019	0.085	0.026	0.014
128	52.86	0.019	0	0.032	0
129	53.35	0.019	0.045	0.174	0
130	53.51	0.019	0.114	0	0
131	53.96	0.019	0.020	0	0.016
132	54.06	0.018	0	0.052	0
133	54.31	0.018	0	0	0.032
134	54.82	0.018	0	0.016	0
135	55.50	0.018	0	0	0
136	55.68	0.018	0.025	0.012	0.030
137	56.10	0.018	0.022	0	0
138	56.25	0.018	0	0	0

Mode	Freq. (Hz)	Period (s)	MP E/W (%)	MP N/S (%)	MP Vert. (%)
139	56.36	0.018	0.123	0.028	0
140	56.61	0.018	0	0.037	0
141	56.71	0.018	0	0.024	0.024
142	56.85	0.018	0	0.046	0.011
143	57.11	0.018	0	0.043	0
144	57.40	0.017	0	0	0
145	57.57	0.017	0.047	0.041	0.055
146	57.84	0.017	0	0.072	0.033
147	58.14	0.017	0.053	0.038	0.054
148	58.24	0.017	0	0.012	0
149	58.94	0.017	0	0	0.038
150	59.04	0.017	0.036	0.128	0.057
151	59.25	0.017	0	0.056	0
152	59.61	0.017	0.199	0	0
153	59.75	0.017	0.102	0.015	0
154	60.00	0.017	0.024	0	0.016
155	60.20	0.017	0.048	0.104	0
156	60.40	0.017	0.142	0.041	0.018
157	60.69	0.016	0.064	0.075	0.034
158	60.88	0.016	0.094	0	0.013
159	61.06	0.016	0	0	0
160	61.31	0.016	0.055	0	0
161	61.44	0.016	0.041	0.017	0
162	61.56	0.016	0.051	0.012	0
163	61.75	0.016	0.039	0	0
164	61.86	0.016	0	0.022	0.014
165	62.34	0.016	0.052	0.043	0.014
166	62.65	0.016	0.076	0.155	0.014
167	62.78	0.016	0.014	0.032	0
168	63.38	0.016	0.069	0.140	0
169	63.69	0.016	0.022	0.040	0.030
170	63.77	0.016	0.058	0	0
171	64.37	0.016	0.115	0.016	0
172	64.49	0.016	0.033	0	0
173	64.55	0.015	0.013	0.103	0.136

Mode	Freq. (Hz)	Period (s)	MP E/W (%)	MP N/S (%)	MP Vert. (%)
174	64.72	0.015	0.016	0.207	0
175	65.35	0.015	0.173	0.014	0
176	65.66	0.015	0.061	0	0
177	65.80	0.015	0	0	0
178	66.14	0.015	0.080	0	0.019
179	66.34	0.015	0	0.031	0
180	66.57	0.015	0	0	0
181	66.94	0.015	0	0.227	0
182	67.16	0.015	0.046	0	0.043
183	67.21	0.015	0.033	0.012	0.035
184	67.62	0.015	0.047	0.030	0.034
185	68.09	0.015	0	0.019	0
186	68.18	0.015	0	0.070	0.063
187	68.33	0.015	0	0	0.102
188	68.35	0.015	0.025	0.020	0.069
189	68.85	0.015	0	0	0
190	69.07	0.014	0.093	0	0.030
191	69.09	0.014	0.033	0.039	0.141
192	69.23	0.014	0	0	0
193	69.45	0.014	0.049	0	0.030
194	69.80	0.014	0.031	0.024	0.053
195	70.04	0.014	0.012	0.014	0.017
196	70.11	0.014	0.055	0.193	0.122
197	70.22	0.014	0	0.012	0.032
198	70.57	0.014	0.012	0	0.073
199	70.77	0.014	0.039	0.025	0.058
200	71.08	0.014	0	0.048	0.039
201	71.20	0.014	0.185	0.046	0
202	71.23	0.014	0.039	0.032	0
203	71.49	0.014	0	0.045	0.026
204	71.67	0.014	0.025	0.011	0.015
205	71.74	0.014	0.024	0.021	0
206	71.88	0.014	0.010	0.047	0
207	72.01	0.014	0.023	0.023	0
208	72.72	0.014	0.028	0	0

Mode	Freq. (Hz)	Period (s)	MP E/W (%)	MP N/S (%)	MP Vert. (%)
209	72.88	0.014	0	0.017	0
210	73.07	0.014	0	0.040	0.045
Residual:	N/A	N/A	9.921	9.771	18.80
Totals:	N/A	N/A	100	100	100